DESIGN AND REASSESSMENT OF TUBULAR JOINTS IN OFFSHORE STRUCTURES

CONFIDENTIAL AS

CHAPTER 6: FATIGUE AND FRACTURE FRACTURE MECHANICS APPROACH

C6060R10.12 REV A OCTOBER 1995

Purpose of Issue	Rev	Date of Issue	Author	Checked	Approved
Sub-Group Review	0	March 1995	MJC	-	-
Final Issue	A	October 1995	MJC	PAS	

BILLINGTON OSBORNE-MOSS ENGINEERING LIMITED
Ledger House
Forest Green Road, Fifield
Maidenhead, Berkshire
SL6 2NR
Telephone (01628) 777707
Fax (01628) 777877

REVISION SHEET

REVISION	DETAILS OF REVISION
0	Issued to Subgroup on fracture mechanics for review.
A	Final issue to all paticipants.

DESIGN AND REASSESSMENT OF TUBULAR JOINTS IN OFFSHORE STRUCTURES

CHAPTER 6: FATIGUE AND FRACTURE FRACTURE MECHANICS APPROACH

CONTENTS

CONTENTS CONTINUED

CONTENTS CONTINUED

CONTENTS CONTINUED

1. FUNDAMENTALS OF FRACTURE MECHANICS

1.1 Introduction

Fracture mechanics is the discipline concerned with the study of cracks and their behaviour. To this end it seeks ways of calculating the parameters and determining the relationships which permit the prediction of such behaviour. This includes evaluation of both sub-critical crack growth by fatigue mechanisms under fluctuating loads, and unstable crack growth by fracture under overloads. The field has developed largely during the past three decades, and the techniques have for some time been used routinely in the aerospace and nuclear industries, and more recently in the offshore industry.

Defect assessment methods, based on fracture mechanics, enable the significance of defects to be evaluated for both fatigue and fracture, taking into account the conditions under which the defective structure operates. Results of such assessments allow decisions regarding the significance of known or postulated defects and any need for remedial action, to be determined on a fitness for purpose basis.

Fracture mechanics based defect assessment methods may be applied to offshore structures in several situations including:

- At the design stage, for assisting designers in making decisions regarding various design aspects, with the aim of reducing the potential for occurrence of fatigue and fracture failures including determining whether post weld heat treatment (PWHT) is required; and for the rationalisation and optimisation of inspection operations during both fabrication and operation.
- During the construction stage, for assessing the significance of fabrication defects.
- During the operation of the structure, for assessing the significance of defects, found by in-service inspection.

The effective use of fracture mechanics results in cost savings, while also offering increased safety. This is achieved by optimising material selection, fabrication and inspection procedures, leading to a reduced probability of in-service failure.

To achieve these objectives the designer must take a number of considerations into account. These include the number and distribution of defects which may occur in the structure, the properties of the various steels considered in the project, the effect of various fabrication procedures on the foregoing and the behaviour of different types of structures. Additionally, the designer must be acquainted with the cost and effectiveness of different inspection procedures.

The logical end product of the application of fracture mechanics to a structure is the fracture control plan. The principal items which must be considered in its development are discussed in Section 1.2, while the remainder of Section 1 is dedicated to outlining the basic principles of fracture mechanics based fatigue and fracture assessments and introducing the key parameters used in such assessments.

1.2 Concepts of Fracture Mechanics Design

1.2.1 Comparison of fatigue design methods

The processes undergone during the life of a structure which fails by fatigue may be divided broadly into three stages, namely crack initiation, crack growth and final failure. In traditional S-N fatigue design methods no distinction is made between the three stages; crack initiation and subsequent growth are treated as a single process, and member failure has an arbitrary definition such as the appearance of a through-thickness crack.

The database for traditional S-N curve fatigue design methods has been derived from numerous fatigue tests performed on standard test specimens and on plate and tubular joints, the tests being carried out under specified conditions relating to parameters which include: geometry, loading, material properties and environment. A major disadvantage is that it is difficult to extend the test data to conditions other than those under which the tests were performed. For example, specimens are tested in the nominally uncracked, ie. defect-free, condition. Consequently, the resulting S-N curves are applicable only to the assessment of defect-free structures.

While, the S-N approach is very convenient for use in design and is relatively much simpler than the fracture mechanics approach, the simplicity of the former is often achieved at the expense of its accuracy and range of applicability. For example, the S-N fatigue life of a tubular joint is related to only the cyclic stress range at the hot spot location excluding the local notch stresses, and without explicit consideration of the effects of stress distribution at adjacent locations around the intersection or through the wall thickness. Such simplifications are bound to introduce some scatter into the data and may lead to reduced accuracy and/or necessitate increased conservatism.

Fracture mechanics enable the effects of parameters which influence the fatigue life, such as component geometry, stress distribution and environmental conditions, to be considered explicitly and assessed individually. As a result, conditions other than those covered by the test data, including the effects of postulated or known defects, may be appraised simply by specifying the relevant input parameters in the fracture mechanics model. Only the parameters under consideration need to be defined based on analytical or experimental data. Thus, the fatigue life under the new conditions may be estimated without having to perform a full fatigue test.

The design of a structure using the fracture mechanics approach involves the selection of portions of the structure requiring closer examination, and then the quantification of the behaviour of defects at these locations. It is assumed a priori that defects exist. The size of the defect is determined mainly by the inspection method used, or it may be related to inherent defects such as those associated with natural weld toe flaws.

Once the initial crack size has been assumed, the next part of the analysis is concerned with calculating the growth of the crack until failure occurs. In this context failure is defined as the onset of unstable crack extension, at which point the affected member will normally cease to act structurally.

The main parameters which determine the onset of fracture are the crack size, the stresses surrounding the crack location and the material toughness. The prediction of failure relies on the techniques of elastic-plastic fracture mechanics (EPFM), although, in some cases linear elastic fracture mechanics (LEFM) may be used.

1.2.2 The fracture control plan

The formal embodiment of the various procedures which are taken to prevent fracture is the fracture control plan. It is considered beyond the scope of this guide to give a detailed account of fracture control plans; examples of some early plans are given by Rolfe and Barsom. However, a brief description of the underlying principles will be given below.

The major advantage in formulating a fracture control plan is that the various measures for fracture control are considered in relation to one another to arrive at the most economic solution for achieving a given level of safety.

Traditionally, a fracture control is achieved by the following methods:

1. Limit design stresses

2. Minimise stress concentrations

3. Use materials of good notch toughness

4. Inspect for cracks.

These measures may be considered independently from one another, but fracture control may be optimised if, in addition, the interaction between the measures is taken into account.

In formulating a fracture control plan, consideration must be given to a number of different aspects, including the following:

(a) Design premise
Definition of postulated initial defect size, environmental conditions, temperature, loads, design life and all other factors affecting fracture.

(b) Design and analysis
Formulation of overall design philosophy to prevent fracture, performing the subsequent detailed design and supporting analyses.

(c) Materials and fabrication
Selection of materials and fabrication procedures to meet toughness requirements, as dictated by the reference defect size and design stress levels.

(d) Inspection
Specification of inspection procedures and intervals to meet the requirements of the other elements of the fracture control plan.

Considering the design stage in greater detail, the fundamental decision to be made concerns design philosophy. The basic choice lies between the adoption of a 'safe-life' or 'fail-safe' approach to structural integrity. For non-redundant structures the former must be used, and is in fact generally adopted for all offshore structures. For redundant structures there is the alternative option of designing the structure so that any failure is localised and may be repaired without the structure being placed at risk. It must be noted that if the 'safe-life' approach is used, in-service inspections form a vital link in the process of fracture control, and these must be performed with high reliability.

During the detailed design, fracture prevention principles must be applied in some degree to all parts of the structure, although effort will be concentrated on those portions of the structure which have greatest significance. Some of the principles by which the structure may be classified are described in Section 1.2.3. For a limited number of critical regions, detailed analyses should be performed to determine crack growth rates and critical crack sizes, thus defining inspection and material property requirements.

The fracture control plan is embodied in specifications covering construction and subsequent operation of the platform. Variations from these specifications should be referred to the designers concerned with the formulation of the fracture control plan.

1.2.3 Classification of types of structures

In the development of a fracture control plan it is necessary to classify each portion of the structure according to several basic criteria which will determine the subsequent approach to fracture prevention.

The first categorisation is to distinguish between members which are loaded primarily in tension and those loaded primarily in compression. The design of the latter will generally be governed by buckling, while fracture is more likely to be an important design parameter for tension members. The designer must then consider the redundancy of the structure. In this context the definition of non-redundant structures is extended

beyond the classical one to include those in which the failure of a single member due to fatigue and/or crack instability causes overloading of other members, leading to further failure. An important indicator of the severity of fatigue loading at a particular member is the ratio of the design fatigue life of the member to the actual required service life.

An additional factor which must be considered in the design methodology is 'inspectability'. In offshore structures certain members must be regarded as 'non-inspectable', being located at great depth or in areas where access is restricted or hazardous. Conversely, members in the air diving range and exposed members are classed as 'inspectable'. The ability to make periodic inspections is an important element in fracture control.

The concept of structure type classification, although inherent in the philosophy of fracture prevention, is not restricted to the fracture mechanics approach. Most current offshore design codes stipulate that when performing a fatigue analysis by S-N methods, the value of the Miner's damage summation factor D, should reflect the nature of the structure involved.

1.2.4 Materials selection and fabrication

The choice of grade of steel has a relatively minor influence on the rate of crack growth, but may influence parameters controlling fracture behaviour, and hence the size of crack which may be tolerated before instability occurs. Such parameters include the toughness and the level of matching between the parent metal and weldment. In general, overmatching which results in preferential straining in the parent metal, shielding the crack from high strains, may be more difficult to achieve in welded high strength steels.

The method of fabrication has a major bearing on all three stages of the fatigue life. For welded joints the welding introduces crack-like defects which, bypass the process of crack initiation. The presence of welding residual stresses increases the rate of crack growth, and together with the relatively poor toughness properties often associated with weldments reduce the critical crack size.

While welded joints often possess inferior mechanical properties, this does not in itself give rise to poor fatigue performance. Seam welds in rolled tubular members seldom fail by fatigue since, owing to the absence of stress raisers, the applied stresses are generally small, and the direction of the principal stress is parallel to the most commonly occurring crack-like defects in the weld. By contrast, welded tubular joints frequently suffer from fatigue problems since the weld is located in the most highly stressed region of the joint, with the plane of the weld normal to the principal stress direction.

From a fracture mechanics standpoint there are clear advantages in departing from traditional fabrication practice, using alternative methods such as cast steel joints, with the prospect of lower residual stresses, reduced incidence of crack-like defects and improved toughness in the critical region. Hybrid

forms of construction might also be considered, such as the use of cast steel inserts in the most highly stressed region of the joint, enabling the welds to be located away from the 'hot-spot'. Alternatively, techniques for improving the fatigue and/or fracture behaviour of welded joints may be considered. These include post weld heat treatment (PWHT), which reduces the level of residual stresses and could improve the toughness, and weld toe grinding which could eliminate inherent crack-like flaws and reduce local stress concentrations.

1.2.5 Inspection methods

Routine inspection is a vital element in fracture control. The choice of inspection method is determined largely by economic considerations taken into account during the development of the fracture control plan. The basis on which the efficiency of an inspection method must be judged is the smallest crack size which may be detected with a high degree of reliability.

The use of fracture mechanics techniques enables the size at which defects become significant to be determined, thereby dictating the required resolution of the inspection methods. Savings on in-service inspections may be made if a crack growth calculation is performed to determine the minimum inspection frequency required at each location. The economics of the inspection method need to be considered at this point; the use of a programme based on minimum inspection frequencies will require the use of a reliable and therefore more expensive inspection method. Nonetheless it is generally possible to make significant savings compared with a programme based on blanket inspections.

The method of inspection at the fabrication yard determines the initial defect size in the as-built structure, which has an important bearing on fatigue life. The potential economics of increasing the level of initial inspection in order to save on in-service inspection and maintenance should be considered.

Current in-service inspection methods for offshore structures are generally based on the philosophy that the structure can only tolerate small defects. Despite important recent developments, most inspection methods remain expensive, requiring extensive cleaning of the area to be inspected, while achieving variable reliability.

The economics of making the structure more defect tolerant, by use of improved materials and fabrication procedures and lower design stresses, must also be considered. The extra initial capital cost may be recovered many times over by reduced in-service inspection requirements.

1.3 Crack Driving Force Parameters

1.3.1 Stress intensity factors

If a crack-like defect exists in stressed material, the elastic stress field in the vicinity of the crack tip can be given by the following series representation of the stress tensor σ_{ij}:

$$\sigma_{ij} = \frac{K_I}{(2\pi r)^{1/2}} f_{ij}(\theta) + \text{higher order terms} \qquad 1.1$$

where r and θ are the polar coordinates of the point under consideration (see Figure 1.2), K_I is the stress intensity factor, and $f_{ij}(\theta)$ is a function of the polar angle θ.

The form of Equation 1.1 indicates that the parameter K_I, termed the 'stress intensity factor' (SIF), characterises the magnitude of the crack tip elastic stress field. The subscript I denotes the Mode I of crack tip displacement. Two other modes exist, Modes II and III. These modes, which are depicted in Figure 1.1 are known as:

Mode I : Opening mode
Mode II : Sliding or in-plane shear mode
Mode III : Tearing or antiplane shear mode

Equations expressed similarly to Equation 1.1 are available to describe the other modes of crack displacement.

Sufficiently close to the crack tip, ie. where r is much smaller than the crack length, the higher order terms in Equation 1.1 are negligible compared to the first term. The elastic solution predicts infinite stresses at the crack tip (r = 0) which cannot occur in practice since there is plastic flow in the highly stressed region near the tip. However, if the region of plastic flow is small compared to the region over which the $r^{1/2}$ term dominates the stress field, it may be assumed that the behaviour of the crack is determined by the elastic parameter K_I. This assumption forms the basis of Linear Elastic Fracture Mechanics (LEFM). Alternatively, if the extent of plastic deformation in the crack tip region is sufficiently large to invalidate LEFM, the behaviour of the crack may be analysed using Elastic Plastic Fracture Mechanics (EPFM). In this case, EPFM parameters such as the Crack Tip Opening Displacement (CTOD) or J integral are used.

In most structural components, the opening mode (Mode I) is of much greater importance than the other two modes which are rarely considered. Consequently, in referring to crack driving force parameters, the subscript I is often dropped, and unless otherwise stated, it is implicitly assumed that just Mode I is implied.

The significance of stress intensity factors may also be seen by consideration of the strain energy release rate, G, defined as:

$$G = -\frac{1}{B}\frac{dU}{da} \qquad 1.2$$

where dU is the change in the total energy associated with the crack advance, da, and B is the thickness of section containing the crack.

K and G are related by the following equation:

$$K^2 = E'G \qquad 1.3$$

where E′ is the effective elastic modulus, equal to E for plane stress conditions and $E/(1 - \nu^2)$ for plane strain conditions.

Thus K represents the force causing crack advance under static loading conditions. In brittle materials, the onset of unstable crack extension occurs under linear elastic conditions and may be characterised by the attainment of critical values of K and G. These are denoted, respectively, as K_c and G_c and are related using Equation 1.3. A lower bound value for K_c is obtained under plane strain conditions. It is thus known as the plane strain fracture toughness, K_{IC}, which is a material property that may be measured according to stringent codified procedures.

The stress intensity factor depends on the state of stress and the structural geometry (including the crack dimensions), and, in general is given by an equation of the form:

$$K_I = Y\sigma\sqrt{\pi a} \qquad 1.4$$

where Y is a compliance factor depending on a number of parameters including the geometry, crack size and type of loading, σ is the tensile stress normal to the crack faces, and a is the crack characteristic dimension (see Figure 1.2).

Values of Y for idealised geometries may be found in handbooks of stress intensity factors (Tada et al 1973, Rooke and Cartwright 1974, Murakami 1986). Simple two-dimensional examples, shown in Figure 1.2, are the centre-cracked infinite plate (Y = 1.0) and the edge-cracked semi-infinite plate (Y = 1.12).

Of great importance are elliptical and semi-elliptical cracks, which may often be used to approximate actual crack geometries, such as the surface crack shown in Figure 1.3. The starting point for stress intensity factor expressions of this type is

the solution of an elliptical flaw in an infinite solid:

$$K_I = \frac{\sigma\sqrt{\pi a}}{Q}\left[\sin^2\theta + \frac{a^2}{c^2}\cos^2\theta\right]^{1/4} \qquad 1.5$$

where a, c and θ are defined in Figure 1.3 and Q is a function of the crack shape.

It can be seen from Equation 1.5 that the SIF varies with the angular position, θ, and that it attains a maximum value at the minor axis ($\theta = 90°$).

Equation 1.5 may be extended to cover the more useful case of a surface crack in a plate of finite thickness. A number of solutions for this case have been reviewed by Scott and Thorpe (1981) and others, and are discussed in Section 6.2.

1.3.2 The crack opening displacement

The relative movement of the faces of a crack is termed the Crack Opening Displacement (COD). Yielding at the crack tip, gives rise to a physical displacement of the crack surfaces at the tip. This is known as the Crack Tip Opening Displacement (CTOD). In the early 1960's, the CTOD was proposed as a parameter for characterising the crack tip region under elastic plastic conditions. It was argued that the plastic strain in the vicinity of the crack tip region controls the fracture process, and that the CTOD (also denoted as δ) is a measure of this plastic strain. Crack extension will then begin at some critical value of the CTOD: δ_c.

Using the Strip Yield Model, the following expression for the CTOD was derived:

$$\delta = \frac{8\sigma_y a}{\pi E}\,\mathrm{Ln}\left[\sec\frac{\pi\sigma}{2\sigma_y}\right] \qquad 1.6$$

where σ and σ_y are the applied remote stress and yield stress, respectively, and a is the crack length.

Under LEFM conditions, Equation 1.6 can be simplified and related to K_I as follows:

$$\delta = \frac{\pi\sigma^2 a}{E\sigma_y} = \frac{K_I^2}{E\sigma_y} \qquad 1.7$$

which shows that the CTOD (or COD) concept is compatible with

LEFM as identified by the stress intensity factor approach.

It should be noted that Equation 1.7 is obtained by considering only the first term of a series expansion of the (Ln sec) part of Equation 1.6, and is only valid under LEFM conditions, ie. for $\sigma/\sigma_y << 1$.

1.3.3 J integral

The J integral concept is based on an energy balance approach. It was proposed on the basis of linear elastic or non-linear elastic material behaviour. The use of J integral for general elastic-plastic applications has been shown to be valid if the loading is monotonic and no unloading takes place within the solid containing the crack. Therefore, in principle, J is applicable at the onset of crack advance, but its use during crack extension when considerable local unloading can take place is debatable. The general form of J in two-dimensional problems is given by:

$$J = \int_{\Gamma} \left(W\,dy - T\,\frac{du}{dx}\,ds \right) \qquad 1.8$$

where Γ is a contour surrounding the crack tip, W is the strain energy density, T is a traction vector acting on a part of Γ, u is a displacement vector, and ds is an element of arc along Γ (see Figure 1.4).

The value of J has been shown to be independent of the path chosen, thus the integral can be evaluated using contours remote from the crack tip.

Similarly to G, the elastic strain energy release rate (Equation 1.2), J can be considered as an elastic-plastic energy release rate per unit crack advance:

$$J = -\frac{1}{B}\,\frac{dU}{da} \qquad 1.9$$

where dU is the total energy released due to elastic and plastic deformation.

For linear elastic material behaviour, J reduces to G, and the relationships between J, G and K, based on Equation 1.3, are:

$$J = G = \frac{K^2}{E'} \qquad 1.10$$

where E′ is the effective elastic modulus.

Thus the J integral concept is compatible with LEFM. Furthermore, because J may be considered as an elastic-plastic energy release rate it is to be expected that there is a critical value, J_c, which corresponds to the onset of crack extension. This is an analogy with G_c and K_c in LEFM.

Application of J integral to elastic-plastic fracture stems from the solutions derived by Hutchinson (1968), Rice and Rosengren (1968). These solutions give the stresses and strains in the vicinity of the crack tip under yielding conditions:

$$\sigma_{ij} = \sigma_o \left[\frac{EJ}{\sigma_o^2 I_n r}\right]^{\frac{1}{n+1}} f_{ij}(\theta,n)$$

$$\epsilon_{ij} = \epsilon_o \left[\frac{EJ}{\sigma_o^2 I_n r}\right]^{\frac{n}{n+1}} g_{ij}(\theta,n) \qquad 1.11$$

where r and θ are the polar coordinates (see Figure 1.2); f_{ij} and g_{ij} are known dimensionless functions of θ and the hardening exponent n; I_n is a constant dependent on n; ϵ_o, σ_o and n are the yield strain, yield stress and hardening exponent, respectively, in a pure power stress-strain representation.

The form of Equation 1.11 indicates that J plays the same role in elastic-plastic fracture as does K in LEFM.

1.4 Principles of Fatigue Assessment

Under fluctuating loads, the fatigue crack growth rate, da/dN, is governed by the variation in crack tip stress intensity, ΔK, during the load cycle. This was first noted by Paris et al (1961), who proposed a power law relation of the form:

$$\frac{da}{dN} = C\ \Delta K^m \qquad 1.12$$

where da/dN is the increment in crack size during a load cycle, C,m are crack growth constants which depend on a number of factors including the material, environment and loading conditions, and ΔK is the cyclic stress intensity range defined as:

$$\Delta K = K_{max} - K_{min} \qquad 1.13$$

where K_{max} and K_{min} are the maximum and minimum stress intensity factors, respectively, in each cycle.

Using Equation 1.4, ΔK may be expressed in terms of the compliance factor Y and the cyclic stress range $\Delta\sigma$ as:

$$\Delta K = Y \Delta\sigma \sqrt{\pi a} \qquad 1.14$$

By substituting Equation 1.14 into Equation 1.12, the fatigue life N, spent in propagating an initial crack a_i to the critical crack size a_f, at a constant stress range, can be expressed as:

$$N = \frac{1}{C \pi^{m/2} \Delta\sigma^{m/2}} \int_{ai}^{af} \frac{da}{Y^m a^{m/2}} \qquad 1.15$$

The complex dependence of Y on the crack size, crack shape and joint geometry precludes an analytical approach and so N is normally computed by numerical integration.

If da/dN versus ΔK for an actual crack is plotted on a logarithmic scale, an approximately sigmoidal curve is obtained (Figure 1.5). Equation 1.12 which plots as a straight line, gives a good approximation for intermediate crack growth rates.

As K_{max} and ΔK approach the plane strain fracture toughness, K_{IC}, the crack growth rate accelerates due to the intervention of fracture processes. Hence the Paris Law underpredicts the growth rate at this range. Under operating conditions, tubular joints in offshore structures are not usually subjected to a significant number of high stress intensity ranges. Thus, from an engineering point of view, the high stress regime may not be important since most of the fatigue life is spent at intermediate and low stress intensity ranges.

For small values of ΔK, a threshold behaviour is observed. When ΔK falls below the threshold value, ΔK_{th}, no growth occurs. The existence of the threshold may be of great importance since one of the methods of guaranteeing the satisfactory performance of critical structural components is to ensure that ΔK is always less than ΔK_{th}. The value of ΔK_{th} depends on a number of factors including the mean stress, material microstructure and environment.

1.5 Behaviour of Flawed Structures under Static Loading

The behaviour of flawed structures under static tension loading is governed by two separate, though interrelated, processes:

- Crack extension (fracture)
- Plastic collapse (yielding)

In general, these two modes interact leading to three basic regimes in which crack extension occurs, namely the linear elastic behaviour, which governs brittle failure, and the elastic-plastic and tearing behaviour, associated with ductile failure.

In the linear elastic and elastic-plastic regimes failure is generally associated with the initiation of crack extension. The tearing regime is concerned with the stability of crack extension after initiation. Although widely used in the nuclear industry, the types of steels and service temperatures limit the applicability of tearing stability methods in the offshore industry. In addition, under storm environment loading, a cracked component in an offshore structure is likely to be subjected to a number of high stress cycles. If one of these causes initiation of crack extension, the subsequent cycles are likely to keep the crack advancing by ensuring that the fracture process resumes if it has not already led to complete failure. The interaction between tearing and fatigue may also lead to a similar outcome. Therefore, the criterion for failure by fracture is initiation of crack extension and the possibility of crack arrest is usually ignored, which is a conservative approach.

In the linear elastic regime, the crack driving force and the material resistance are characterised, respectively, by the stress intensity factor, K, and the plane strain fracture toughness, K_{IC}. However, modern offshore steels and weldments have generally good toughness properties, which, at moderate temperatures, preclude brittle fracture and render linear elastic analysis methods of secondary interest.

In the elastic-plastic regime, both the crack driving force and the material resistance may be characterised by the crack tip opening displacement, CTOD, or the J integral. The two parameters are somewhat interchangeable although the CTOD is much more widely used in the offshore industry. An important difference compared to the linear elastic regime is that the crack driving force is not proportional to the load, typically varying with the square of the load.

Some basic principles of assessment for initiation of crack extension under static loading, referred to hereafter as fracture assessment, are outlined below. In particular the concept of the failure assessment diagram approach is introduced.

1.6 Principles of Fracture Assessment using the FAD Approach

In its simplest form, a fracture mechanics based fracture assessment consists of comparing the severity of applied crack tip conditions, characterised by a crack driving force parameter (applied K, CTOD or J), with the material resistance to crack extension (critical value of K, CTOD or J). For a defect to be acceptable, the crack driving force must be less than the material resistance.

Several fracture mechanics based procedures for assessing the integrity of structures containing defects are available. Such procedures are based on the fitness for purpose approach, which consists of using rational analysis methods to show objectively that during the intended lifetime of a flawed structure, failure will not occur under foreseen loading and environmental conditions by any recognised mechanism.

Since the failure of a flawed structure is governed by crack extension and/or plastic collapse, a fundamental aspect of any assessment procedure is the manner in which the two failure mechanisms are considered. A simple approach may be based on treating each mechanism separately within the confines of a failure interaction curve. Such an approach is typified by the Failure Assessment Diagram (FAD) procedures of the CEGB R6 document (Milne et al 1986) and the BSI published document PD 6493: 1991.

The failure assessment diagram defines limits between safe and unsafe loading of flawed structures with regard to brittle fracture (represented on a vertical axis), plastic collapse (represented on a horizontal axis), and the intermediate ductile fracture regime (defined by the assessment curve). A known or postulated defect is assessed by evaluating a fracture parameter and a plastic collapse parameter and plotting the resulting coordinates as a point on the FAD. The defect is acceptable only if the point falls within the assessment curve. If the point lies outside the curve, the defect is deemed unacceptable because failure is possible ie. the curve defines safe loading regimes rather than best estimates of failure conditions. If the point lies on the curve, the input parameters are considered to correspond to a critical condition, eg. with regard to defect size and/or load level. For example, in order to estimate the tolerable flaw size corresponding to a severe loading condition, the procedure is repeated for a range of flaw sizes. The intersection of the resulting locus with the assessment curve indicates the minimum flaw size which would cause failure.

A typical FAD is shown in Figure 1.6. The fracture parameter, denoted as K_r or $\sqrt{\delta_r}$ and plotted on the vertical axis, is the ratio of the applied elastic crack driving force to the fracture toughness (obtained either by the K or CTOD approaches). Only the elastic component of the applied crack tip driving force is used in the calculation, since the effects of crack tip plasticity are allowed for by the shape of the failure assessment diagram reducing in height as the applied stress increases towards yield. Thus, the FAD approach allows an elastic-plastic assessment to be made using only elastic crack driving force values. The plastic collapse parameter, denoted as S_r or σ/f_y and plotted on the horizontal axis, is the ratio of the applied load to the plastic collapse load, ie. it characterises the proximity of the flawed structure to failure by yielding mechanisms. Failure on the vertical and horizontal axes, takes place when K_r (or $\sqrt{\delta_r}$) = 1 and S_r = 1, respectively. Interpolation between these two limiting regimes is provided by a function relating K_r (or $\sqrt{\delta_r}$) and S_r.

As an alternative to the FAD approach, the total crack driving force including plasticity effects, may be estimated using standard solutions or elastic-plastic finite element analyses, and compared with the appropriate material fracture toughness. However, additional checks must be made to safeguard against plastic collapse.

1.7 Parameters for Consideration

1.7.1 General

The input parameters required for performing fatigue and/or fracture assessment of defects, are associated with data on defect dimensions, applied stresses and material properties. To obtain meaningful results, input parameters which represent the defect under consideration as accurately as possible, should be used within the framework of appropriate theoretical and/or empirical models for fatigue and fracture assessment procedures.

Features of some basic input parameters are outlined below. Aspects of evaluation of these and other parameters are addressed in more detail later in this chapter.

1.7.2 Defect characterisation and dimensions

Defect characterisation refers to the procedure of determining idealised shapes and dimensions of defects in order to approximate their known or postulated profiles with simple geometrical shapes. Such characterisation enables fracture mechanics treatments to be applied and aims at maximising the severity of the idealised defects in order to ensure conservative assessments. In general, defects are represented by equivalent planar cracks. While such modelling is appropriate for fatigue cracks and lack of fusion or lack of penetration defects, it is very conservative for volumetric defects. Basic aspects of characterisation of planar defects may be outlined as follows:

Defect shape

The shapes of surface, embedded and through thickness defects are typically idealised using semi-elliptical, elliptical and rectangular profiles. Idealisation of a part thickness defect involves circumscribing the defect with a rectangle, then inscribing the rectangle by a semi-ellipse or an ellipse to represent a surface defect or an embedded defect, respectively. A through thickness defect needs only be circumscribed by a rectangle. If the applied stresses change along the front of a part-thickness defect, consideration should be given to the position of the deepest point(s) in the idealised defect with regard to location of the peak stress. If the latter coincides with the position of the deepest point(s), the most severe condition is usually obtained.

Defect orientation

In order to maximise the severity with regard to Mode I, the orientation of a defect or of the applied stress may be idealised according to two alternative approaches:

1. The applied stress is resolved according to the planes perpendicular and parallel to the defect, and only the stress component perpendicular to the plane of the defect is considered in the assessment.

2. The defect is resolved onto planes perpendicular to the principal stresses, and only the defect projection perpendicular to the maximum principal stress is considered in the assessment.

Defect interaction

The severity of a defect may increase in the presence of adjacent defects. Therefore, possible interaction must be accounted for when considering multiple defects. Criteria for interaction are normally based on linear elastic solutions for the stress intensity factor, and are given in simple rules in terms of the defect length and/or height. If interaction is deemed to occur, the defect dimensions should be revised. Then, further interaction of the resulting defect, corresponding to the revised dimensions, with adjacent defects should be checked. This iterative process should be repeated until interaction is considered not to occur.

1.7.3 Stresses

Models for through thickness stress distribution

The elastic stress field acting on the section containing a defect may be considered in three different ways depending on the level and purpose of the assessment being considered. In decreasing levels of conservatism, and in general, increasing complexity of analysis, the three stress models are:

- Maximum tensile stress
  This approach provides a very conservative model for fracture assessments. The stress considered is the maximum tensile stress, which is taken to be uniform across the thickness and equal to the sum of all stress components.

- Linearisation of stress distribution
  This is the most commonly used approach for fatigue and fracture assessments. The stress distribution in the vicinity of the flaw is split into membrane and bending components, denoted respectively, with the subscripts m and b. Components of both the primary and secondary stresses may be obtained by linearisation. Any linearised stress distribution would be acceptable provided that it is greater than or equal to the magnitude of the real distribution over the flaw.

- Actual stress distribution
  This most realistic and least conservative model may involve a mathematical curve fit representation of the stress distribution in the vicinity of the flaw.

Types of stresses for consideration

Stresses for consideration in the assessment of defects can be classified into three categories:

- Primary stresses:
  These are the stress components which contribute to plastic collapse, ie. fulfil the equilibrium conditions between internal and external forces and moments. They are normally split into membrane, σ_m, and bending, σ_b, components.

- Secondary stresses:
  These are self equilibrating over a cross section. Welding residual stresses and thermal stresses are normally included in this category. While these stresses do not contribute to plastic collapse, they may magnify the severity of local conditions at the crack tip, ie. intensify the crack driving force. Their magnitude may be influenced by heat treatment and the loading history of the structure. Secondary stresses may be split into membrane, Q_m, and bending, Q_b, components as for primary stresses.

- Notch stresses:
  These may be due to local stress concentrations at structural discontinuities such as sharp corners or weld toes. In tubular joints, they are normally associated with the local stress magnification at the weld toe. This results in a sharp increase in stresses in the vicinity of the surface down to approximately 20% of the depth through the plate thickness. The effects of the weld notch stresses on stress intensity factors is usually quantified using the parameter Mk (see Section 6.3).

1.7.4 Material properties

Data on the fatigue, fracture and tensile properties for the part of the component under consideration are required to characterise the material resistance in fatigue and fracture assessments.

Key material properties, in relation to fatigue, are the crack propagation data which include the constants C and m of the Paris Law, and the threshold stress intensity factor range, ΔK_{th}. Alternative crack propagation laws, which are modified versions of the Paris Law, may require additional data (see Appendix D).

Fracture assessments require data on the fracture toughness and tensile properties, to characterise the material resistance to fracture and plastic collapse, respectively.

Fracture toughness data may be in the form of K_{IC}, δ_c (or CTOD), or J_c. When no toughness data are available and only Charpy data exist, empirical correlations may be used to infer estimates of the fracture toughness from Charpy values.

Tensile properties consist of the yield or 0.2% proof strength, tensile strength, and the modulus of elasticity. In certain cases, eg. fracture assessments of high strain hardening materials, a complete stress-strain curve may be required.

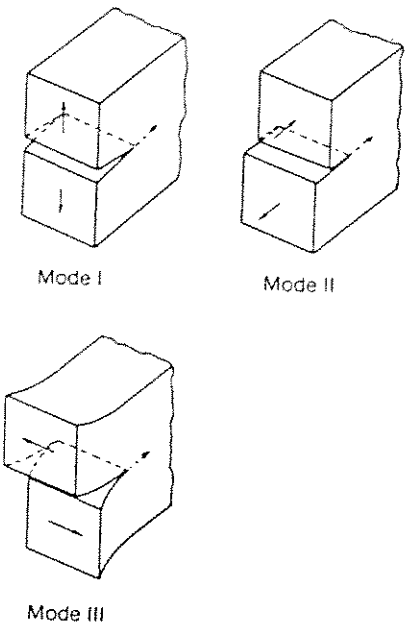

Figure 1.1 Crack opening nodes

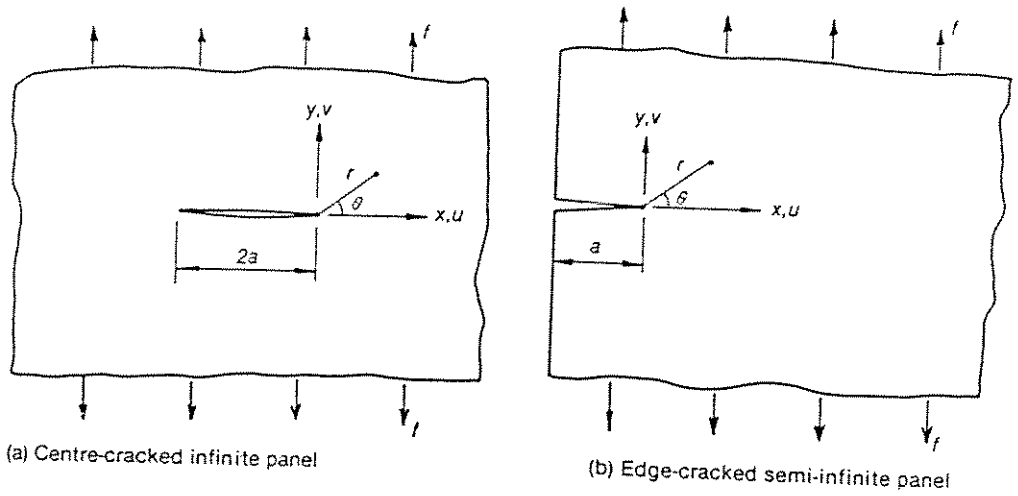

Figure 1.2 Typical two-dimensional crack problems

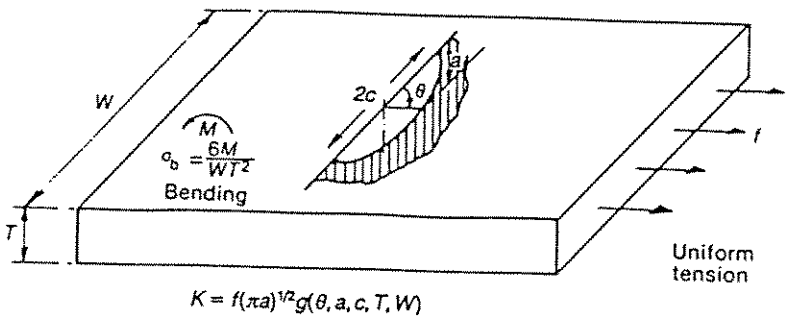

Figure 1.3 Semi-elliptic crack in a finite plate

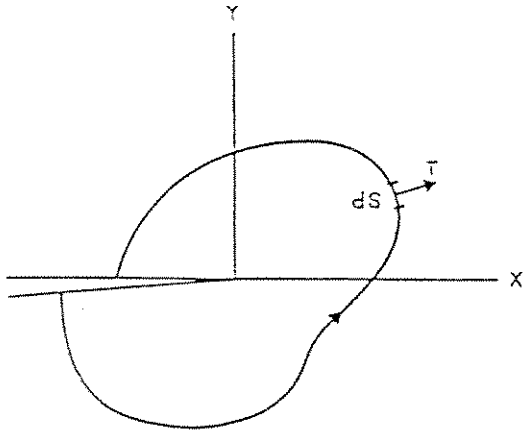

Figure 1.4 Parameters associated with J-integral

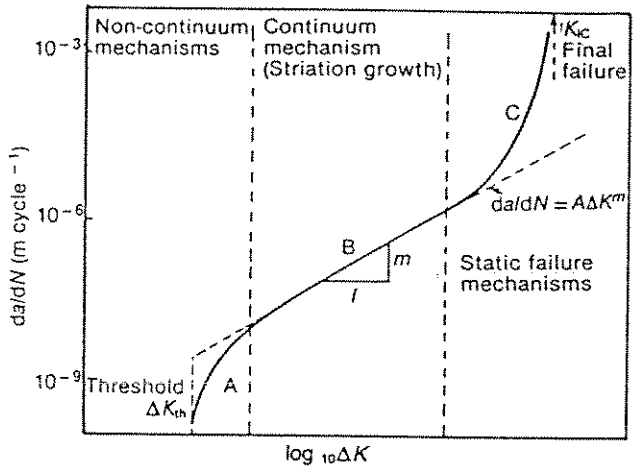

Figure 1.5 Schematic da/dN versus ΔK plot

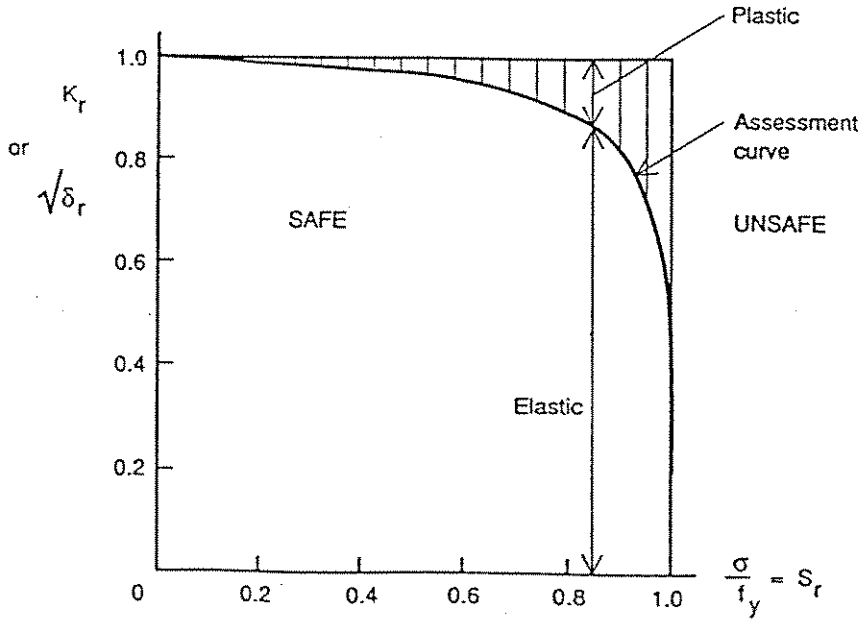

Figure 1.6 A typical failure assessment diagram

2. DATA ON CRACK DEVELOPMENT IN TUBULAR JOINTS

A considerable number of welded joints have been tested to determine their fatigue life. During some of these tests measurements were made of the fatigue crack length and depth as a function of the number of cycles. Such measurements have enabled some understanding of the mechanics of crack growth to be deduced and used for several applications including:

- Derivation of simple models which allow lowerbound estimates of the residual fatigue life to be inferred from data on surface crack length and/or crack depth (eg. Tweed and Freeman, 1987).
- Formulation and validation of fracture mechanics models for fatigue crack growth intended to match and/or predict safe estimates of crack growth data (eg. Hsu, 1990).

This section reports some data relevant to the above two applications with the aim of providing a basis for discussions in the following sections on modelling fatigue crack growth.

Although some aspects of the mechanics of fatigue crack growth have been noted to depend on joint type, joint loading or test environment, the following three distinct phases of crack growth have been observed in all valid tubular joint fatigue tests:

i) crack initiation and coalescence

ii) crack propagation

iii) joint failure.

Initiation occurs at inherent weld toe defects such as undercuts which develop into small embryo cracks. While the welding process has a major influence on the occurrence and distribution of initial weld toe defects, the number of cracks initiated from these defects has been found to increase with increasing stress range and plate thickness (Vosikovsky et al, 1985). Crack initiation sites are grouped around the 'hot spot' for joints loaded in bending, while under axial loading they are more widely spaced, reflecting the lower stress gradient around the weld toe (ASME 1980).

Observations of the fatigue fracture surface complemented by beachmarking studies and/or potential drop measurements show that the initiated embryo cracks grow independently in a roughly semi-elliptical shape before joining up to form larger cracks. This process, known as crack coalescence, may be repeated a number of times, until a single dominant crack is formed (Burns et al, 1987). Figure 2.1 shows a schematic model for crack growth and coalescence in plate welded joints (Bell and Vosikovsky, 1992).

Fatigue crack shape may be expressed in terms of the aspect ratio (crack depth/crack half length) or a/c. Crack shape development is often characterised by plotting the aspect ratio versus the relative crack depth (crack depth/plate thickness) or a/T.

Coalescence resulting in the formation of a single dominant crack is often associated with a sharp drop in the aspect ratio. Data reported by Topp and Dover (1986) suggest that the resulting a/c is around 0.05. Data on shape development of the dominant cracks in large scale T joints (chord diameter $\geq$457mm) tested in air as part of UKOSRP I, have been analysed by Clayton (1982) and are reproduced in Figure 2.2. This shows the aspect ratio to rise slowly as the crack grows to a value between 0.061 and 0.341. This range corresponds to two standard deviations around the mean which is 0.144 and appears to remain constant throughout most of the fatigue life. However, the Alternating Current Potential Drop (ACPD) technique used to measure the crack depth in the UKOSRP I tests was then in its infancy and thus some doubts remain about the quality of the data.

Tweed (1987) discusses crack depth information and crack shape development data from two recent fatigue programmes where the information is expected to be of better quality than the earlier UKOSRP I data:

- UKOSRP II (crack depth measured by hand held ACPD probes)
- UCL/SERC, UCL/DEn (crack depth measured using fixed ACPD probes).

Since the UKOSRP II programme is largely based on investigating the effect of geometrical loading, heat treatment and environmental factors on the fatigue of a specific T joint geometry, Tweed analyses the data in comparison with a reference case specified by the following conditions:

- D = 914mm, β (= d/D) = 0.5
- T = 32mm, τ (=t/T) = 0.5
- γ (= D/2T) = 14
- α (=2L/D) = 5.3
- Θ (chord/brace angle) = 90°
- Axial loading
- Constant amplitude loading
- Minimum load/maximum load ratio (R) = 0
- Air environment
- As-welded condition.

Detailed data on relative crack length and depth (2L/T and a/T respectively) versus endurance normalised with respect to the endurance for through thickness cracking (N/N_3) are presented and compared with the reference case. In addition data on crack shape development (a/c vs. a/T) are contrasted with the corresponding data from the reference case. Only the latter information are considered in this section. Table 2.1 provides a summary of the parameters considered and comments on the crack development data.

These, reproduced in Figures 2.3a-c and 2.4a-j allow the following observations to be made:

- For the reference conditions crack depth tends initially to increase slowly (see Figure 2.3b) so that by 50% of N_3 the crack depth is around 20% of the chord thickness or less. After about $0.6N_3$ crack depth increases roughly linearly to through-thickness cracking.

  Crack shape development data for this reference case (see Figure 2.3c) shows a broad band of aspect ratios between about 0.1 and 0.2 for depths greater than about 0.35t. Early crack growth is reported to have given near-linear cracks ($a/c \sim 0$) and so the early trend is towards increasing aspect ratio. This is similar to the trends reported earlier in connection with the UKOSRP I data (see Figure 2.2). While both sets of data indicate a mean a/c of about 0.15, the scatter band associated with the reference case is narrower. This is not surprising since the latter refers to three identical joints tested under similar conditions except for the stress range. The broader scatter band of UKOSRP I is associated with in excess of 40 tests involving axial, IPB and OPB loading.

- The UKOSRP II results on crack shape development in seawater with cathodic protection appear to suggest deeper cracks (higher a/c) than those derived in air environment for a/T 0.6. However, the corresponding UCL results in seawater with cathodic protection seem to fall well within the air environment data. While Tweed suggests that this apparent anomaly may be due to the crack measurements procedure adopted in the UKOSRP II tests, more recent data reported by Tubby et al (1994) support the UKOSRP II results. The new data, introduced in Figure 2.5, are obtained from constant and variable amplitude IPB tests on large scale joints (D = 914mm, T = 32mm). Significant differences in crack shape development in air and seawater with CP are reported. While multiple cracking along the weld toe led to very low aspect ratios during early growth in air, in seawater a single crack tended to dominate throughout the life, with its aspect ratio varying from 0.2 at small depth to about 0.1 on breaking through the chord wall.

  Tubby et al (1994) attribute this difference in behaviour to the higher fatigue crack growth threshold value observed in seawater with CP. Berge et al (1994) who report what appear to be the same data with more measurements of a/c during early crack growth ($a/T < 0.2$) note that suppression of crack initiation due to CP may be responsible for the effect of seawater with CP on crack shape development (see Figure 2.6). Similar arguments are put forward by Lambert (1992), based on a series of tests on pipe-plate and plate-plate specimens. These tests, aimed at illustrating the influence of seawater environment on crack shape development, show that seawater with CP has a beneficial effect on initiation behaviour in comparison with air. This is attributed to the formation of calcareous deposits on the surface which tend to plug nascent cracks, thus reducing the cyclic stress range and increasing the threshold to initiation, especially at low applied stress levels. However, seawater with free corrosion is reported to lead to more rapid and uniform initiation, leading to the formation of a long shallow crack early in the fatigue life.

Particular(s) investigated	Reference case	Joint size	Joint geometry and loading	Joint geometry and loading	Joint geometry and loading	Light stiffening	Heavy stiffening	Variable amplitude loading	Environment seawater + CP	Environment seawater + CP	PWHT
Number of joints	3	4	4	1	4	3	3	4	4	2	4
Number of dominant cracks	3	5	4	1	7	5	6	7	4	2	6
Joint type	T	T	Y	K (Gap)	K (Lap)	T	T	T	T	T	T
Joint loading	Axial	Axial	IPB	IPB	Bal. Ax	Axial	Axial	Axial	Axial	Axial	Axial
Chord D * chord T (mm)	914*32	182*76	457*16	457*16	457*16	914*16	914*16	914*32	914*32	457*19	914*32
As-welded/PWHT (AW/PWHT)	AW	AW	AW, PWHT	AW	AW	AW	AW	AW	AW	PWHT	PWHT
Constant/variable amplitude	CA	CA	VA	CA	CA	CA	CA	VA	CA	CA	CA
Minimum load/maximum load (R)	o	-1	+ve	-1	0	0	0	-1	0	0.3	-1
Environment	Air	Air	Air	Air	Air	Air	Air	Air	Seawater	Seawater	Air
Project	UKOSRP II	UKOSRP II	UCL/SERC	UCL/SERC	UKOSRP II	UKOSRP II	UKOSRP II	UKOSRP II	UKOSRP II	UCL/DEn	UKOSRP II
Data on crack aspect ratio (a/c) versus scatter band data on a/c from the reference case (RC)	Figures 2.3a-c	Scatter within and above RC for a/T<0.25, and within RC thereafter	Lower than RC across the a/T range	Very close to lower bound of RC. Higher than RC for a/T<0.35 and lower thereafter	Widely scattered especially at a/T<0.35	Mostly within RC but stiffness failure caused a/c below RC	Widely scattered but stiffener cracking may have led to a/c below RC for a/T>0.5	Mostly around the lower bound of RC	Higher than RC for a/T<0.6 and around upper bound thereafter	Within RC	Within RC but nearer to lower bound
Figure 2.4		a	b	c	d	e	f	g	h	i	j

Table 2.1
Data on crack shape development (Tweed, 1987)

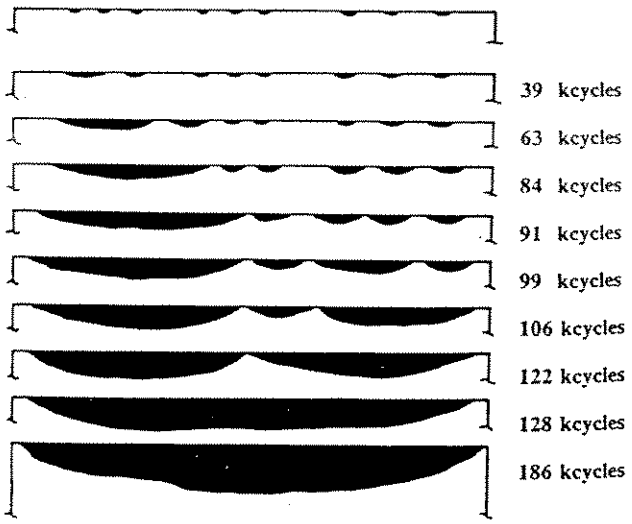

Figure 2.1 A schematic of a typical initial array of cracks and the progression of growth and coalescence of cracks (Bell and Vosikovsky 1992)

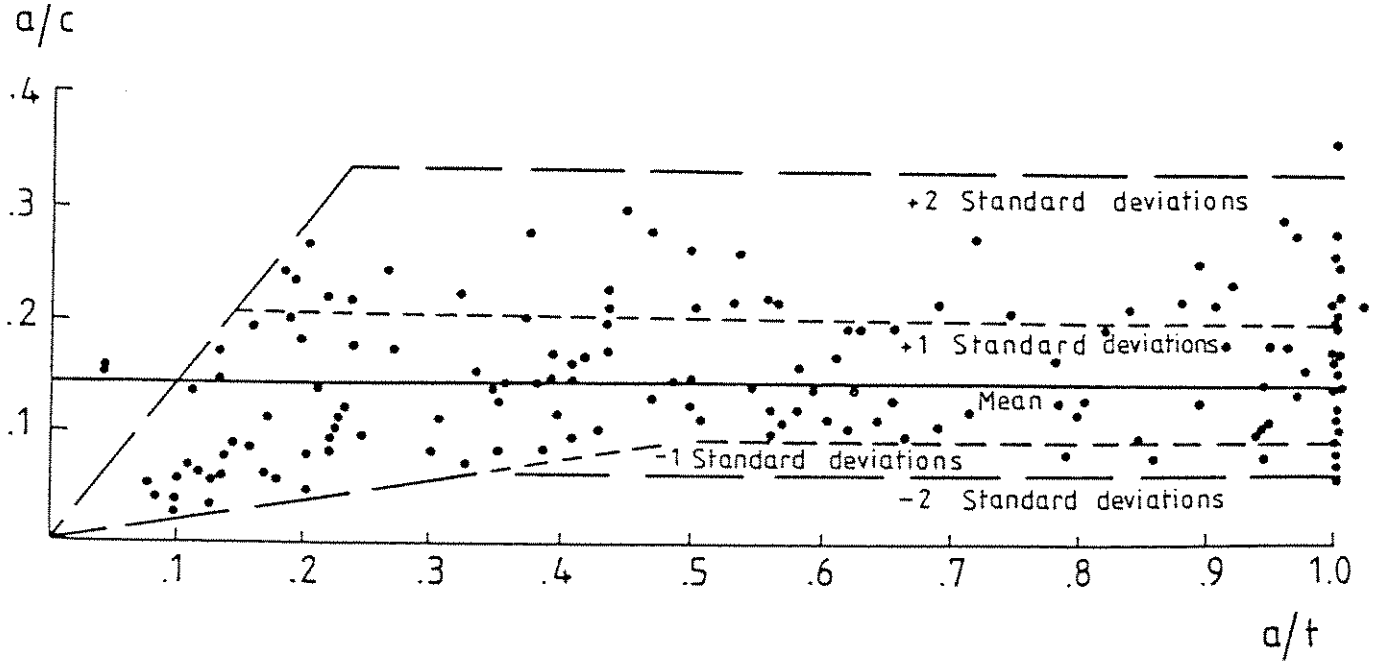

Figure 2.2 Crack aspect ratio vs crack depth for tubular T connections (Clayton 1982)

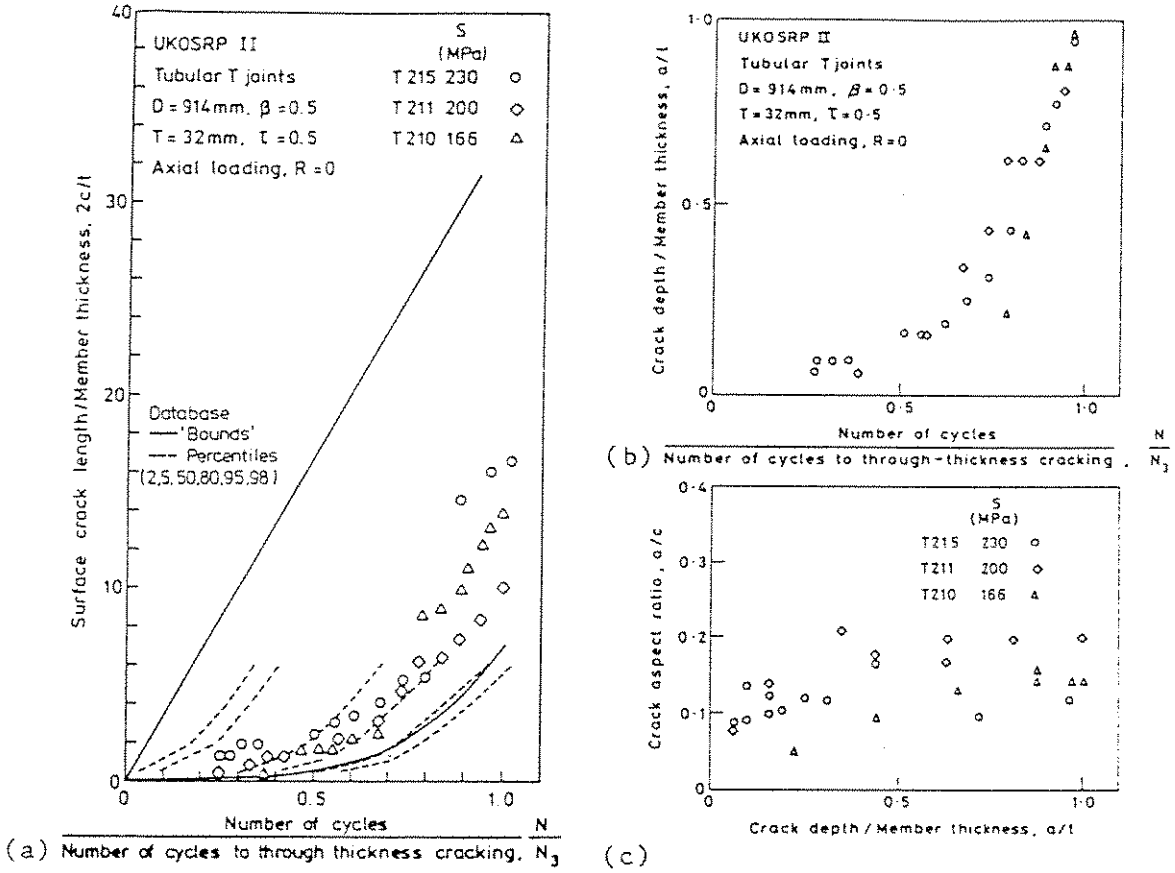

Figure 2.3a-c Crack growth data for the reference condition (D=914mm, T=32mm, β= 0.5, τ=0.5, axial loading, R=0)

a) Normalised surface crack length vs normalised endurance
b) Normalised crack depth vs normalised endurance
c) Crack aspect vs normalised crack depth
(Tweed 1987)

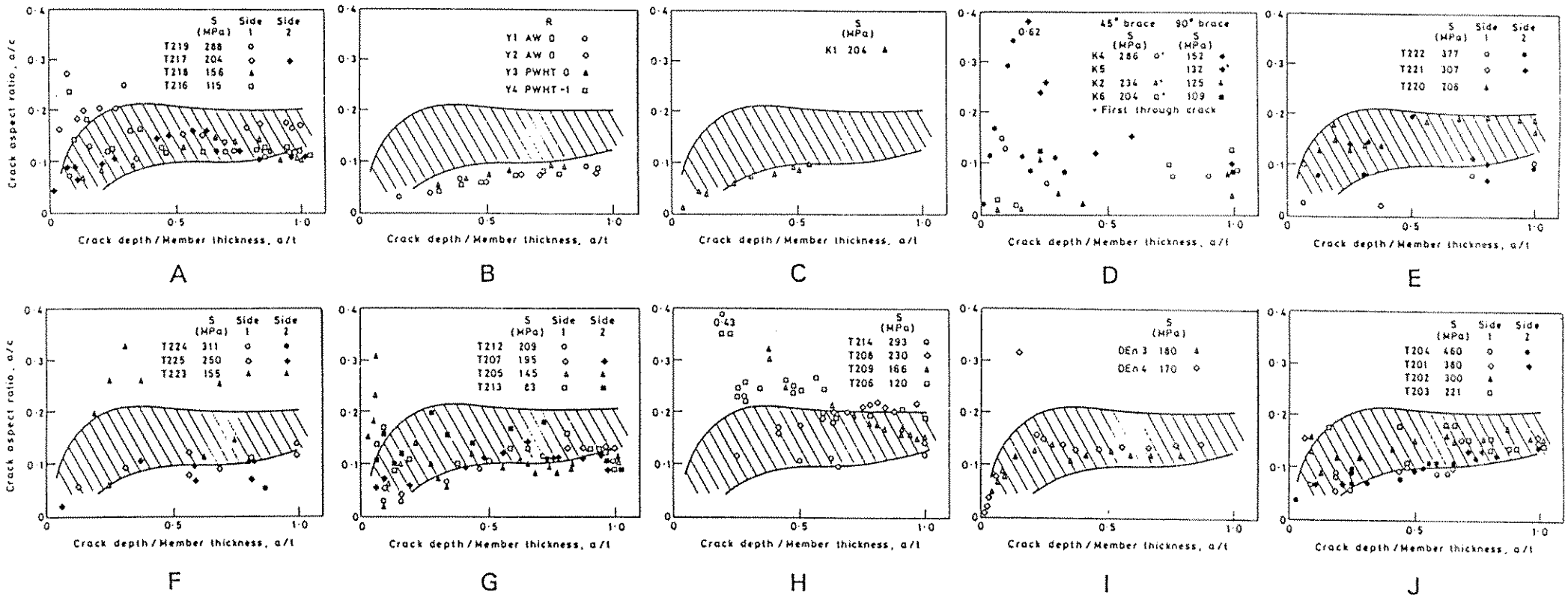

Figure 2.4a-j Crack growth data (See Table 2.1) (Tweed 1987)

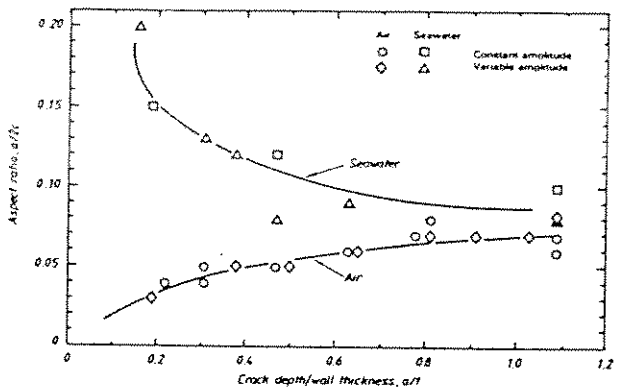

Figure 2.5 Variation of aspect ratio with crack depth (Tubby et al 1994)

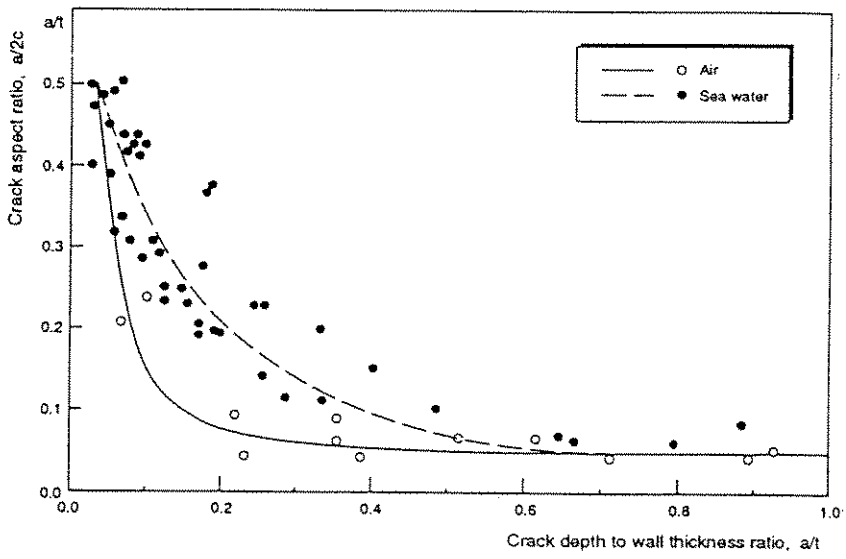

Figure 2.6 Aspect ratio development of fatigue crack in tubular joint in air and in sea water with cathodic protection (Berge et al 1994)

3. DATA ON STATIC STRENGTH OF CRACKED TUBULAR JOINTS

3.1 Introduction

Whilst the static strength of intact tubular joints has been relatively well researched, very limited attention has been given to the static strength assessment of cracked joints.

The shortage of relevant data has led to a number of recent investigations which have addressed aspects relating to plastic collapse and/or fracture behaviour of cracked tubular joints. The resulting data are mainly used for validation and/or formulation of models for assessing the behaviour of flawed joints under static overload conditions, ie. models for fracture assessments. Most of the data are obtained from laboratory tests, and in some cases from both experimental and numerical investigations.

All known experimental data are considered in this section with the exception of test results where information on 'important' parameters were not reported or measured. The importance of such parameters is assessed on the basis of the potential use of the data. For example, where plastic collapse is the governing failure mode, yielding properties are considered more important than fracture toughness properties. However, the latter properties become critical when fracture is the dominant failure mode and fracture rather than plastic collapse data are sought. In all cases, data on initial crack dimensions, prior to testing, are considered essential. Fortunately, in most recent programmes, all relevant parameters have been recorded though not necessarily reported in the published literature.

Numerical data are covered in various investigations, most of these are part of the MTD/SERC Defect Assessment Programme and have been surveyed by Cheaitani (1994). Only the main conclusions are reported here in the relevant sections.

3.2 Failure Modes of Cracked Tubular Joints

Cracked tubular joints may fail by any of the modes identified in connection with uncracked tubular joints exhibiting load deformation characteristics which may be similar to those of uncracked joints. However, loads which induce tension along the crack front (eg. brace tension or IPB in a direction that causes crack opening) may lead to onset of crack extension. This may initiate a brittle or a ductile fracture failure which precedes other conventional failure modes (eg. plastic collapse or yielding failure associated with uncracked joints) or interacts with them.

Modern offshore steels and weldments are relatively tough. Consequently, the failure of cracked joints at moderate temperatures is likely to be ductile.

3.3 Failure Criteria of Cracked Tubular Joints

The behaviour of a cracked tubular joint under static tension loading is governed by crack extension (fracture) and/or plastic collapse (yielding). In general, these two processes interact leading to three basic regimes in which crack extension may occur, namely the linear elastic regime, which governs brittle failure, and the elastic-plastic and tearing regimes, associated with ductile failure.

In the linear elastic and elastic-plastic regimes failure is generally associated with the initiation of crack extension. The tearing regime is concerned with the stability of crack extension after initiation. As discussed in Section 1.5, the applicability of tearing stability methods to offshore structures is limited due to the prevalent loading, environmental and material aspects.

If crack extension is preceded or governed by plastic collapse failure, several failure criteria may be considered including:

- Local collapse
- Global collapse
- Deformation limit

Local collapse applies only to part-thickness cracks and refers to local failure of the uncracked ligament adjacent to the crack front. Global collapse takes place when the deformations become unbounded and the whole structure becomes a mechanism. It is thus compatible with conventional yielding failure modes of uncracked joints, especially the ultimate load criterion. The distinction between local and global collapse arises only in joints containing part-thickness cracks. For through thickness cracks, global collapse is the only relevant plastic failure criterion. In general local collapse occurs at lower load levels than global collapse and if the difference between the corresponding failure loads is large, the implications with regard to the FAD approach may be significant.

Alternatively, failure may be associated with postulated deformation limits, such as those of Yura (1980), which are expressed in terms of brace displacement and rotation for axial and bending loading, respectively. Another limit may be defined as corresponding to the load at which the load-deformation curve is intersected by a line from the origin with slope equivalent to twice the compliance of the initial elastic loading (ASME 1986 and Miller 1987).

3.4 Methods for Estimating the Plastic Collapse Load of Cracked Structures

The following is a brief outline of the most commonly used methods for estimating the plastic collapse load (yielding capacity) of structures containing defects. Such estimates are primarily required to provide input for evaluation of the plastic collapse parameters, S_r and L_r, for use in FAD type fracture assessments. Analytical methods, such as limit load and finite element methods normally exclude crack extension and its effects. Laboratory tests, eg. on steel specimens, can reflect to some extent both crack extension and plastic collapse effects on the ultimate capacity. However, specimen scale in general and the absolute crack size in particular have significant effects on the interaction between the fracture and plastic collapse failure modes in a laboratory test.

Limit load analysis and approximate methods

An accurate assessment of the plastic collapse load of a flawed structure would take into account material strain hardening, large strain and large deformation effects, in a model which represents accurately the geometry of the structure, especially the region surrounding the flaw. Commonly, however, most conventional limit load analysis methods neglect these effects or adopt approximate approaches to take some of them into account.

Since complete solutions are often hard to calculate, lower and upper bounds to the limit load of a structure may be obtained by using the lower bound and upper bound theorems respectively. Usually a conservative estimate of the limit load is required, and a lower bound estimate is appropriate, eg. to use as denominator in the plastic collapse parameters S_r or L_r.

In deriving lower or upper bound solutions, elastic-perfectly plastic material behaviour is assumed. Work hardening is taken into account approximately by replacing the yield stress by the flow stress.

A list of available limit load analysis solutions for common structural geometries is given by Miller (1987). Most of the solutions given are effectively two dimensional, being derived from plane strain, plane stress or thin shell assumptions. When it is unclear whether plane strain or plane stress solutions are applicable, the plane stress solution is preferable, since it provides a more conservative estimate.

Finite element analysis

This numerical technique offers exceptional facilities for the analysis of cracked joints which include:

- Evaluations of LEFM and EPFM crack driving force parameters. These allow fracture assessments to be carried out and CEGB/R6:Option 3 or PD6493:Level 3 failure assessment diagrams to be constructed.

- Calculation of the plastic collapse load of cracked joints. The crack is assumed to remain stable throughout the analysis, thus the resulting failure load is due purely to plastic collapse. In model or large scale laboratory tests, it may be difficult to prevent crack extension from affecting the failure of the cracked section. As a result, additional care needs to be exercised when inferring plastic collapse loads from test results.

Model and Full Scale Tests

An accurate estimate of the plastic collapse load of a flawed structure can probably be obtained from a large or full scale test, in which the geometry and loading are simulated with reasonable accuracy. This technique may be the most accurate but its practical implementation can be very difficult or prohibitively expensive. Instead, a small scale model of the flawed structure can be tested taking care that the geometry is scaled accurately. However, this may be difficult in the case of welds in tubular joints.

One advantage of testing small scale models is that the absolute size of the crack is scaled down, the crack driving force in the small scale model, is therefore less severe than the crack driving force in the equivalent full scale model at comparable load levels. As a result, fracture is less likely to intervene and plastic collapse is more likely to take place.

A disadvantage of testing small scale models can be inferred from the previous argument. Because fracture behaviour depends on the absolute size of the crack, unlike plastic yielding behaviour, the fracture behaviour of a small scale model does not represent the fracture behaviour of the corresponding full scale model. Care is therefore required for interpreting small scale experimental results and for drawing conclusions relevant to full scale behaviour.

Multiple axis loading

Plastic collapse load solutions are usually given for unidirectional loads. For example, solutions for plates may be given for pure tension and for pure bending, but it may be desirable to estimate the collapse load of a plate under combined tension and bending.

Miller (1987) showed that a conservative estimate of the collapse load under combined loading can be obtained by using the 'convexity lemma'.

For example, if the limiting value of the stress resultants in a plate under pure tension, and pure bending are given by $|N| \leq N_o$ and $|M| \leq M_o$, respectively, then a lower bound to the limit load under combined tension and bending is given by:

$$(|N| / N_o) + (|M| / M_o) \leq 1 \qquad 3.1$$

In the case of tubular joints, solutions are usually given for unidirectional brace loads. The following relationship has been shown to account for brace load interaction effects in uncracked joints (API RP2A 1993):

$$|P_a/P_c| + (M_{ai}/M_{ci})^2 + |M_{ao}/M_{co}| \leq 1 \qquad 3.2$$

where P_a and P_c are the applied and ultimate axial loads, M_{ai} and M_{ci} are the applied and ultimate in-plane bending moments, and M_{ao} and M_{co} are the applied and ultimate out-of plane bending moments.

Applying the same equation to the case of a cracked tubular joint, with (P_c, M_{ci} and M_{co}) corresponding to plastic collapse and adjusted to take account of the crack, would give a combined plastic collapse ratio, S_r. This approach, however, is yet to be verified.

4. STRESSES IN TUBULAR JOINTS

Unlike the traditional S-N approach where only the stress range magnitude (excluding notch stresses) on the outer surface is considered, fracture mechanics calculations require detailed information on the actual stress distribution acting in the anticipated crack region. In general, knowledge of the detailed stress distribution through the wall thickness and around the intersection of tubular joints is of primary importance for the evaluation of crack driving force parameters and the production of meaningful results.

4.1 Applied Stress Distribution

The required stress distribution in uncracked tubular joints may be quantified using the following parameters:

- Stress Concentration Factor (SCF)
- Degree Of Bending (DOB)
- Notch stress

The SCF refers to the outer surface global (or geometric) stress concentration obtained by extrapolating stresses to the weld toe from a region where the decay in stress is approximately linear. Thus, the local notch stresses, dependent on the weld geometry, are excluded. Various aspects of determination of the SCF parameter are dealt with in detail in Chapter 4.

Notch stresses due to the weld geometry are usually quantified using the Mk parameter. This is the ratio of SIF, for a crack, including notch stresses to SIF, for the same crack, without notch stresses. Sections 5 and 6 which deals with methods for determining stress intensity factors provide a detailed review of aspects of determining Mk.

The remainder of this section is dedicated to the Degree Of Bending parameter (DOB) which describes the stress distribution through the thickness.

Degree Of Bending (DOB)

The Degree Of Bending (DOB) describes the proportion of the through thickness stress which is due to bending. It is defined as follows:

$$DOB = \Omega = \frac{\sigma_b}{\sigma_{total}} = \frac{\sigma_b}{\sigma_m + \sigma_b} \qquad 4.1$$

where σ_b is the pure bending stress, σ_m is the membrane stress, and σ_{total} is the total outer surface stress.

σ_{total} may also be denoted as σ_{outer} in order to contrast it with the total inner surface stress, σ_{inner}. In this case, σ_b and σ_m may

be expressed in terms of σ_{outer} and σ_{inner} as follows:

$$\sigma_b = \frac{\sigma_{outer} - \sigma_{inner}}{2} \qquad 4.2$$

$$\sigma_m = \frac{\sigma_{outer} + \sigma_{inner}}{2} \qquad 4.3$$

By combining Equations 4.2 and 4.3 and normalising the inner and outer stresses by the nominal stress in the brace, the DOB can be expressed as:

$$DOB = \Omega = \frac{SCF_{outer} - SCF_{inner}}{2\ SCF_{outer}} \qquad 4.4$$

where SCF_{outer} is the conventional SCF and SCF_{inner} is the corresponding parameter on the inner surface.

It should be noted that DOB does not account for the weld notch stresses. The outer surface stress and SCF parameters used in defining the DOB are all global (geometric) stresses which are normally obtained by extrapolating stresses to the weld toe from a region where the decay in stress is approximately linear. The inner surface stress required to quantify the DOB is not affected by the notch stresses, but it should be measured at positions which correspond to those considered on the outer surface. Therefore the DOB and SCF parameters are fully compatible in that they both represent the global (geometric) stresses and exclude the weld notch stresses.

There are relatively far fewer data on DOB in tubular joints than on SCFs. The most significant work on DOB is that undertaken at UCL by Connolly and co-workers as a part of the MTD/SERC Defect Assessment Programme (Connolly et al 1990). This study involved a series of nearly 900 finite element analyses of a wide range of T and Y joint geometries under axial, IPB and OPB loading. The following geometric parameters were considered:

$$6.21 \leq \alpha \leq 13.1$$
$$0.20 \leq \beta \leq 0.80$$
$$7.60 \leq \gamma \leq 32.0$$
$$0.20 \leq \tau \leq 1.00$$
$$35° \leq \theta \leq 90°$$

Although α was limited to a maximum of 13.1, Connolly et al note that the DOB is weakly dependent on α, so that increasing α (ie. increasing the chord length) will produce little or no change in the results.

The analyses were performed with the program PAFEC using semi-loof thin shell finite element models. The principal stresses at the inner and outer tube surfaces were used to determine the relative amounts of bending and membrane stresses. The numerically greatest principal stress on the outer wall was always chosen but selection of the corresponding stress on the inner surface is reported to have been more problematic due to rotation of the principal stresses especially for the 35° and 45° Y joints. Although not stated by the authors it is believed that the stresses at the brace/chord intersection were used rather than the values corresponding to the imaginary weld toe position.

The results of the analyses were curve fitted into parametric equations for the DOB on both the brace and chord sides of the intersections. These give the DOB at the saddle and hot spot positions in the cases of axial loading or out-of-plane bending, and at the crown and hot spot positions for in-plane-bending. The equations are reproduced in Appendix A.

A limited comparison of DOB results obtained using three different meshes was performed on an axially loaded T joint with the following parameters: α = 8.67, β = 0.67, γ = 15.0 and τ = 0.8. Two of the meshes consisted of thin and thick shell elements, respectively, while the third was constructed using a combination of three-dimensional solid elements (in the weld region) and thin shell elements. The results indicate that while there is little difference between the thin and thick shell element predictions, the DOB solutions obtained using the solid-shell element combination are consistently lower than the values from the shell element analyses (Table 4.1). Although this conclusion may be seen to cast some doubt over the data, limited data generated by other investigators appear to agree reasonably with predictions based on the above equations (Bowness and Lee 1993, GMTC 1992).

Other work on DOB has been performed at UMIST by Chan and Manteghi on T joints and large gap K joints. The results, reported by Burdekin el al (1986), are given for both the saddle and crown positions in the case of axial loading. Data for out-of-plane and in-plane bending are also given.

More recently, Thurlbeck, working at UMIST within the MTD/SERC Defect Assessment Programme, performed a limited FE study with the aim of providing models to calculate DOB at any location around the brace/chord intersection of a tubular joint and under any brace loading, including combinations of axial, IPB and OPB.

To achieve the above objectives which include establishing principles for superposition of DOB values, in a similar manner to the treatment of SCF and hot-spot stress ranges, finite element stress analyses were carried out on a series of tubular T joints with β ratios of 0.3, 0.5, and 0.8. The analyses, performed using mainly thin shell elements, enabled investigation of the circumferential DOB due to axial, IPB and OPB loads, applied separately and in combination. The DOB was defined using the absolute maximum principal stress on both the outer and inner surfaces.

By observing the basic distributions of the DOB around the circumference, functions were developed which permit the interpolation of DOB between hot-spot positions. These functions enable the DOB value to be calculated at any angular location around the intersection for axial, in-plane, and out-of-plane loading. They are arranged such that they may be programmed without developing the infinite values which may occur when the outer surface stress approaches zero (eg. at the crown position of OPB loaded joints). The equations have been recently published together with additional background information by Cheaitani et al (1995) and are reproduced in Appendix A.

With regard to combining DOB values due to single loading modes in order to produce DOB estimates for multiple axis loading, Thurlbeck found that a simple addition of the chord outer stresses from the simple loadcases produced accurate estimates for the combined loadcase. But, this was not the case for stresses on the chord inner surface. Such a result is not surprising since the addition of stresses involves principal stresses with orientations differing between the outer and inner surfaces. On the chord outer surface, under the influence of brace stiffness, the principal stresses are orientated in approximately the same direction as the direct stresses and so addition is possible. However, on the chord inner surface this effect does not apply and the stresses are not orientated with the direct stresses. This does not occur on the brace side of the connection where, under the influence of the intersection with the chord, the maximum principal stresses are orientated on both the outer and inner surfaces in such a way that simple addition is possible.

In order to overcome the apparent problem of combining chord stresses on the inner surface, Thurlbeck proposed a simple model to estimate these from the values at the saddle or crown positions, by assuming that the principal stresses were orientated with the direct stresses as radial stresses. The correction involves redefining the inner surface stress by calculating them from the outer surface stress and the DOB. Thus, the inner surface stresses are defined as:

$$\sigma(\phi)_{AX(inner)} = \sigma(\phi)_{AX(outer)} \left[1 - 2\,\Omega(\phi)_{AX}\right] \qquad 4.5a$$

$$\sigma(\phi)_{IPB(inner)} = \sigma(0°)_{IPB(outer)} \left[1 - 2\,\Omega(0°)_{IPB}\right] \cos\phi \qquad 4.5b$$

$$\sigma(\phi)_{OPB(inner)} = \sigma(90°)_{OPB(outer)} \left[1 - 2\,\Omega(90°)_{OPB}\right] \sin^2\phi \qquad 4.5c$$

where the subscripts inner and outer denote the inner and outer surfaces, respectively; ϕ is the angular location around the brace/chord intersection; $\Omega(0°)$ is the DOB at ϕ = 0°, corresponding to the crown position; and $\Omega(90°)$ is the DOB at ϕ = 90°, corresponding to the saddle position.

A similar arrangement was proposed for the opposite side positions at 180° for IPB and 270° for OPB loading.

The combined outer surface stress at any position, ϕ, around the joint on either the brace or chord side of the connection is given by:

$$\sigma(\phi)_{outer} = \sigma(\phi)_{AX(outer)} + \sigma(\phi)_{IPB(outer)} + \sigma(\phi)_{OPB(outer)} \qquad 4.6a$$

where each stress component is the outer surface stress component due to the applied loads at any position ϕ around the brace intersection circumference, and the inner surface value of stress is calculated from:

$$\sigma(\phi)_{inner} = \sigma(\phi)_{AX(inner)} + \sigma(\phi)_{IPB(inner)} + \sigma(\phi)_{OPB(inner)} \qquad 4.6b$$

where the individual inner surface stress "components" are calculated from the redefined equations 4.5a-4.5c at the position ϕ around the intersection circumference for the chord side of the connection or from:

$$\sigma(\phi)_{inner} = \sigma(\phi)_{(AX,IPB,OPB)outer} \left[1 - 2\Omega(\phi)_{(AX,IPB,OPB)}\right] \qquad 4.7$$

in the case of the brace side. The combined DOB at any position ϕ around the circumference is then simply calculated from:

$$\Omega(\phi) = \frac{\sigma(\phi)_{outer} - \sigma(\phi)_{inner}}{2\,\sigma(\phi)_{outer}} \qquad 4.8$$

- Work on DOB at UMIST by Chan and Manteghi on T joints and large gap K joints. Data at both the crown and saddle positions were produced.
- Work on DOB at UMIST by Thurlbeck on T joints subjected to simple axial, OPB and IPB loads, applied separately and in combination. Equations for circumferential variations of DOB around the circumference were proposed.
- Work on DOB at British Gas by Haswell on complex tubular joints.

4.2 Residual Stresses

The term 'residual stresses' may be used to refer to the following two different types of stresses:

i) Welding residual stresses: These are local stresses which are locked in the zone adjacent to the weld line. They are due to the combined effects of the thermal history (heating followed by cooling) of material in the weld region, and the restraint offered by the adjacent joint components.

ii) Long-range stresses (also referred to as fit-up or locked-in stresses): In contrast with the above type of residual stresses, long-range stresses may be considered on a global member level rather than in relation to the local weld toe region. Within the context of steel offshore structures, they are associated mainly with weld shrinkage which can generate net forces in the adjacent welded member. Their magnitude depends on a number of parameters including the relative stiffness of members, the heat input, size of root gap, member length and the fabrication sequence.

Both types of stresses can have important effects on the fatigue and fracture behaviour of welded joints. However, due to the lack of data on long-range stresses, these are not usually accounted for in routine defect assessment and will not be considered further in this section. Rather, attention will be restricted to welding residual stresses which, for simplicity, are referred to hereafter as residual stresses.

Although self equilibrating across the thickness, residual stresses can have a detrimental effect on the structural integrity of welded joints. This is due to the tensile residual stresses which can be of up to yield magnitude. The interaction of these with applied stresses results in more severe crack tip conditions than under the influence of applied stresses alone, and consequently can promote failure by fatigue and fracture.

With reference to the local direction of welding, components of residual stresses are classified as either transverse or longitudinal. These are, respectively, normal and parallel to the local direction of welding. Cracks which develop along the weld toe will therefore be subjected to the transverse stresses which act in the Mode I opening direction. For such cracks, longitudinal stresses are less important and will not be considered further in this section.

There are relatively limited data on the distribution and magnitude of residual stresses in welded joints. Data relating to tubular T and Y joints, pipe-to-plate joints, and T-butt/fillet joints, have been reported by a number of researchers including Goff et al (1985 and 1987). Based on these references and a recent review by Stacey (1993), the following general observations can be made:

- In the vicinity of the weld toe, transverse tensile stresses of up to yield magnitude can occur. However, as the depth increases, these stresses fall sharply and may

become compressive near the mid-thickness region before increasing and becoming tensile near the inner surface.

- In tubular joints (simple T and Y configurations), the magnitude and distribution of residual stresses do not appear to vary significantly along the weld toe between the saddle and crown positions. In addition, the distribution of transverse residual stresses is similar to that found in T-butt/fillet joints.

- With regard to effects on defect assessment, the lack of comprehensive data on residual stress distributions necessitates conservative assumptions which can lead to very conservative defect assessments and uncertainties with regard to interpretation of the results.

Typical transverse residual stress distributions in tubular joints and in T-butt/fillet joints are shown in Figures 4.1a and 4.1b. In addition, estimates of such distributions based on a model recommended in PD 6493:1991 are shown alongside the experimental and analytical data.

The PD 6493 model is intended to allow the extent of the tensile component of transverse residual stresses in T-butt/fillet joints to be estimated conservatively, as a function of the heat input of the adjacent weld run and yield strength. The resulting stress distribution can then be converted into membrane and bending components enabling the corresponding stress intensity factor to be quantified using parametric equations such as those of Raju and Newman (Figure 4.2). However, such equations are intended for idealised pure membrane and bending stress distributions. Consequently , they are inappropriate for quantifying stress intensity factors for alternative nonlinear residual stress distributions. The latter require the use of numerical or weight functions methods. Stress intensity factor solutions for typical residual stress distributions can have been reported by Stacey (1993).

Redistribution of residual stresses as a result of interaction with applied stresses is covered in Section 8.

Values of α and β for axial and bending loading				
Loading Mode	L/T	a/T	α	β
Axial	≤ 2	$\leq 0.05(L/T)^{0.55}$ $>0.05(L/T)^{0.55}$	$0.51(L/T)^{0.27}$ 0.83	-0.31 $-0.15(L/T)^{0.46}$
	> 2	≤ 0.073 >0.073	0.615 0.83	-0.31 -0.20
Bending	≤ 1	$\leq 0.03(L/T)^{0.55}$ $>0.03(L/T)^{0.55}$	$0.45(L/T)^{0.21}$ 0.68	-0.31 $-0.19(L/T)^{0.21}$
	> 1	≤ 0.03 >0.03	0.45 0.68	-0.31 -0.19

Table 4.1
Mk Solutions PD 6493:1991

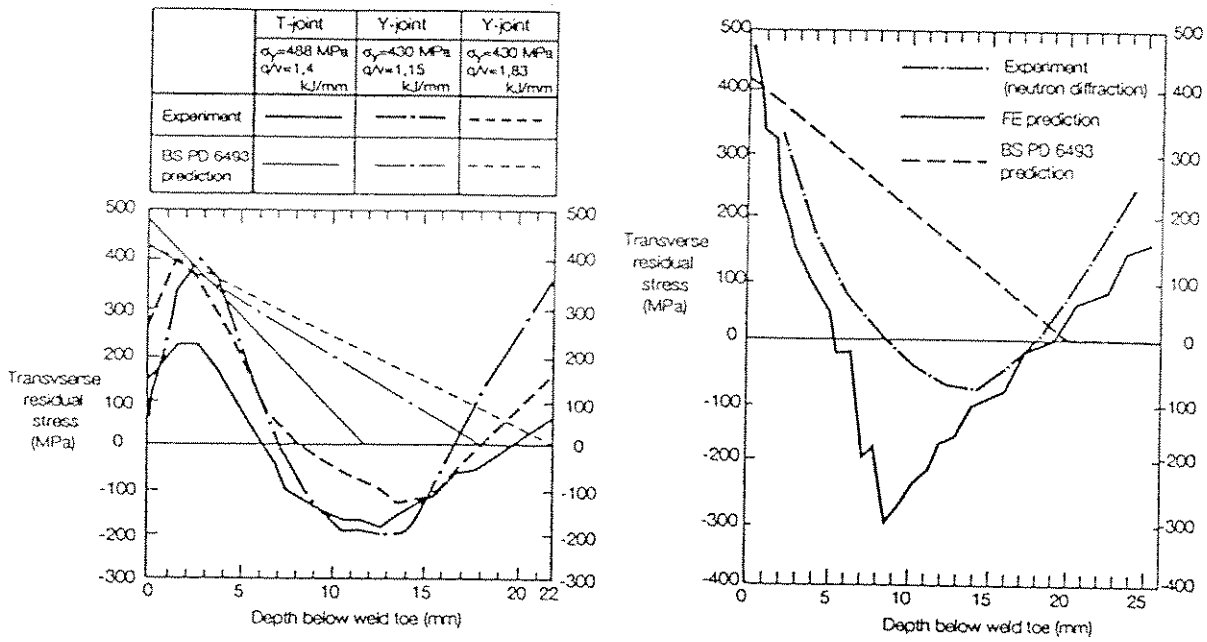

Figure 4.1 Residual stress distribution in: a) nodal joints, b) T-butt/fillet joints (Stacey 1993)

(a) Variation through-thickness of base plate of transverse residual stresses at toe of fillet or T-butt weld	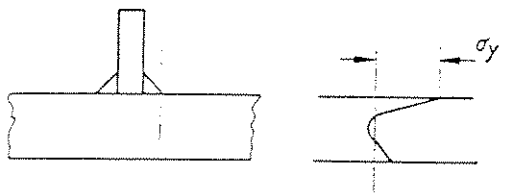
(b) Idealized distribution of transverse residual stresses at toe of fillet or T-butt weld	For carbon manganese steel $y = \left(\frac{122}{\sigma_y}\frac{q}{v}\right)^{0.5}$ where q/v is the heat input of the weld run adjacent to flaw (in J/mm), y (in mm), σ_y (in N mm^{-2}) and $y < B$. If $y > B$, assume residual stress σ_y throughout thickness. Then for $a < y$ $Q_m = \sigma_y [1 - (B/2y)]$ $Q_b = \sigma_y (B/2y)$ and for $a \geq y$ $Q_m = Q_b = 0$ 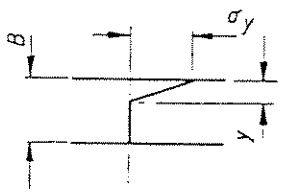

Figure 4.2 Typical distributions of residual stresses (PD 6493 : 1991)

5. METHODS FOR DETERMINING STRESS INTENSITY FACTORS

5.1 Introduction

The determination of stress intensity factors for defects located in tubular joints is a difficult task, owing to the complexities introduced by the three-dimensional structural geometry and the nature of the local stress fields. There is however a need for simplified expressions for stress intensity factors for cracks in tubular joints, similar to the parametric formulae for SCFs, to enable fracture mechanics to be used for the purpose of fatigue and fracture assessments.

While the three modes of crack displacements (opening, in-plane and anti-plane shear) characterised by the corresponding stress intensity factors, have been considered in some studies (eg. Rhee 1991, Du and Hancock 1989), to date the offshore tubular joint problem has been mostly dealt with in the context of pure Mode I behaviour. In the following the subscript I, denoting Mode I, is dropped and unless otherwise stated the symbol K is used to represent the Mode I stress intensity factor (ie. K_I). The methods which are generally used to calculate stress intensity factors are as follows:

1. Numerical methods, the most popular is the FE method.

2. Empirical methods, based on simple interpretations of experimental crack growth data.

3. Classical solutions of idealised simple geometries, corrected to represent tubular joints.

Of these approaches only numerical methods have the ability to account explicitly for all the governing parameters. In using the empirical or classical approach it is necessary to introduce simplifying assumptions which often affect the reliability of the resulting solutions and/or their range of applicability.

A basic technique which is common to a number of methods presented in this section relies on the principle of superposition. With this approach, shown schematically in Figure 5.1, the analysis is performed as a two-stage process:

- The stresses in the uncracked body, including the local stress distribution along the fictitious crack face, are determined initially.

- The stress intensity factor is then calculated by analysing the crack region for crack face loading obtained by reversing the local stress distribution from the analysis of the uncracked body.

The benefit of using such a technique is that the stress distribution acting on the plane of the crack need only be evaluated once for the uncracked body. Stress intensity factors for any crack along the plane can then be calculated without the need to evaluate the stresses in the whole body for every crack.

5.2 Classical Solutions

A number of stress intensity factor solutions are available for idealised crack geometries in essentially simple structural components under simple loading conditions. Such solutions are published in handbooks such as those of Tada et al (1973), Rooke and Cartwright (1974), and Murakami (1986). The experienced analyst is frequently able to modify the solution for an idealised cracked body in order to approximate the stress intensity factor for a crack in a body of a more complex geometry. This involves the application of correction factors to account for one or more of the features relating to the crack in the component under consideration.

As an example, for a surface crack in a welded cruciform joint, the correction factor Y may be expressed as:

$$Y = Y_E\, Y_S\, Y_W\, Y_G\, Y_K \qquad 5.1$$

where Y_E accounts for the crack shape, for part-thickness cracks, Y_S is the front free surface correction ($Y_s \leq 1.12$), Y_W is the finite width correction, Y_G corrects for non uniform applied stresses, and Y_K is the correction for the geometrical discontinuity caused by the presence of the adjacent weld.

Using existing published solutions, it is often possible to evaluate the correction factors individually. Solutions for cracks under the action of wedge opening forces are of particular value since these may be used to calculate the correction factor Y_G for arbitrary loading conditions (see Figure 5.2); this approach may be used with the superposition method, shown in Figure 5.1, and the weight function technique (Section 5.4) to extend the solutions to more complicated configurations, the method of compounding may be used (Smith, 1982). Examples of the derivation of stress intensity factors for particular cases from classical solutions have been reported by Gurney (1979) and Rooke (1981).

5.3 Empirical Methods

Dover and co-workers at UCL have proposed an experimentally based method for determination of stress intensity factors of cracks at tubular joints. If the expression for stress intensity factor range is written in the general form:

$$\Delta K = Y \Delta\sigma \sqrt{\pi a} \qquad 5.2$$

where Y is the correction factor for crack growth in the depth direction, $\Delta\sigma$ is the stress range at the hot spot, and a is the crack depth, and if it is assumed that the Paris' law governs the rate of crack growth (Equation 1.12) then the correction factor may be expressed as:

$$Y = \frac{\Delta K}{\Delta\sigma\sqrt{\pi a}} = \frac{(da/dN)^{1/m}}{C^{1/m}\,\Delta\sigma\sqrt{\pi a}} \qquad 5.3$$

Hence, if C and m are known for the particular material and environment under consideration, Y may be determined for a given tubular joint by conducting a fatigue test on that joint and measuring the quantities da/dN, $\Delta\sigma$ and a. Some values of Y for a number of tubular joints, as determined by this procedure, are plotted as a function of the non-dimensional crack depth, a/T, in Figure 5.3. These curves can be approximated by an expression of the form:

$$Y = A\left[\frac{T}{a}\right]^{j} \qquad 5.4$$

where A and j are constants which must be determined from crack growth measurements recorded in full scale tubular joints fatigue tests.

Experimentally determined values of A and j exhibit considerable scatter between joints, and it is suggested that these quantities should in fact depend primarily on the average value of the stress concentration factor, SCF_{av}, defined as:

$$SCF_{av} = \frac{1}{\pi}\int_{0}^{\pi} SCF(\phi)\,d\phi \qquad 5.5$$

for joints under axial or OPB loading, and as:

$$SCF_{av} = \frac{1}{\pi}\int_{-\frac{\pi}{2}}^{\frac{\pi}{2}} SCF(\phi)\,d\phi \qquad 5.6$$

for joints under IPB loading

where $SCF(\phi)$ is the stress concentration factor as a function of the angular position around the intersection, ϕ ($\phi = 0°$ at crown position).

Based on crack growth data from a limited number of tubular joint fatigue tests, Dover and Dharmavasan (1982) recommended the 'Average Stress' (AVS) model. In this Y is estimated using A and j values dependent on the chord thickness, T, and the non-dimensional factor, S, defined as:

$$S = SCF_{HS} / SCF_{av} \qquad 5.7$$

where SCF_{HS} is the maximum stress concentration factor at any location around the intersection.

Recognising that the average stress approach places too much emphasis on the stress distribution away from the hot spot stress site, and prompted by the need to produce an equivalent stress that can be used to correlate fatigue data from joints of different geometries, Dover and Connolly (1986) proposed a refinement to the parameter S. This consists of using an average stress weighted for the distance from the hot spot stress site (eg. with an exponential function), thus providing distinction between circumferential stress distributions associated with joints of different geometries.

In the light of new crack growth data for joints of different chord wall thicknesses, Kam et al (1989) proposed improving the AVS model by considering crack growth in two phases: The 'early crack growth' phase and the propagation phase. In the new model, known as the Two Phase Model (TPM), Y is expressed as follows:

$$Y = M.B. \left[\frac{T}{a} \right]^k \qquad 5.8$$

where, similarly to A and j of the AVS model, M, B and k are determined from crack growth measurements recorded in full scale tubular joints fatigue tests (see Section 6.4 where the new equations are reported in detail).

Although the AVS and TPM models incorporate implicitly all factors influencing fatigue behaviour of the tubular joints considered in their derivation, both models have significant limitations including:

- The stress intensity factor is assumed to depend on one dimension of the crack only, the depth, the crack length and the aspect ratio are not explicitly considered.

- Averaging of the stresses is performed over the complete stress field around the joint (ϕ = 0 to π). Greater accuracy would be obtainable if the averaging were performed over the current crack length, and if the variation of stress in the thickness direction were taken into account.

- The Y values are determined using data on crack growth rates inferred from assumed fatigue constants C and m. The scatter inherent in determining C and m, and the differences in constraint conditions which may exist between tubular joints and the specimens used to estimate C and m, are bound to affect the reliability of the computed Y values.

- The effects of errors in crack depth measurements are increased due to differentiating these data in order to determine Y (Equation 5.3)

- A large number of important parameters, such as joint, crack and weld geometries, and local primary and residual stress distributions through the thickness, are not accounted for explicitly. As a result, the Y models, derived from a limited set of test results, cannot be applied to other tubular joints where the parameters influencing fatigue strength may be different.

However, the extensive crack growth data and the associated Y functions can be useful for validating other approaches to estimate stress intensity factors such as the numerical approach.

5.4 Numerical Methods

Determining stress intensity factor solutions, directly or from J integral predictions, may be simplified significantly if the three-dimensional structural geometry of cracks in tubular joints is approximated using simpler structural models. For example, a two-dimensional planar model may be used to simulate the geometry and loading of a section across the deepest point of a semi-elliptical crack. Such a model may provide a reasonable estimate of the required solution especially if appropriate correction factors are applied to account for the effects of parameters not accommodated in the model.

However, in addition to simplified structural modelling, there are a large number of parameters which can influence the accuracy of numerical stress intensity factor solutions including:

- Local stress distribution in the vicinity of the crack. This may be affected by:
  - Global geometry of the structural component and restraint conditions.
  - Local geometry in the vicinity of the crack, eg. modelling of stress raisers such as the weld geometry and local weld toe profile.
  - Explicit modelling of the crack. This affects stress redistribution, eg. due to load shedding to the adjacent uncracked ligament.
  - Stress model, eg. relating to stress changes along the crack front and through the thickness.
- Crack geometry, eg. crack aspect ratio and orientation.
- Solution method, eg.
  - Direct approach involving explicit crack modelling, or indirect approach using stresses in the uncracked condition.

- Use of local solutions such as displacements or stresses near the crack tip, or global energy based solutions.

Some of the above and other aspects of numerical determination of stress intensity factors are outlined in the following sections.

It should be noted that there are no reference stress intensity factor solutions for cracks in tubular joints. However, NAFEMS, the National Agency for Finite Element Methods and Standards, has recommended a number of 2D benchmark linear elastic fracture mechanics problems for relatively small geometries (Pang and Leggatt 1992).

5.4.1 Direct methods

Direct methods are those in which the calculation of the stress intensity factor is performed in a single-stage analysis of a model involving explicit crack idealisation. At present the finite element method is the best established and most widely used method. Boundary integral equation methods, known as BEM, have not found extensive acceptance despite being valuable for certain cases. The main advantage of these methods is that two-dimensional problems can be effectively treated in one dimension and, similarly, three-dimensional problems can be reduced to two dimensions. Thus, significant savings in computing costs may be possible especially for analyses involving bulky structures where the ratio of surface to volume of the body under consideration is low. However, the availability of increasingly powerful computers at relatively affordable costs may have contributed, together with other technical issues, to the relatively low interest in boundary integral methods. As a result, the vast majority of methods for calculation of stress intensity factors using direct methods, rely on the FE method.

Direct methods for evaluating stress intensity factors can be broadly classified in two categories. The first includes methods using calculated displacements or stresses at nodes in the immediate vicinity of the crack tip, while the second encompasses energy based approaches to evaluate the elastic J integral (equal to the strain energy release rate G). The main features of these methods and some related applications are described below.

Methods using local crack tip displacements

In this approach, displacement predictions in the vicinity of the crack tip are substituted into Irwin's theoretical displacement equations (Barsom and Rolfe 1987, Ingraffea and Manu 1980). Nodes located on radial lines emanating from the crack tip at fixed values of the polar coordinate angle (θ) are considered. This allows values for K_I, K_{II}, and K_{III} to be inferred along the radial lines and subsequently extrapolated to the crack tip position. Similar calculations can be performed using stress predictions, but finer meshes or higher order elements may need to be used to achieve similar accuracy to that associated with displacement predictions.

Arguing that conventional procedures for computing stress intensity factors from the nodal displacements of three-dimensional quarter point elements (Ingraffea and Manu, 1980), is not applicable to problems involving curved crack fronts, Rhee and Salama (1987) developed a procedure to handle weld toe cracks with flat crack surface and curved crack front. More recently, Rhee (1989) developed a procedure applicable to cracks with both curved surface and curved front. This is intended mainly for weld toe surface cracks in tubular joints which often propagate following a curved path to result in doubly warped crack surfaces. Rhee argues that the new method has an important advantage over the conventional method by allowing the accuracy of the solutions at a single crack front point to be assessed using more than one set of results.

Energy based methods

As originally proposed this approach enables the strain energy release rate G to be evaluated from two analyses on two cracks with slightly different dimensions. Two values for the strain energy per unit thickness (U and U+dU) are computed corresponding , respectively, to two crack dimensions (a and a+da). G can be approximated as (-dU/da) and the stress intensity factor may be calculated using Equation 1.3. Applications of this method, known as the compliance technique, to tubular T joints containing through thickness cracks have been reported by Brown (1986).

A more efficient version of this approach, which requires one analysis only, has been proposed by Parks (1974). This method, known as the Virtual Crack Extension (VCE) technique, consists of perturbing nodes on and around the crack front numerically to simulate a postulated small increment in crack size. The resulting change in the strain energy is then computed enabling G to be evaluated without the need to perform a second separate analysis of the whole model. Cheaitani (1994) reported good agreement between J integral values (equal to G in the elastic range), predicted using both the original compliance and the VCE techniques.

One advantage of energy based methods is that they are based on domain integral rather than crack tip quantities. As a result, they can provide reasonably accurate solutions even if the crack tip is modelled with conventional elements in relatively coarse meshes.

However, solutions derived using the VCE technique depend on the direction of the virtual crack extension used to evaluate the correspondin genergy release rate. Consequently, implementation of the VCE technique can be problematic in the presence of mixed mode behaviour where the direction of crack extension is not known in advance, ie. it is a part of the solution. In practice the effects of the aforementioned problems depend on the mixed mode content of the problems and on the sensitivity of the solution to direction of crack extension, i.e on differences between Mode I and mixed mode solutions. Such differences have been recently shown to be very small in a typical simple T joint containing semi-elliptical cracks (Bowness and Lee 1994).

The parameter G or J, evaluated using energy based methods, enables an equivalent stress intensity factor, K_e, to be estimated. In general, K_e characterises the combined effect of Mode I, Mode II and Mode III. The contribution of each of these modes can be quantified approximately by assuming that the relative displacements of the crack faces in the immediate vicinity of the crack tip are proportional to the stress intensity factor of the corresponding mode (Ingraffea and Manu 1980).

Line spring modelling

The line spring model, originally proposed by Rice and Levy (1972), provides a simplified economical method for the analysis of surface cracks in both plate and shell models. It consists of replacing the part thickness crack with equivalent distributed springs which match the compliance introduced into the structure by the crack. The stiffness of each spring, which varies with crack depth, is based on matching the local compliance of the crack with that of a plain strain single edge notch specimen. A principal limitation for this technique is that it cannot handle the local weld stress concentration due to the geometry of welded attachments in plate joint and tubular joint configurations. This stress concentration is effective in the vicinity of the weld toe down to approximately 20% of the thickness. Beyond this region, Huang et al (1988), and Du and Hancock (1989), report that line springs produce reasonably accurate results at the deepest point of tubular joint weld toe surface cracks, with crack depth / thickness ratios up to 0.8 (see Figure 5.4). Another limitation is that line spring models appear to be restricted to cracks normal to the shell surface, while cracks in tubular joint tests generally curve under the weld toe (Bowness and Lee 1993, Abel and Wu 1993).

An important aspect of using line spring elements in shell element models where the weld in not included, is placing the elements in a position close to the notional weld toe crack and at the same time ensuring conservative predictions. Since SCF predictions in uncracked shell models may be unconservative if the stresses at the notional weld toe are considered, it would be expected that placing the line spring elements at the geometrically correct notional weld toe position might result in unconservative stress intensity factor solutions. This conclusion is supported by analyses reported by Bowness and Lee (1993), who recommend placing the line springs as close as possible to the intersection of the brace and chord shell mid-surfaces (eg. at 5mm away from the intersection of a 12.5 mm thick brace with a 30mm thick chord, with β = 0.5). However, Huang et al (1988) reported good agreement between SIF solutions at the deepest point of semi-elliptical cracks (a/T = 0.6 and 0.9; and β = 0.71) modelled using three-dimensional solid elements and line spring elements, when in the latter case the elements were placed at one brace thickness away from the intersection of the brace and chord shell mid-surfaces.

Singular elements for crack tip modelling

Calculation of crack driving force parameters using finite elements may be made more accurate if elements that incorporate the crack tip singularity are used to model the crack tip. A simple technique to produce such elements consists of moving the midside nodes of isoparametric elements to the quarter point positions. In two-dimensional analyses, the eight noded isoparametric element has the property that if the midside nodes on the sides of the element connected to the crack tip are displaced to the quarter points nearest to the crack tip, the element strain field naturally exhibits a $1/\sqrt{r}$ singularity characteristic of linear elastic material (Henshell and Shaw 1975, Barsoum 1976). In addition, if one side of the element is collapsed (all three nodes have the same geometric location), the predicted angular strain variations become more accurate. Constraining the three coincident nodes to move together maintains the $1/\sqrt{r}$ singularity, but leaving them free to move independently produces a $1/r$ singularity characteristic of elastic-perfectly plastic material. Singularities characteristic of power law hardening materials ($1/r^{(n/n+1)}$), can be obtained if isoparametric elements of sufficiently high order are used.

The approach described above for two-dimensional isoparametric elements can equally be applied to three-dimensional isoparametric elements.

Crack driving force at the free surface points

Determining crack driving force parameters at the free surface points of a semi-elliptical surface crack at the weld toe is a difficult task. Unlike the deepest point where reliable solutions may be obtained using three-dimensional or approximate two-dimensional idealisations, known solutions at the surface points are characterised by scatter and uncertainties due to modelling difficulties. These are associated with a number of factors including:

- Double curvature of the crack front: This increases as the crack approaches the surface and meets the weld toe. The resulting complex three-dimensional configuration is difficult to model using finite elements and require careful meshing and substantial refinement in the vicinity of the surface points if distorted elements are to be avoided.

- Sharp increase in local stresses: This is due to the local weld geometry. Very fine meshing is essential for capturing the associated stress gradient and its effects on crack tip stress intensity.

Three-dimensional finite element studies where stress intensity factor and/or J integral values at the surface points are evaluated have been reported by a number of researchers including Rhee et al (1991) and Kristiansen and Fu (1993). These studies indicate the following:

- J integral predictions using the VCE technique are contour dependent, therefore unreliable.

- Stress intensity factors predicted using local crack tip displacements depend on the region from which the solutions are inferred, ie. the solutions do not converge at the surface point.

Kristiansen and Fu argue that the above difficulties may be associated with the assumption of plane crack singularity at the free surface points, and suggest that the true singularity depends on Poisson's ratio. Further studies of variations of the singularity order are reported by Fu (1990).

While the factors influencing the solutions at the surface points are yet to be fully understood, it would appear that a key limitation of the majority of the reported finite element models is their relative 'coarseness' in the vicinity of the surface points. In a recent study where a relatively fine mesh was used, Bowness and Lee (1994) claim that solutions at the surface points obtained from local crack tip displacements, correlate reasonably well with empirical data.

An alternative to direct evaluation of stress intensity factors at the surface points consists of using plate solutions in conjunction with the Mk factor approach. This is described in Section 6.3.

5.4.2 Indirect methods

Indirect methods are those in which a stress analysis of the unflawed body is performed initially, and, making use of superposition principles, the stresses acting on the crack surfaces are used in a separate calculation to compute the stress intensity factor.

Efficient procedures are available for performing both tasks, and generally less expenditure of effort is required than in direct methods. In particular, stresses in the unflawed body need be computed only once, enabling stress intensity factors for any number of cracks to be evaluated. This feature is one of the principal advantages of indirect methods in fatigue crack growth computations since analyses of various crack configurations, tracing the history of crack growth, may be performed economically. However, the approximations and simplifying assumptions, often made when applying indirect methods, are bound to influence the generality, and may affect the accuracy of the resulting stress intensity factor solutions. In general, the accuracy of indirect methods decreases as the crack depth increases.

Weight function methods

One of the powerful methods for computing stress intensity factors for general stress fields is the weight function method (Bueckner 1970, Rice 1972). This is based on the superposition principle (Figure 5.1, and requires that for one reference loading condition the stress intensity factor, $K_{I,r}$, and the

displacement field normal to the crack face, v_r, should be known. Then, the mode I stress intensity factor for any other loading condition, in two-dimensional problems, is given by:

$$K_I = \frac{E'}{2K_{I,r}} \int_{\text{crack faces}} \sigma_y \frac{dv_r}{da} ds \qquad 5.9$$

where σ_y is the crack face loading in the uncracked body. Equation 5.9 must generally be evaluated by numerical methods.

While there are many reference solutions for $K_{I,r}$, the corresponding crack opening displacement solutions are less available.

Petroski and Achenbach (1978) have proposed a method to address this problem, which, for a known $K_{I,r}$ solution, involves specifying the displacement field in an approximate form satisfying certain conditions.

Niu and Glinka (1987) adopted this approach to derive weight functions for a T-butt welded joint, and using these, they studied the effect of weld profile parameters on stress intensity factors for edge cracks, and reported that their predictions agreed satisfactorily with similar finite element results.

Similarly Shen and Glinka (1991) and Shen et al (1991) derived weight functions which enable the calculation of stress intensity factors at the surface points and deepest point of a semi-elliptical crack in a finite thickness plate. A comparison functions, with numerical results is reported to indicate very good agreement for a wide range of crack aspect ratio and crack depth, i.e $0.2 \leq a/e \leq 1.0$ and $0 \leq a/T \leq 0.8$.

The 'O' integral weight function

Oore and Burns (1980) proposed a generalised weight function for an embedded irregular flaw of the following form:

$$W_{QQ'} = \frac{K_{PQQ'}}{P_Q} = \frac{\sqrt{2}}{\pi l_{QQ'}^2 \left[\int_s \frac{ds}{\rho_Q^2}\right]^{1/2}} \qquad 5.10$$

where Q' is a point on the crack front and Q is a point on the crack surfaces at which, P_Q, a pair of symmetrical opening forces act (see Figure 5.5). $K_{PQQ'}$ is the resulting opening mode stress intensity factor at Q', while, $l_{QQ'}$ and ρ_Q denote, respectively, the distances between Q and Q', and between Q and a point s at the centroid of an elemental length ds of the crack front.

Oore and Burns argued that for an arbitrary stress field σ_Q, computed in the uncracked body, an estimate of the stress intensity factor, $K_{Q'}$, at point Q', may be given by the integral:

$$K_{Q'} = \iint_A W_{QQ'} \sigma_Q \, dA_Q \qquad 5.11$$

where A_Q is an infinitesimal area around point Q, and A is the area of the crack surface.

To extend the approach to semi elliptical surface cracks, it was proposed to apply correction factors, functions only of the geometry under consideration, to the solutions for equivalent embedded elliptical cracks. Developments and/or applications of the 'Q' integral approach to surface semi elliptical cracks in tubular joints have been reported by Burdekin et al (1986), and by Dover and Connolly (1986). Both groups reported good agreement between their stress intensity factor predictions and data from fatigue tests on tubular joints. More recently Forbes et al (1991 and 1992) reported similar studies and argued that better predictions of stress intensity factors in tubular joints, especially for deep cracks, can be achieved by considering the load shedding effect (Section 7.9).

Albrecht and Yamada

Albrecht and Yamada (1977) suggested a simple method for estimating stress intensity factors for cracks subjected to non-uniform stress fields. The method consists of applying correction factors, that account for the non-uniform stress distribution in the structural detail under consideration, to known solutions corresponding to uniform stresses. The correction factors are obtained by integrating the stresses normal to the anticipated crack plane, evaluated in the uncracked body, over the length of the crack. The following sum expression for the correction factors, based on the known SIF solution for a central crack of length 2a in an infinite plate with two equal pairs of splitting forces P applied symmetrically around the crack centre (Figure 5.6), was proposed:

$$F_G = \frac{2}{\pi} \sum_{i=1}^{n} \frac{\sigma_{bi}}{\sigma} \left[\arcsin \frac{b_{i+1}}{a} - \arcsin \frac{b_i}{a} \right] \qquad 5.12$$

where σ and σ_{bi} are the stresses normal to the crack plane, corresponding to the remote uniform stress and actual local stress, respectively; and n is the number of segments along the crack length, over which the stresses are discretised (Figure 5.7).

5.4.3 Effects of structural modelling

This section is restricted to reporting the findings of a recent study by Haswell (1991) who investigated the significance of structural modelling on stress intensity factor predictions using the line spring finite element technique.

The study concerns predicting stress intensity factors for a range of surface cracks in a tension loaded tubular T joint. The cracks, located at the chord weld toe, are semi-elliptical with a low aspect ratio (a/2c = 0.1) and depths in the range a/T = 0.2 to 0.8. The tubular joint was first analysed in the uncracked condition enabling the through thickness elastic stress distribution at the saddle position, corresponding to the deepest point in the cracks, to be estimated as a combination of a membrane and a bending stress. These stresses were then applied to the following structural models which were idealised using shell or plane strain finite elements (see Figure 5.8):

- Full tubular joint.
- A cylinder with and without attachment.
- A plate under different boundary and loading conditions.
- A two-dimensional slice through the brace/chord intersection.

The cracks in all the models were idealised using line spring elements, except in the two-dimensional slice model where conventional plane strain elements and the VCE technique were used to compute J integral and equivalent stress intensity factors which were then corrected to account for the finite crack length. Comparisons of the predictions at the deepest point indicated good agreement between the various models for crack depths in the range: a/T = 0.2 to 0.4 (Figure 5.9). For deeper cracks predictions from the simple models were up to 45 % higher than those from the tubular joint and cylinder with attachment models. These differences were attributed to the effects of structural restraints and/or load shedding. In addition, predictions from the plate model appear to depend significantly on the plate length/width (L/W) ratio and end restraint conditions with convergence reported to be obtained for L/W = 64.

It should be noted that findings of the above study apply to SIF predictions at the deepest points of cracks in the range a/t = 0.2-0.8. Solutions for the deepest points of shallower cracks ($a/T \leq 0.2$), and for the surface points of all cracks, is likely to be more affected by modelling of the non linear stress distribution associated with weld notch stresses than by the nature of structural modelling.

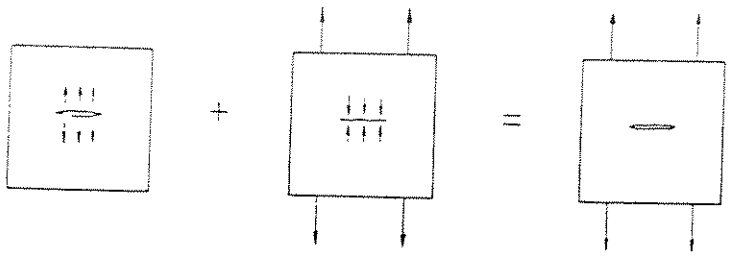

Figure 5.1 Principle of superposition applied to LEFM problems

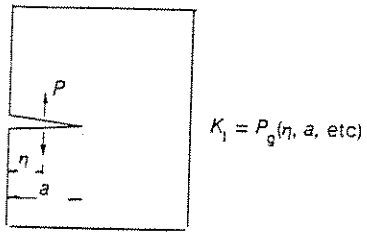

(a) Original solution for wedge forces P

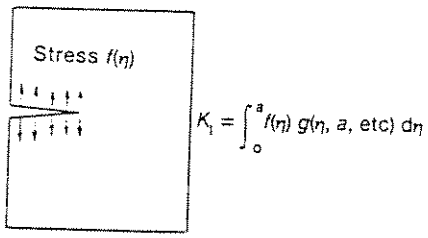

(b) Derived solution for crack face loadings $f(\eta)$

Figure 5.2 Development of stress intensity solutions from the case of wedge opening forces

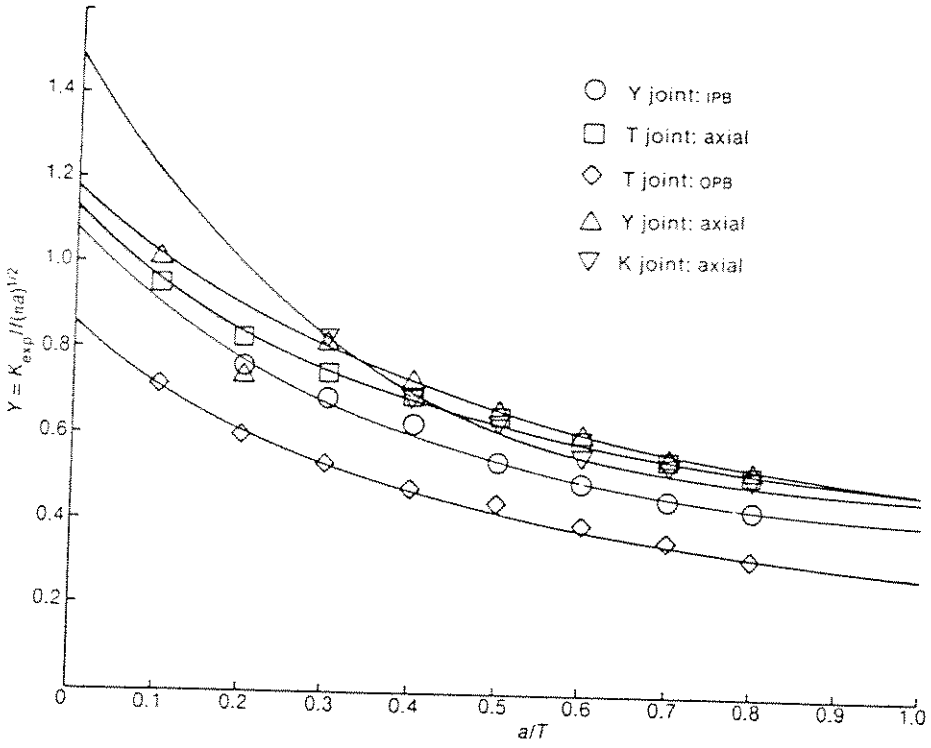

Figure 5.3 Experimentally determined values of y for various joints (Dover and Dharmavasan 1982)

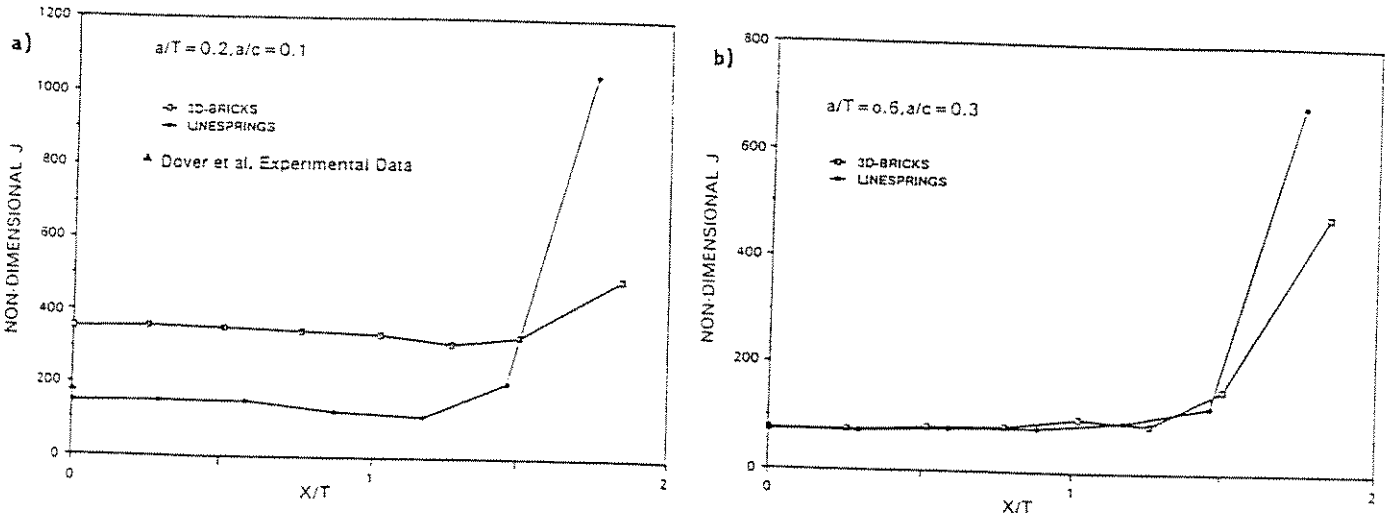

Figure 5.4 A comparison of the non-dimensional J parameter calculated by line spring and brick elements (Du and Hancock 1989)

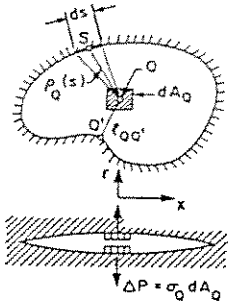

Figure 5.5 Equivalent embedded crack for O - integral formulation

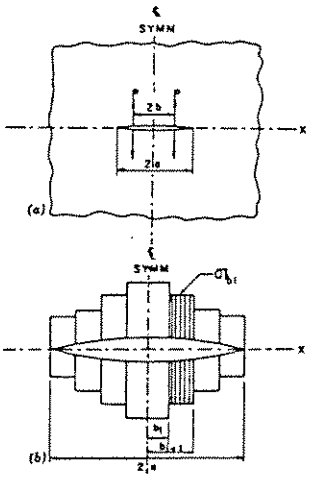

Figures 5.6 and 5.7 Crack in infinite plate subjected to:
a) two pairs of equal splitting forces, b) pairs of discrete stresses

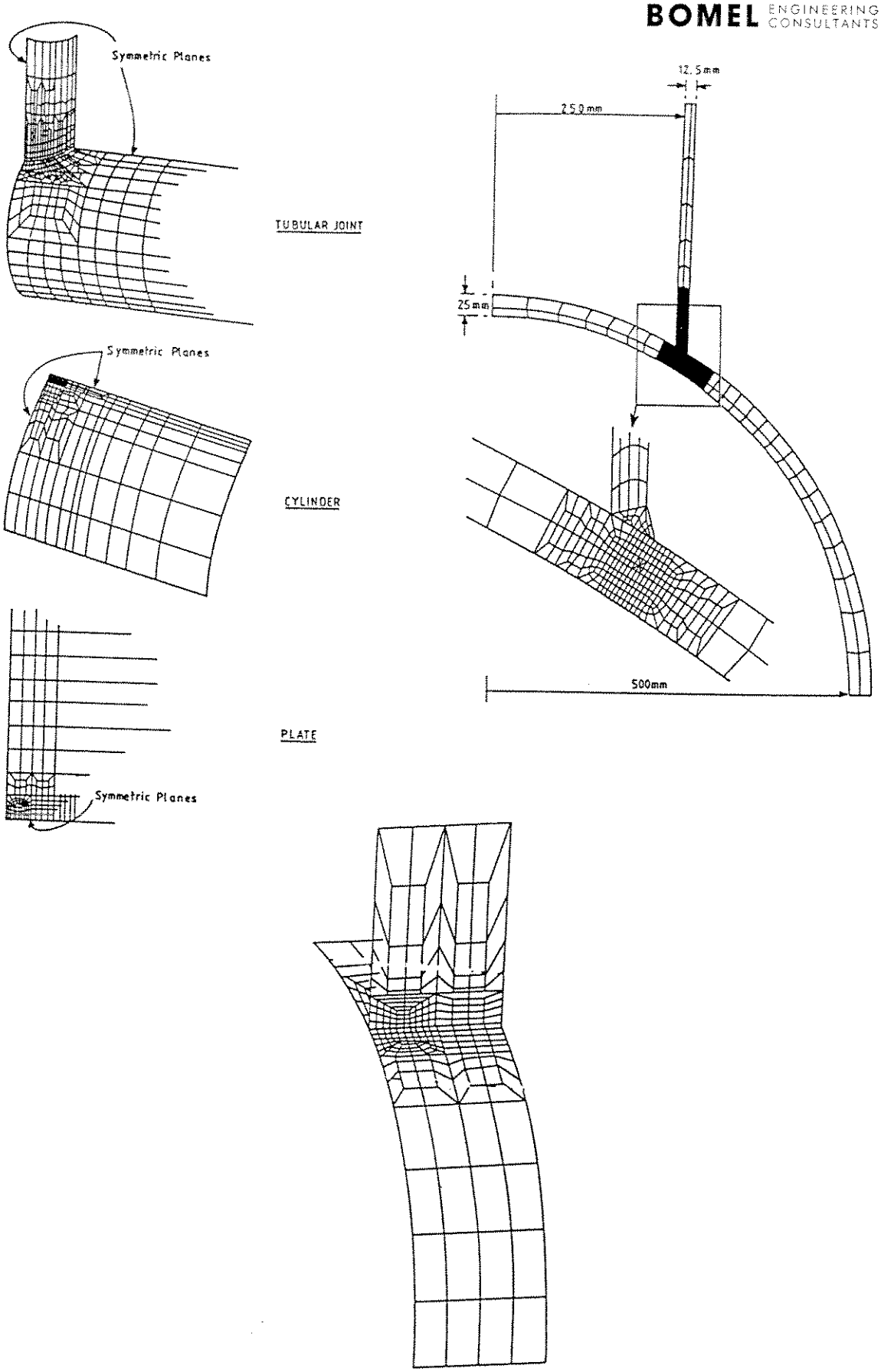

Figure 5.8 Structural models considered by Haswell (1992)

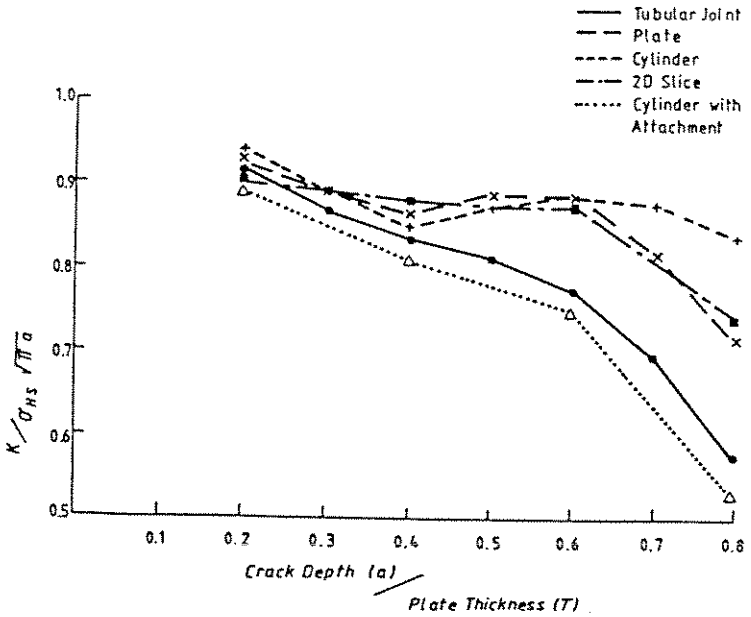

Figure 5.9 Comparison between simple models and full-scale joint model (Haswell 1992)

6. PARAMETRIC EQUATIONS FOR STRESS INTENSITY FACTORS

6.1 Surface Semi-Elliptical Cracks in Finite Plates

A number of parametric equations for stress intensity factors of surface semi-elliptical cracks in plain plates are available. Scott and Thorpe (1981) used the development of fatigue crack shape, as a diagnostic tool, to test the accuracy of some of these equations in predictive fatigue crack growth calculations. They concluded that the most accurate solutions were those of Newman and Raju (1979) for tension, and the Koterazawa and Minamisaka solutions for pure bending (1977). To modify these equations for finite width effects, Scott and Thorpe recommended the correction factors of Holdbrook and Dover (1979).

Straalen et al (1988) reported a more recent review which involved:

- The equations recommended by Scott and Thorpe
- A more recent version of the Raju and Newman equations including solutions for bending and corrections for finite width effects (Newman and Raju 1981 and 1984)
- Equations for tension by Dufresne (1981)
- Equations for tension and bending by Isida, Nogushi and Yoshida (1984).

Comparative plots of the infinite plate solutions show reasonable agreement for small crack depths but significant differences for deeper cracks. However, over most of the crack depth range for the geometries considered, the Newman and Raju predictions appear to lie nearer to the upper end of the scatter band. Straalen et al conclude by recommending the use of the Newman and Raju solutions because they are the most complete and are supported by the general agreement with the other solutions.

Thurlbeck (1991) compared the equations of Raju and Newman (1981), Scott and Thorpe (1981), and Huget et al (1983). The latter are intended for cracks with aspect ratio less than or equal to 0.2. After considering a range of crack depths and aspect ratios the following was concluded:

- There is little difference between the formulae of Raju and Newman and those of Scott and Thorpe for $a/T \leq 0.2$ and $a/c > 0.2$ for both tension and pure bending at the surface and deepest point positions.
- For deep low aspect ratio cracks, the Raju and Newman results are closer to those of Huget et al than the Scott and Thorpe results, and, in the majority of the cases larger in magnitude, thus providing a more conservative assessment.

Based on the above, Thurlbeck found the Raju and Newman solutions to be the most appropriate.

A feature common to all the above parametric equations is that they are applicable to cracked plain plates under pure tension and/or pure bending stress fields. Non linear through thickness stress distributions such as those found in fillet welded T-butt joints (associated with the local weld stress concentration) may be dealt with using plain plate solutions in conjunction with the Mk factor. This approach is considered in the next section.

6.2 Surface Semi-Elliptical Cracks in Fillet Welded T-Butt Joints

An attachment welded to a plain plate has a stress raising effect on nominal through thickness stress distribution. This effect, local to the immediate vicinity of the weld toe, decreases as the distance from the plate surface through the thickness increases, and almost vanishes at approximately 20% of the plate thickness (see Figures 6.1 and 6.2). Consequently, If a shallow surface crack (eg. $a/T < 0.2$) is present at the weld toe, its stress intensity factors at the deepest and surface points will be higher than the corresponding values of an identical crack in a plain plate.

The factor Mk, first proposed at TWI, is intended to quantify the effect of local weld stress concentration factor on the stress intensity factor, K, of surface cracks as follows:

$$Mk = \frac{\text{K for a crack in a plate with attachment}}{\text{K for same crack in same plate with no attachment}} \qquad 6.1$$

For three-dimensional semi-elliptical cracks, Mk may be defined at various points on the crack front. However, for practical purposes, only the deepest point and two surface points are considered. In two-dimensional cracked geometries, Mk is defined at a single point representing the crack tip which is equivalent to the deepest point of an infinitely long crack ($a/c = 0$). Both configurations are shown in Figure 6.3.

Mk is a function of crack size and geometry, weld size and profile, and applied loading. For a semi-elliptical crack, Mk can be expressed, for tension or pure bending, in terms of the following parameters:

- Relative crack depth: a/T
- Crack aspect ratio: a/c
- Non-dimensional attachment width: L/T
- Non-dimensional weld toe radius: r/T
- Weld toe angle: θ

where T is the plate thickness (see Figure 6.3).

In general, Mk can be determined according to Equation 6.1, from stress intensity factor analyses of a plain plate and the same plate with attachment for a variety of crack geometries. Since three-dimensional analyses are much more complex than two-dimensional analyses, the latter have been used as the basis for the majority of studies on Mk. This approach allowed approximate methods to be inferred from two-dimensional results and adapted to three-dimensional configurations.

Published Mk studies allow the following trends and results to be identified:

1. When a/T decreases, Mk increases exponentially. 2D results, corresponding to straight fronted cracks and considered relevant only to the deepest point on the front of semi-elliptical cracks, indicate power law expressions of the form:

$$Mk = \alpha \left(\frac{a}{T} \right)^{\beta} \qquad 6.2$$

where α and β are functions of the crack size and welded joint geometry (see Table 4.1 for the values of α and β derived at TWI and recommended in PD 6493:1991). As a/T increases, Mk decreases to reach 1.0 at approximately a/T = 0.25. An upper bound for Mk, as a/T approaches 0.0, has been suggested to correspond to the free surface weld toe stress concentration factor, K_t. An alternative to using K_t, is to assume that Mk at the free surface corresponds to a very small crack, such as, a = 0.15mm. The latter approach is compatible with the fact that crack-like defects of this order are likely to exist at the toe of welded steel joints. However, Pang (1990,1991 and 1993) argues that using such an approach leads to over conservative results, particularly if Mk is kept constant, and proposes that, based on 3D results published by Bell (1987), a less conservative estimate for Mk at the free surface can be made using the expression:

$$Mk_c = Mk_a + 1.15 \exp\left[-9.74 \left(\frac{a}{T} \right) \right] \qquad 6.3$$

where Mk_c and Mk_a are Mk values at the free surface points and deepest point, respectively and $a/T \leq 0.15$. Mk_a is determined using Equation 6.2.

2. In general, if L/T or θ increase or r/T decreases, K_t and Mk increase. However, the relative effects of changing these parameters vary, with r/T being the most influential (Thurlbeck and Burdekin 1992).

3. Limited FE studies, reported by Dijkstra et al (1989), indicate that for the same relative crack depth, a/T, Mk based on 2D analyses are consistently higher than the

corresponding Mk from 3D analyses. This can be attributed to the constraint, offered by the uncracked section on either side of a finite length semi-elliptical crack, which restrains crack opening. Such constraints are modelled in 3D, whereas, 2D idealisations imply a straight fronted crack configuration. Dijkstra et al recommend correction factors in order to adapt 2D Mk results to 3D geometries. They suggest the values 0.9 and 0.8 for the deepest point and surface points, respectively, for both tension and bending loading (ie. Mk(3D) / Mk(2D) $\approx$0.9 or 0.8).

4. 3D studies, reported by Fu et al (1993), indicate that the effects of a welded attachment on Mk can be decoupled into two separate functions. One function, f_2, accounts for a/T and the position on the crack front, and can be determined from 2D studies taking specific weld geometries into consideration. The other function, f_1, depends on a/c and accounts for the constraint offered by the attachment. Lower and Upper bounds for f_1 correspond, respectively, to the semi-circular crack (a/c=1.0) and straight fronted crack (a/c=0.0) configurations. It is suggested that only a limited number of 3D analyses are required to determine f_1.

5. Thurlbeck and Burdekin (1992) introduced a stress undershoot parameter, Ma, for use in conjunction with Mk derived from 2D studies. The new factor is based on the observation that stresses across the plate thickness at the toe of a welded attachment are self equilibrating, ie. the steep increase near the surface (associated with Mk) is balanced by a fall below the plain plate nominal stress at larger depths further into the section. As a result, the SIF in this region would be lower than for a plain plate solution (Figure 6.4). The proposed Ma factor, intended to account for this SIF reduction, is based on the 3D results of Fu et al (see 4. above). In addition, it corrects the 2D based Mk values for the 3D semi-elliptical crack condition (see 3. above). The factor is given in terms of a/T and a/c and incorporates a number of assumptions (see Appendix B).

A large number of Mk studies have been undertaken. Most of these are based on 2D analyses and some on combinations of 2D and 3D analyses.

Pang (1990 and 1991) reviewed a number of the earlier studies, involving cruciform and T welded connections, and outlined the methods commonly used for evaluating Mk. Most of Pang's conclusions have been covered above. In the remainder of this section, The attention will be restricted to a number of the most recent Mk studies on welded T configurations intended to represent the conditions in tubular joints, and which have been published in the form of parametric equations.

Thurlbeck and Burdekin (1992)

As part of the MTD/SERC Defect Assessment Programme comprehensive 2D FE studies were performed involving the following parameters:

$0.375 \leq L/T \leq 3.0$
$0.01 \leq r/T \leq 0.5$
$22.5° \leq \theta \leq 90°$

These studies provided detailed information on stresses in the uncracked condition, which, in conjunction with the Albrecht and Yamada (1977) method, were used to calculate 2D Mk values for varying crack depths. Based on these, parametric equations, describing effects of the three parameters (L/T, r/T, and θ), and interaction between r/T and θ, were produced for both tension and bending loading. The equations are of the following form:

$$Mk_{combined} = Mk_{(L/T)} * \frac{Mk_{(\theta)}}{Mk_{(\theta = 45°)}} * \frac{Mk_{r/T}}{Mk_{(r/T = 0.01)}} * f\left(\frac{r}{T}.\theta\right) \qquad 6.4$$

where $Mk_{(L/T)}$, $Mk_{(\theta)}$, and $Mk_{(r/T)}$ are described in terms of the sum:

$$C_o + C_1\left[\log\frac{a}{T}\right] + C_2\left[\log\frac{a}{T}\right]^2 + C_3\left[\log\frac{a}{T}\right]^3 \qquad 6.5$$

where coefficients C_0, C_1, C_2, and C_3 are functions of L/T, r/T, or θ. These Mk equations, in addition to the Ma equations (see 5. above), are reported fully in Appendix B.

Dijkstra et al (1989 and 1993)

Equations based on 2D Mk results incorporating the following parameters were proposed:

$0.562 \leq L/T \leq 1.31$
$0.0071 \leq r/T \leq 0.125$
$25° \leq \theta \leq 65°$

The equations, which assume no interaction between the parameters, are of the following form:

$$Mk = g_L\left(\frac{a}{T}, \frac{L}{T}\right) * \frac{f_\theta\left(\frac{a}{T}, \theta\right)}{f_\theta\left(\frac{a}{T}, 70°\right)} * f_r\left(\frac{a}{T}, \frac{r}{T}\right) \qquad 6.6$$

where the functions g_L and f_r are based on Mk data generated by Dijkstra et al and published, respectively, in 1993 and 1989. These data are based on 2D FE analyses of T plate joints, which involved modelling of cracks with a/T in the range 0.007-0.5, and using the VCE technique to evaluate the strain energy

release rate and the corresponding stress intensity factors. The function f_θ is a curve fit of the Smith and Hurworth (1984) Mk data from 2D FE analyses of cruciform joints. It is proposed to apply correction factors, described in 3. above (0.8 and 0.9), in order to adapt the 2D Mk estimates to the general 3D condition. Equations 6.6 are reported in detail in Appendix B.

Fu et al (1993)

Simple equations based on 3D FE studies for T plates, were proposed as the sum of two functions as follows (see 4. above):

$$Mk\left(\frac{a}{c}, \frac{a}{T}, \phi\right) = f_1\left(\frac{a}{c}\right) + f_2\left(\frac{a}{T}, \phi\right) \qquad 6.7$$

where $f_1(a/c)$ are as follows:

a/c	$f_1(a/c)$ Tension	$f_1(a/c)$ Bending
0.00	1.0000	1.0000
0.20	0.9219	0.9108
1.00	0.8860	0.8395

It is recommended to estimate values of $f_1(a/c)$, for intermediate a/c, by interpolating the above data. Expressions for $f_2(a/t,\phi)$, where ϕ is the crack front parametric angle, are given for tension and bending in Equations 6.8 and 6.9, respectively. (ρ=0 and ρ=90 correspond to the surface point and deepest point, respectively).

The 3D plate models represent attachments with L/T = 1.0, θ = 45°, and a sharp transition at the weld toe corresponding to a very small radius. Cracks with relative depths, a/T, in the range 0.05-0.4 were considered. The Mk data were based on stress intensity factors derived from strain energy release rate predictions. These were obtained using the VCE technique applied to meshes involving explicit crack modelling. The Fu et al equations are unique in allowing Mk to be estimated at any point along the semi-elliptical crack front except at the two free surface points. At these points, Fu et al note that the VCE predictions are unreliable because of the singularities associated with the crack meeting the free surface, and the sharp notch at the weld toe.

$$f_{2t}\left(\frac{a}{T}, \phi\right) = -0.0245 + 1.7261\left[1.0 + 76.9069\,\frac{a}{T}\sin\phi\right]^{-1.2879} \qquad 6.8$$

$$f_{2b}\left(\frac{a}{T}, \phi\right) = -0.0751 + 2.9014\left[1.0 + 266.4478\,\frac{a}{T}\sin\phi\right]^{-0.7916} \qquad 6.9$$

6.3 Surface Semi-Elliptical Cracks in Tubular Joints

Haswell (1992)

This work is based on an extensive FE study of over 70 planar tubular joint models in both the uncracked and cracked conditions subjected to axial and OPB loads. The joints considered included T, Y, K, X, and KT joints (see Table 6.1). These were modelled using 8-noded shell elements and analysed using the ABAQUS software (Hibbitt et al 1989). The cracked joints contained semi-elliptical surface cracks in the chord at the saddle positions. These were modelled using line spring elements located along the weld toe position, which was assumed to be radially offset 25mm from the brace mid-shell surface. The brace thickness was 12.7 mm in most cases. Brace thicknesses equal to 7.6mm and 20.32mm were also considered. Cracks with relative depths, a/T, of 0.2, 0.4, 0.6, and 0.8 were analysed. The aspect ratio, a/c, was constant at a/c = 0.2.

The cracked models were used to provide data on SIF at the cracks deepest points, while the uncracked models enabled detailed information on the stress distribution, at the saddle position coinciding with the crack centre, to be quantified in terms of the SCF and DOB parameters. The SIF results were expressed in a non-dimensional Y form as follows:

$$Y = \frac{K_I}{\sigma_n \, SCF \, \sqrt{\pi a}} \qquad 6.10$$

where K_I is the Mode I SIF at the deepest point on the crack front, σ_n is the nominal stress in the brace, and a is the crack maximum depth. The relationships between Y, a/T, SCF and DOB are illustrated in Figures 6.5 to 6.7. Haswell noted that, for each crack depth SIF/σ_n increases with SCF and $SIF/(\sigma_n * SCF)$ decreases when DOB increases. In both cases the relationships are approximately linear. Haswell proposed a simple model relating the SIF, SCF, and DOB at each crack depth as follows:

$$\frac{SIF}{SCF * \sigma_n} = (A + dA) + B * DOB \qquad 6.11$$

where A and B are constants obtained from a linear regression analysis of the data (see Table 6.2), and dA is the maximum absolute scatter at each crack depth. dA is intended to account approximately for the scatter in the data attributed to Mode II contribution and to crack plane restraint which varies with joint geometry and loading.

Haswell suggests that the model represented by Equation 6.11 can be used to estimate the SIF at the deepest point of crack geometries similar to those considered in the study, and that variations in joint geometry, loading and crack position are characterised by the SCF and DOB values at the crack position. It is recommended to estimate these SCF and DOB parameters from FE shell element analysis of the uncracked joint.

It should be noted that although, the line spring predictions are reported to agree reasonably well with the 3D SIF results of Ritchie and Voermans (1986) especially at medium crack depths ($a/T \approx 0.5$), locating the cracks at 25mm away from the mid-shell surface may lead to unconservative SIF predictions (Bowness and Lee 1993). This may be related to the associated SCF and DOB predictions. The values calculated at the mid-shell intersection appear to be in better agreement with predictions from a number of commonly used parametric equations, than the values calculated at a position 25mm away from the mid-shell intersection (Table 6.3).

The range of application of the proposed SIF model (Equation 6.18) would appear to be severely limited by the format of the equation and nature of the constants A and B. Examining the terms in the equation reveals that A and B must have a dimension of $(\text{length})^{1/2}$, eg. $(\text{mm})^{1/2}$. This anomaly may be attributed to the term $\sqrt{(\pi a)}$ which does not appear in Equation 6.18. As a result, for a fixed stress distribution (determined by SCF, DOB and σ_n) SIFs predicted according to the above equation would appear to be independent of the absolute crack size. Consequently, the proposed model appears to be applicable only to joints having absolute chord thickness and crack sizes similar to those considered in the finite element studies. It is understood that all the tubular joint models used to provide the finite element data have a chord thickness of 25mm.

Rhee et al (1991)

Earlier work by Rhee (1985-1988) involved a series of 3D FE analyses of semi-elliptical cracks in tubular joints of various configurations. These included an X joint (β = 0.68), a K joint (β = 0.67) and a multiplanar K joint (β = 0.6). In the FE models, 3D solid elements were used to model the cracks (assumed normal to the chord surface) and the brace/chord intersection region, while shell elements were used to model the remaining parts of the joint. SIFs for Modes I, II, and III were extracted from displacements in the vicinity of the crack tip.

More recently, arguing that there is a need for empirical SIF equations for weld toe surface cracks in tubular joints similar to those available for SCF evaluation, Rhee suggested that such SIF equations can be derived based on systematic 3D FE analyses. The first step towards achieving this 'mammoth' objective consisted of performing 40 analyses of a series of semi-elliptical crack geometries in T joints subjected, separately, to tension, IPB, and OPB loads. The following geometrical parameters were considered:

- Joint parameters:
  $0.4 \leq \beta \leq 0.8$
  $10.0 \leq \gamma \leq 20.0$
  $0.3 \leq \tau \leq 1.0$
  $\alpha = 12.0$

- Crack parameters:
  $0.05 \leq a/T \leq 0.80$
  $0.05 \leq 3c/d \leq 1.20$

All the cracks were located in the chord at one saddle position along the weld toe. The FE models for the joints and cracks, in addition to the method of SIF evaluation were similar to those adopted in Rhee's earlier work.

The SIF results were converted into an equivalent SIF parameter, K_e, which is intended to account for the contributions of Modes I, II, and III:

$$K_e = \left[\frac{K_I^2 + K_{II}^2 + K_{III}^2}{(1 - \nu)} \right]^{1/2} \qquad 6.12$$

where, ν, is Poisson's ratio. Based on regression analyses of the K_e data, equations of the following form were proposed:

$$\text{Ln} \left(\frac{K_e}{\sigma_n \sqrt{\pi a}} \right) = f(\text{Ln}\beta, \text{Ln}\gamma, \text{Ln}\tau, \text{Ln } a', \text{Ln } c') \qquad 6.13$$

where σ_n is the nominal brace in the brace, $a' = a/T$, and $c' = 3c/d$. Function f in Equation 6.13 was expressed in terms of three functions: F_g, F_s, and F_i as follows:

$$e^f = F_g * F_s * F_i \qquad 6.14$$

where F_g is a joint geometry factor, F_s is a crack size factor, and F_i is a joint and crack coupling factor. Details of the joint and crack geometries and the proposed K_e equations for the crack deepest and surface points are given in Appendix C.

The above equations can be very useful for estimating SIF for saddle cracks in joint geometries similar to those considered in the study. However, It should be noted that it is not clear whether the meshes used in the analyses were sufficiently fine to capture the sharp increase in stresses near the surface (see Section 6.3 in connection with the parameter Mk).

Such stresses, associated with the weld geometry, will affect K_e at all points on the fronts of shallow cracks ($a/T \leq 0.2$) and K_e at the surface points of deeper cracks. In addition, similarly to most recent FE results, K_e predictions at the crack front surface points are less reliable than the predictions at the deepest point.

Ho and Zwerneman (1995)

This recent study provides significant and valuable data on methods for determining SIF solutions for semi-elliptical cracks in tubular joints. The study, undertaken at OSU has a number of features similar to those of the earlier OSU work (Rhee et al, 1991), and it may be considered as a follow on to that work.

Noting that the reliability of existing methods for determining SIF solutions for tubular joints, has been studied only on a very small scale, Ho and Zwerneman, declare that the major purpose of their research is to conduct a thorough comparison of the aforementioned methods to 'exact' finite element solutions. In order to achieve this objective, a large number of finite element analyses on both uncracked and cracked tubular Y joints were performed using the Package SESAM, and its Module Pretube as a preprocessor. Findings from analyses of the uncracked joints were aimed at producing data on SCF, DOB and hot spot angle. These were then used to assess a number of parametric equations such as those of Efthymiou (1988) and Connolly et al (1990).

The results of these assessments are not considered here. Rather, attention is restricted to the work on cracked joints which consists of approximately 1200 analyses on 60° Y joints subjected to brace axial tension. Each joint contains a semi-elliptical crack at the hot spot along the weld toe on the chord outer surface. The crack surface is assumed normal to the chord wall.

Geometrical parameters of the joints are as follows:

- Joint parameters: D = 1000 mm
  $0.6 \leq \beta \leq 0.8$
  $10.0 \leq \gamma \leq 35.0$
  $0.2 \leq \tau \leq 1.0$
  $\alpha = 12.0$

- Crack parameters: $0.1 \leq a/T \leq 0.8$
  $0.1 \leq a/c \leq 0.4$

Similarly to the earlier work by Rhee et al, 3D solid elements were used to model the cracks and the brace/chord intersection region, while shell elements were used to model the remaining parts of the joint. Stress intensity factors for Modes I, II, and III were extracted from displacements in the vicinity of the crack tip using POSTSIF which is a module of SESAM. Although, Rhee et al used a different postprocessor which incorporates the procedure proposed by Rhee (Section 5.4.1), a comparison of solutions obtained by both postprocessors for 30 joints containing a wide range of semi-elliptical cracks, reveals very close agreement in the vast majority of cases.

The SIF results were expressed in a nondimensional form as follows:

$$Y_{ia} = \frac{K_{ia}}{\sigma_n \sqrt{\pi\, a}} \qquad 6.15$$

where
K = Stress intensity factor
σ_n= Nominal brace stress, and
i = 1,2,3 which refers to the mode of fracture

The subscript 'a' refers to solutions at the crack deepest point. Y_{1a}, Y_{2a}, and Y_{3a} were then converted into an equivalent parameter, Y_{ea}, as follows:

$$Y_{ea} = \sqrt{Y_{1a}^2 + Y_{2a}^2 + \frac{Y_{3a}^2}{(1-\nu)}} \qquad 6.16$$

The results presented in tabular form, indicate that similarly to findings from other investigations, Y_{2a} and Y_{3a} are much smaller than Y_{1a} which, as a result, is very close to the equivalent parameter Y_{ea}.

The Y_{1a} data were then evaluated and compared to solutions obtained by applying simplified methods including:

i Raju and Newman equations for flat plates together with the Mk approach assuming that the weld leg length is 1.5 times the brace thickness (this method is referred to by Ho and Zwerneman as the BSI PD6493 method)

ii as above but including a correction factor to account for load shedding according to the linear moment release approach (Section 7.8).

Results of the evaluation and comparison studies can be outlined as follows:

1 The SIF estimates obtained by applying Method (i) are higher than the finite element solutions. Differences between the two sets of results increase as the cracks become deeper, i.e. a/T increases. Therefore Method (i) is conservative (Table 6.4 and Figures 6.8 and 6.9).

2 The majority of SIF estimates obtained by applying Method (ii) are lower than the finite element solutions. Therefore, Method (ii) is unconservative (Table 6.4).

3 The parameter Y_{1a}/SCF does not change significantly as the joint parameters β, γ and τ change, i.e. joints with different β, γ or τ values all have nearly the same values of Y_{1a}/SCF. However, the crack parameters a/T and a/c appear to have the most significant influence on the value of Y_{1a}/SCF.

4 Based on the last observation, Ho and Zwerneman derived a simple linear equation for calculation of Y_{1a}/SCF as follows:

$$\frac{Y_{1a}}{SCF} = A - B\,(a/T) \qquad 6.17$$

The constants A and B were found by curve fitting the finite element data and introducing adjustments aimed at reducing the errors associated with the resulting simplified curves. Values for A and B are given in Table 6.5 and the curve for (a/c = 0.2) is shown in Figure 6.10.

With regard to the high percentage errors shown in Table 6.5, Ho and Zwerneman note that these are associated with cases where Y_{1a} is small, and that the maximum errors occur when γ, τ, a/T and a/c are large. They propose that the above simplified method (Equation 6.17) can be used for computing a first estimate of SIF and that if the associated fatigue life is found to be inadequate, then a more sophisticated form of analysis may be employed.

It should be noted that apart from the excessive conservatism which may be associated with the proposed model, its applicability is restricted to the deepest point of saddle cracks in the geometries considered to derive the basic data and to axial loading only. The most valuable contribution of this work is that it provides data on effects of the geometric parameters β, γ and τ, in addition to a comprehensive database of SIF solutions which can be used in the future in conjunction with SIF data from other sources in order to produce improved or alternative approaches to estimate SIF for a wide range of joint geometry under various loading conditions. Furthermore, the study proves that simplified methods applicable to a wide range of geometries and loading conditions, such as those based on the equations of Raju and Newman, and possibly incorporating correction factors, can provide conservative SIF solutions.

Kam, Topp, and Dover (1989)

This work is based on the UCL empirical approach for estimating stress intensity factors. Section 5.3 provides a detailed description of the approach and the relevant parameters, and discusses its main limitations. Equations describing the latest model, known as the Two Phase Model (TPM), are given here. This model is apparently based on crack growth data from seven tubular joints of chord wall thicknesses in the range 16mm - 45mm (Figure 6.11). The joints are of T, Y, and X configurations. Five joints were tested under axial loading, one under IPB and one under OPB. Crack growth is considered in two phases: The 'early crack growth' phase and the propagation phase. The data are fitted to a Y expression of the form:

$$Y = M.B.\left(\frac{T}{a}\right)^{k} \qquad 6.18$$

$M = 1$ for $a > 0.25T$ (propagation phase)

$M = (0.25T/a)^{-p}$ for $a < 0.25T$ (early growth phase)

$B = (0.669 - 0.1625S)\,(T/0.016)^{0.11}$

$k = (0.353 + 0.057S)\,(T/0.016)^{-0.099}$

$P = 0.231\,(T/0.016)^{-1.71}\,(\beta)^{0.31}\,(S_c)^{0.18}$

B and k are functions of the chord thickness and the average stress parameter S (described in Section 5.3). The exponent p is a function related to the early crack growth phase, and is considered dependent on the local weld profile and the associated notch stress effect. S_c in the hot spot stress concentration factor denoted as SCF_{HS} in Section 5.3.

It is suggested that the remaining life to failure, corresponding to through thickness penetration, for a joint with a crack of depth a, can be obtained in a closed form by integrating Paris law:

$$N = N_1 + N_2 \qquad 6.19$$
$$N_1 = (a^u_{int} - a^u_s)/(U * F * (0.25T)^{-pm})$$
$$N_2 = (T^v - a^v_{int})/(V * F)$$

where
$$F = C * \Delta\sigma^m * \pi^{m/2} * B^m * T^m$$
$$U = 1 + m * (k - 0.5 - p)$$
$$V = 1 + m * (k - 0.5)$$

and if
$a_s > 0.25T$, $a_{int} = a_s$, $N_1 = 0$
$a_s < 0.25T$, $a_{int} = 0.25T$

In the above equations, the crack depth, a, and the chord wall thickness, T, are expressed in metres.

Dharmavasan and Dover (1988) reported the following validity limits for the above model:

1. $0.51 < \beta < 0.76$
2. $2.66 < SCF_{HS} < 9.4$
3. $1.81 < SCF_{AV} < 6.35$
4. Solution is not derived from experimental data if T is not 16mm
5. $16mm < T < 45mm$

Comments on the advantages and disadvantages of the TPM model are given in Section 5.3.

	Geometry	β	τ
AXIAL	T	0.3	0.5
	T	0.5	0.3
	T	0.5	0.5
	T	0.5	0.8
	T	0.8	0.5
	KT	0.5	0.5
	X	0.5	0.5
	Y	0.5	0.5
	K	0.5	0.5
OPB	T	0.3	0.5
	T	0.5	0.3
	T	0.5	0.5
	T	0.5	0.8
	T	0.8	0.5
	KT	0.5	0.5
	X	0.5	0.5
	Y	0.5	0.5
	K	0.5	0.5

Table 6.1
Uncracked joint geometry, Haswell (1992)

a/T	Slope B	Intercept A	
		Mean	Upper Bound
0.2	-0.248	4.028	4.228
0.4	-3.865	7.938	8.138
0.6	-9.407	13.096	13.436
0.8	-14.196	16.317	16.717

Table 6.2
Linear Y-calibration model for tubular joints
(a/2c = 0.1), Haswell (1992)

	β	τ	SCF			DOB		
			FE		HCD	FE		CHDS
			W/T	INT		W/T	INT	
AXIAL	0.3	0.5	3.69	9.2	9.91	0.774	0.864	0.834
	0.5	0.3	5.6	6.7	5.03	0.78	0.883	0.822
	0.5	0.5	7.3	9.9	9.84	0.796	0.888	0.841
	0.5	0.8	13.62	15.7	19.36	0.824	0.894	0.868
	0.8	0.5	3.59	6.9	5.8	0.63	0.884	0.808
OPB	0.3	0.5	4.01	5.1	7.3	0.85	0.92	0.968
	0.5	0.3	3.25	4.5	5.17	0.83	0.906	0.929
	0.5	0.5	5.76	7.3	8.61	0.836	0.905	0.932
	0.5	0.8	9.8	11.0	13.8	0.856	0.911	0.94
	0.8	0.5	4.7	7.5	8.8	0.86	0.905	0.893

Table 6.3
Comparison of FE and parametric SCF and DOB predictions for T joints Haswell (1992)

a/c	Ho's method	BSI PD6493 Method (i)	Modified PD6493 Method (ii)
0.1	-7% to +88%	-11% to +111%	-41.2% to +13.3%
0.2	-8% to +100%	-3% to +111%	-34.5% to +24.8%
0.3	-5% to +155%	+3% to +149%	-25.5% to +68.7%
0.4	-19% to +327%	+7% to +304%	-20.3% to +209.8%

Table 6.4 Comparison of range of errors among simplified methods (Ho and Zwerneman 1995)

a/c	A	B
0.1	1.22	0.69
0.2	1.07	0.84
0.3	0.96	0.83
0.4	0.87	0.81
Valid range of parameters: θ=60°, β=0.6 & 0.8, γ=10-35, τ=0.2-1.0		

Table 6.5
Constants for A and B for new simplified method (Ho and Zwerneman 1995)

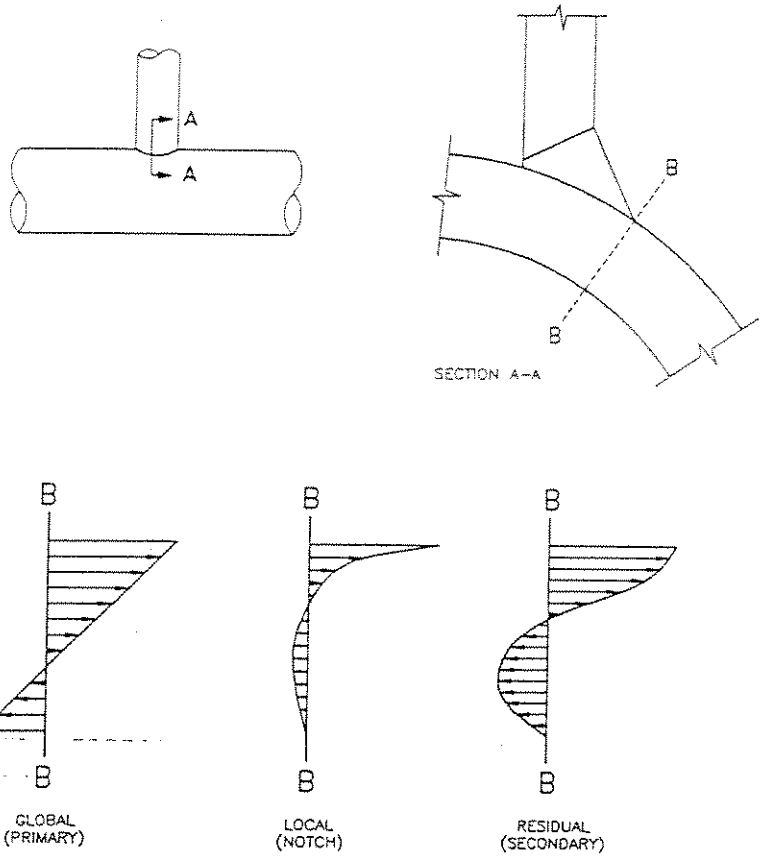

Figure 6.1 Schematic representation of stresses in tubular joints

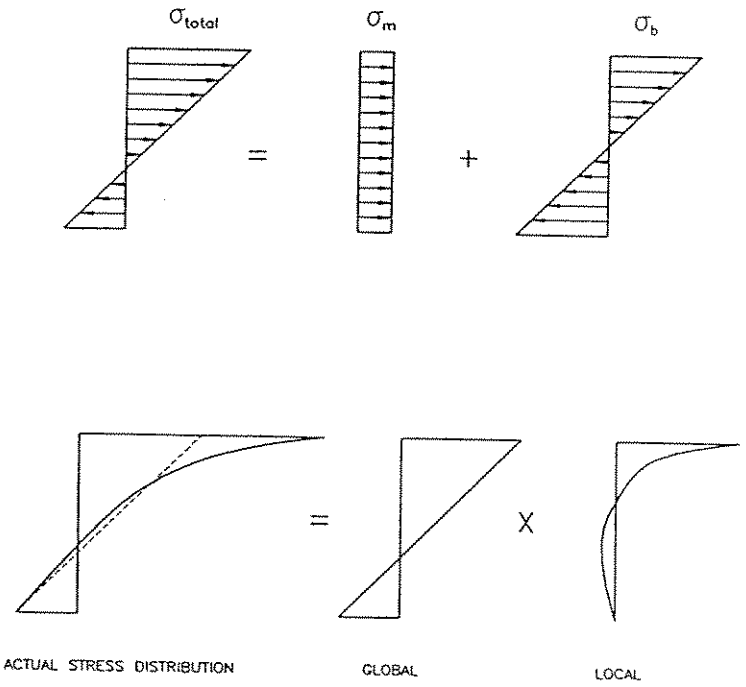

Figure 6.2 Components of global and local stresses in tubular joints

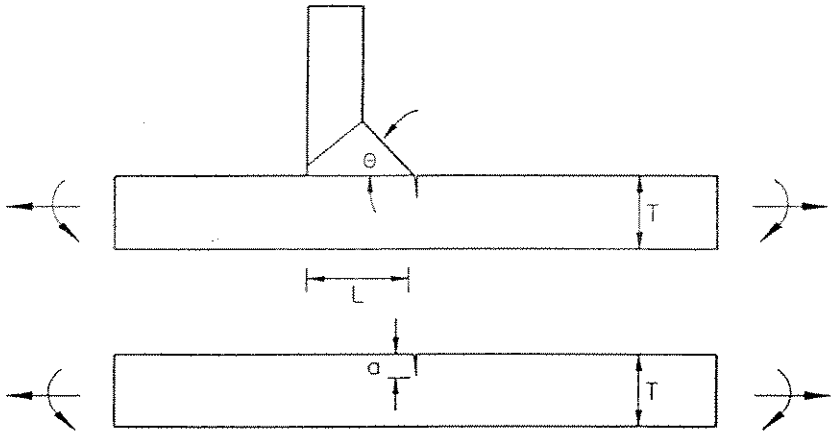

$$Mk\ (2D) = \frac{K_{joint}}{K_{plate}}$$

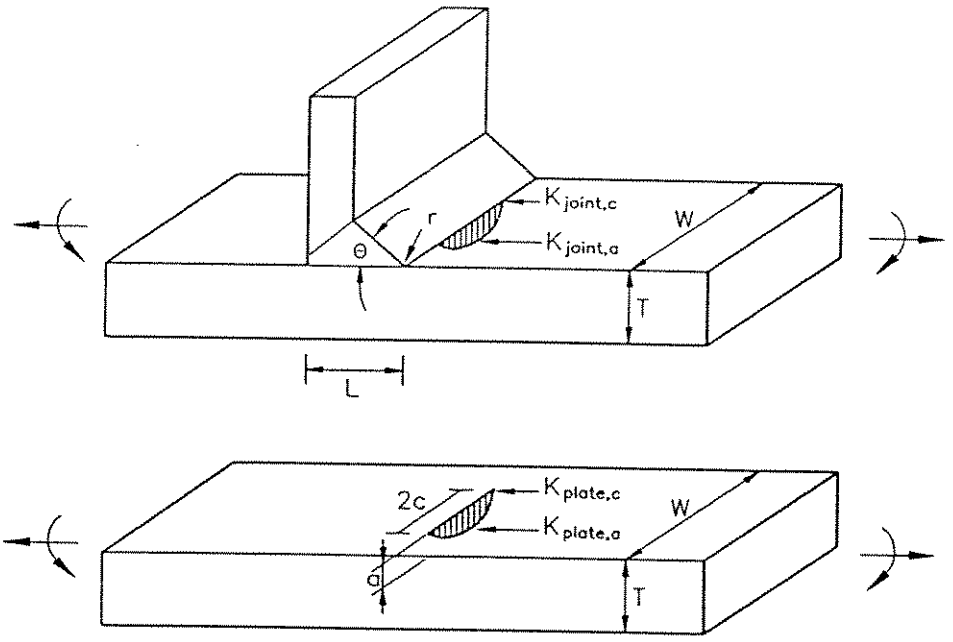

$$Mk_a\ (2D) = \frac{K_{joint,a}}{K_{plate,a}}$$

Figure 6.3 Definitions of Mk

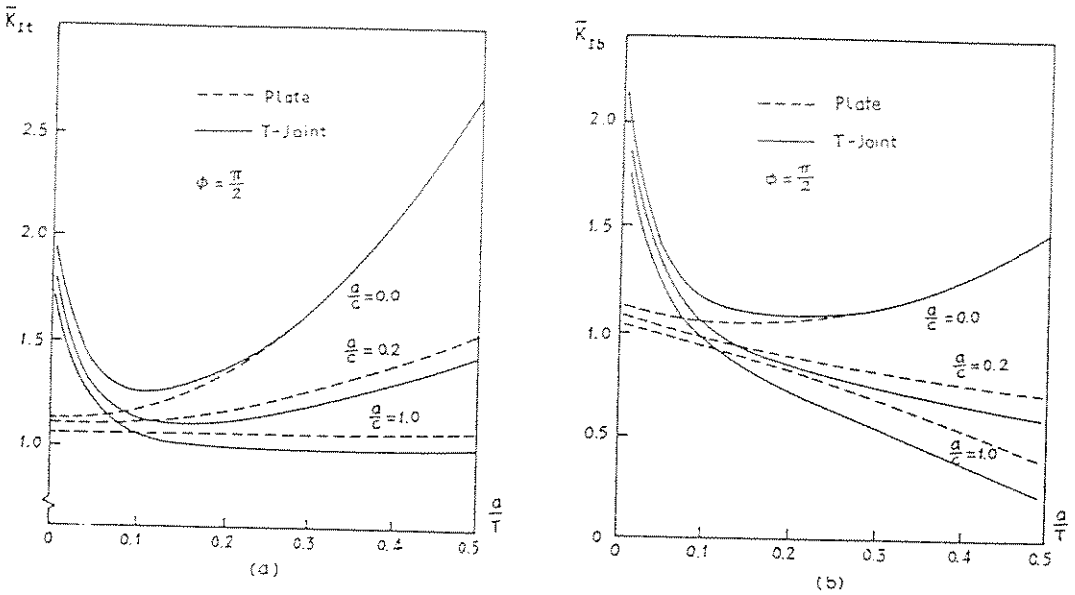

Figure 6.4 Comparison of normalised SIF values for deepest point of the surface of the surface crack front in the welded T butt joints and the plain plates subjected to:
a) tension and b) bending
(Fu et al 1993)

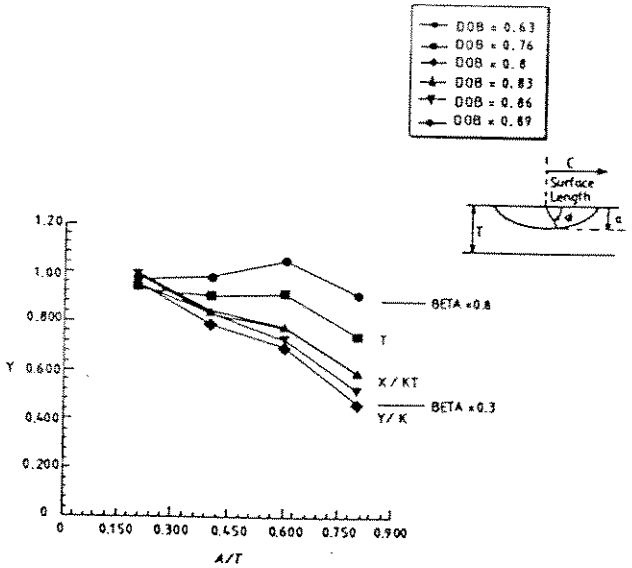

Figure 6.5 Variation of Y with DOB (Haswell 1992)

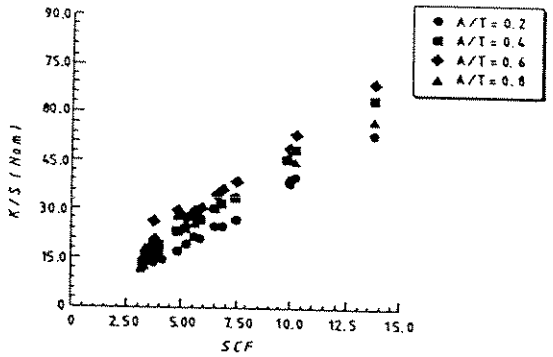

Figure 6.6 Variation of SIF with SCF (Haswell 1992)

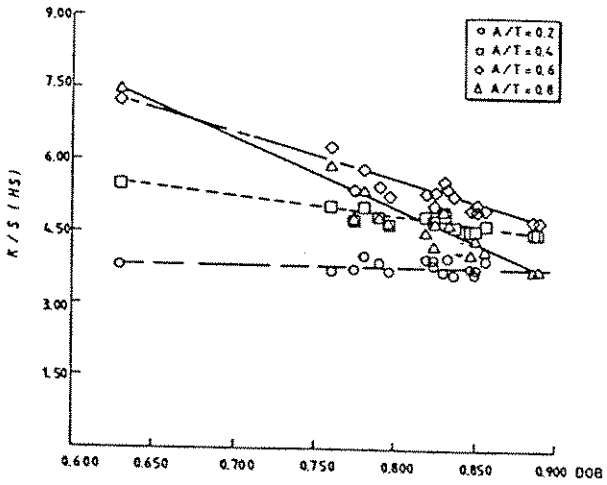

Figure 6.7 Variation of SIF with DOB and proposed model (Haswell 1992)

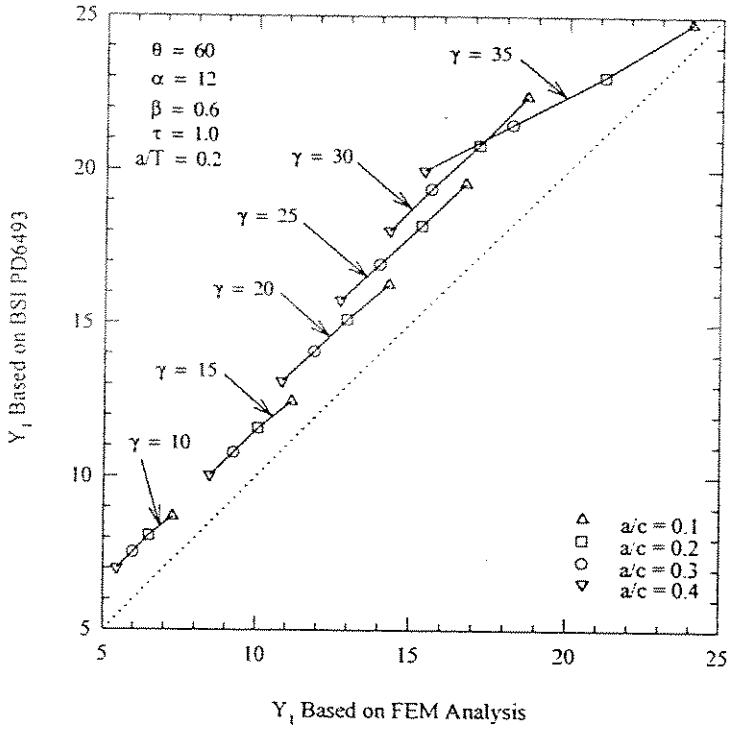

Figure 6.8 Comparison of SIF with BSI's method (method (i)) for a/T = 0.2 (Ho and Zwerneman 1995)

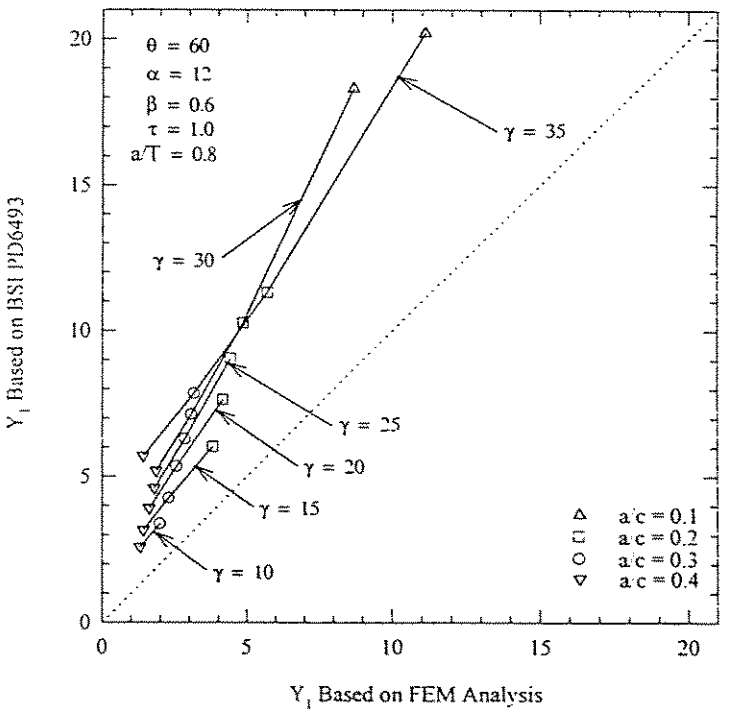

Figure 6.9 Comparison of SIF with BSI's method (method (i)) for a/T = 0.8 (Ho and Zwerneman 1995)

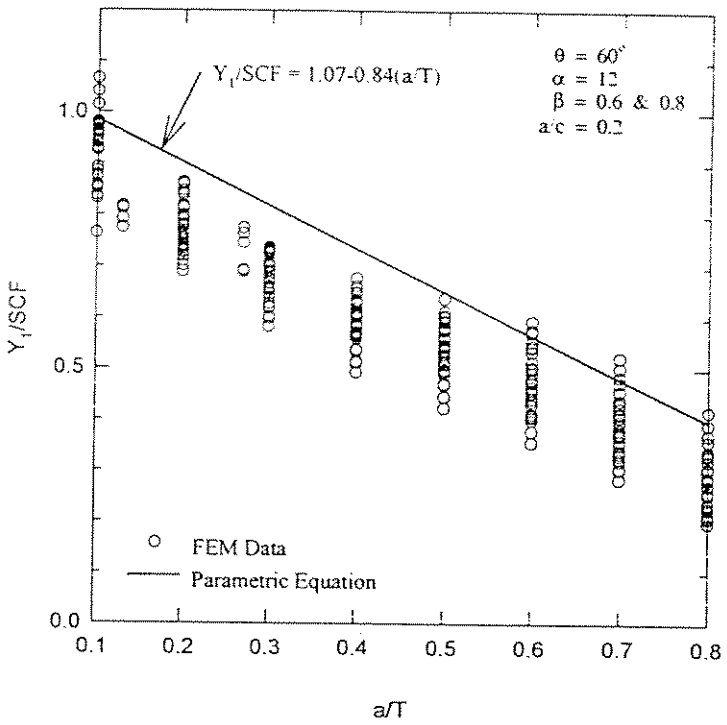

Figure 6.10 Curve fitting for a/c = 0.2 (Ho and Zwerneman 1995)

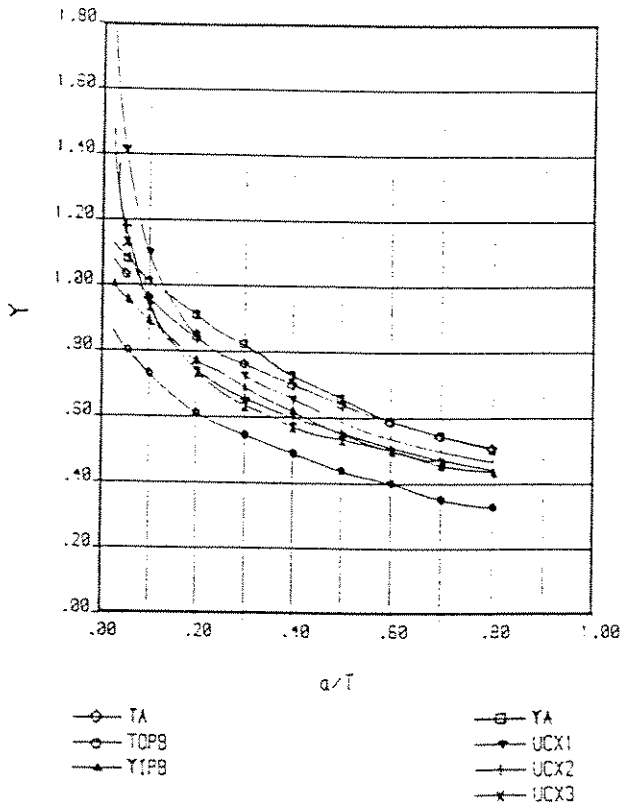

Figure 6.11 Y distribution data (Kam et al 1989)

7. FACTORS AFFECTING FATIGUE ASSESSMENTS

7.1 Residual Stresses

The principal effect of residual stresses is to change the stress intensity factor experienced at the crack tip during load cycling. The different cases of applied stress ratio are considered separately:

1. Positive stress ratio ($R \geq 0$). Effects of tensile residual stress are:

   - K_{max} and K_{min} increased
   - ΔK unchanged
   - Average value of K during load cycle increased.

2. Negative stress ratio ($R < 0$). Effects of tensile residual stress are:

   - K_{max}, ΔK increased
   - K_{min} either unchanged (=0) or increased (>0) depending on relative magnitude of applied and residual stresses
   - Average value of K during load cycle increased.

For both cases 1 and 2 the possibility of fracture is increased, since K_{max} has been increased. Additionally there will be a small increase in crack growth rate, owing to the increase in the average value of K during the cycle (see Section 7.2). For case 2 there will also be a marked increase in crack growth rate, owing to the increase in ΔK (see Equation 1.12). At low stress ranges, for case 2 in particular, there may also be changes in crack growth because of threshold effects.

Assuming that the response is elastic the incorporation of residual stress effects into a crack growth calculation is straightforward. The actual stress intensity factor experienced by a crack is

$$K = K_{app} + K_{res} \qquad 7.1$$

where K_{app} is the stress intensity factor from externally applied loads and K_{res} is the stress intensity factor from the residual stresses, applied as a crack face loading.

During the load cycle, the maximum and minimum stress intensity factors experienced at the crack tip are thus

$$K_{max} = (K_{app})_{max} + K_{res} \qquad 7.2$$

$$K_{min} = (K_{app})_{min} + K_{res} \qquad 7.3$$

where $K_{min} \geq 0$. The variation in stress intensity factor may be calculated from Equation 1.13.

It is generally accepted that in the as-welded condition, yield magnitude tensile residual stresses will exist at the surface of a welded joint. During load cycling at a constant amplitude stress range of $\Delta\sigma$, it is normally assumed Gurney, 1979) that the stress range at the surface will vary between σ_y and (σ_y - $\Delta\sigma$).

Limited information is available for residual stress levels in welded tubular joints. This information, in addition to data for pipe-on-plate and plate joints are reviewed in Section 4.2. Residual stresses will be changed by stress-relieving heat treatments, and may be reduced by in-service loads which cause high stresses at the joints (such as storm loading or installation loads).

7.2 Stress Ratio Effects

In the presence of residual stresses, the effective stress ratio, denoted as R_{eff}, may be expressed as:

$$R_{eff} = \frac{(\sigma_{app})_{min} + \sigma_{res}}{(\sigma_{app})_{max} + \sigma_{res}} \qquad 7.4$$

If $((\sigma_{app})_{max} + \sigma_{res}) \geq \sigma_y$, eg. if $\sigma_{res} = \sigma_y$, R_{eff} may be expressed as:

$$R_{eff} = \frac{\sigma_y - [(\sigma_{app})_{max} - (\sigma_{app})_{min}]}{\sigma_y} = \frac{\sigma_y - \Delta\sigma}{\sigma_y} \qquad 7.5$$

The effect of stress ratio on fatigue crack growth rates for unwelded steels in air is shown schematically in Figure 7.1. The fatigue crack growth rate accelerates at stress intensity ranges approaching the critical fracture toughness K_{IC} in steels of relatively low toughness, due to the intervention of static failure processes. However in most ductile structural steels this does not occur and the crack growth rate increases linearly until the test piece ruptures plastically (Maddox et al, 1978). At intermediate stress intensity ranges the crack growth rate in steels depends only weakly on R, unlike aluminium alloys or stainless steels which show large mean stress effects. The crack growth rate over this region is best described by the simple Paris law given by Equation 1.12. Modifications to the Paris law, reported in Section 7.6, allow the combined effects of residual stresses, stress ratio and threshold to be accounted for.

Maddox et al (1978) have reported that the crack growth rate at an R ratio of 0.5 was between 1.3 and 2.0 times the growth rate at R = 0 for structural steels with yield stresses in the range 256 to 435 N mm^{-2}. Under fully reversed loading the crack growth rate, based on the tensile stress range only, was between 1.65 and 2.5 times the growth rate at R = 0. Similar results have been reported by Johnson and Bretherton (1979) for BS 4360: Grade 50D steel with an increase in growth rate of at most twice for tests conducted at R = +1 over those at R = 0.

7.3 Crack Growth Thresholds

At low stress intensity ranges the fatigue crack growth rate decreases rapidly, ceasing altogether at a limiting threshold value of the stress intensity range. Growth rates close to the threshold are generally found to be more sensitive to mean stress and environmental factors as well as material characteristics. The mean stress effect on fatigue thresholds has been attributed to a reduction in effective stress intensity due to the closure of the crack surface during part of the fatigue cycle. Theoretical crack growth models predict that the crack becomes wedged open by a wake of plastically deformed material adjacent to each fracture surface, although oxide debris or contact between fracture surface asperities may have a predominant effect in practice. Figure 7.2 shows the detrimental effect of high mean stresses and higher tensile strength on fatigue thresholds for steels in air (Richards and Lindley, 1972). A minimum threshold of 2 MPa $m^{(1/2)}$ is found at R ratios above 0.7.

Garwood (1979), has found the following lower bound relationship between fatigue threshold and stress ratio for steels in air:

$$\Delta K_{th} = 6.0 - 4.55R \quad \text{MPa m}^{1/2} \qquad 7.6$$

For weldments, where the effective stress ratio is as given by Equation 7.5, Equation 7.6 becomes:

$$\Delta K_{th} = 1.45 + 4.55 \frac{\Delta\sigma}{\sigma_y} \quad \text{MPa m}^{1/2} \qquad 7.7$$

$$\begin{aligned} \Delta K_{th} &= 170 \quad \text{Nmm}^{-3/2} && \text{for } R < 0 \\ \Delta K_{th} &= 170-214\ R \quad \text{Nmm}^{-3/2} && \text{for } 0 \leq R \leq 0.5 \\ \Delta K_{th} &= 63 \quad \text{Nmm}^{-3/2} && \text{for } 0.5 < R \end{aligned} \qquad 7.8$$

Austen (1983), based on analysis of published data for carbon and carbon manganese steels in air and seawater, proposed the following relationships for 97.7% probability of survival:

If $\sigma_{res} = \sigma_y$, Equation 7.8 becomes:

$$\begin{aligned} \Delta K_{th} &= 214 \frac{\Delta\sigma}{\sigma_y} - 44 \quad \text{Nmm}^{-3/2} && \text{for } \frac{\sigma_y}{2} < \Delta\sigma \\ \Delta K_{th} &= 63 \quad \text{Nmm}^{-3/2} && \text{for } \frac{\sigma_y}{2} \geq \Delta\sigma \end{aligned} \qquad 7.9$$

If there is doubt about the level of residual stress, it is generally recommended that σ_{res} is assumed equal to σ_y, thus Equation 7.9 applies. PD 6493: 1991 recommends Equation 7.8 and allows the use of a, more convenient, constant value of ΔK_{th} when considering variable amplitude loading. The value recommended for as-welded joints is 63 N $mm^{-3/2}$.

A recent review of fatigue crack growth rates in both ferritic and austenitic steels (Section 7.4) indicates that the present PD 6493:1991 recommendations, with regard to ΔK_{th}, are suitable for air and seawater with cathodic protection. However, the study recommends that no fatigue crack growth threshold is assumed for ferritic steels under free corrosion conditions (King, 1985, and King and Stacey, 1996).

7.4 Fatigue Crack Growth Rates

The material constants C and m are key parameters of the Paris Law and of alternative fatigue crack growth laws. These and other relevant parameters such as ΔK_{th} depend on a number of factors including: material, loading, environment, stress ratio, test frequency, wave form and temperature. The choice of values relevant to the applied conditions is an important first step towards obtaining meaningful fatigue life estimates.

With regard to offshore structures, data on crack growth rates in offshore-specific materials such as BS 4360 50D steel have been generated in various environments including air and seawater with and without cathodic protection. Such information together with data on other materials have been reviewed in a number of studies including: Morgan et al (1981) and Booth and Dobbs (1986). These and other studies enabled the experimentally measured crack growth rates to be represented more accurately mainly within the context of the Paris Law. However, as more data have been generated, especially in order to examine environmental effects and growth rates in higher strength steels, it became apparent that in some cases, especially in seawater with cathodic protection, applying the relatively simple Paris Law across the ΔK range may lead to over simplification of the actual behaviour and subsequently to erroneous results (Lambert, 1992 and Tubby et al, 1994).

The above and other issues have been considered in a recent reassessment of fatigue crack growth data in a study which has been performed on behalf of the HSE with a view to providing recommendations for the forthcoming revision of PD 6493:1991 (Offshore Research Focus 1995, King 1985, and King and Stacey, 1996). This review includes:

- Medium and higher strength steels with yield strengths up to 1000 N/mm^2, in air and in seawater under freely corroding conditions and with cathodic protection at levels of -850 and -1050 mV Ag/AgCl.

- Data for austenitic stainless steels in an air environment.

- Threshold stress intensity factors for both ferritic and austenitic steels.

- The effect of R ratio due to mean and residual stress effects.

- Benchmarking the recommendations of the study against experimental SN data for welded joints.

A summary of recommendations from the study to the WEE/37 committee, which is revising PD 6493:1991, has been made available to the Tubular Joints Group on a confidential basis. These recommendations can be outlined as follows:

7.4.1 Air environment

Examination of crack growth data for an air environment has shown a significant effect of R-ratio even within the Paris region. Recommendations have therefore been separated into a low R regime (~0.1), and a high R regime ($\geq$0.5) applicable to as-welded construction. These data include information for high strength steels and are considered appropriate for all ferritic steels with a yield strength up to 1000 MPa.

Air R ~ 0.1

Stage 1	Mean line	$da/dN=1.21\times10^{-26}\ \Delta K^{8.16}$
	Design line (+2 Std. Devn.)	$da/dN=4.37\times10^{-26}\ \Delta K^{8.16}$
Stage 2	Mean line	$da/dN=3.98\times10^{-13}\ \Delta K^{2.88}$
	Design line (+2 Std. Devn.)	$da/dN=6.77\times10^{-13}\ \Delta K^{2.88}$

Air R $\geq$0.5

Stage 1	Mean line	$da/dN=4.80\times10^{-18}\ \Delta K^{5.10}$
	Design line (+2 Std. Devn.)	$da/dN=2.10\times10^{-27}\ \Delta K^{5.10}$
Stage 2	Mean line	$da/dN=5.86\times10^{-13}\ \Delta K^{2.88}$
	Design line (+2 Std. Devn.)	$da/dN=1.29\times10^{-12}\ \Delta K^{2.88}$

In the above Stage 1 refers to the near threshold region whilst Stage 2 is applicable to higher values of ΔK. The crossover point varies with R ratio and to a smaller extent on whether mean or design lines are being used.

Simplified Paris Constants for Air

The following constants can be used for a simple Paris Law approach rather than the bi-linear constants recommended above, however the resulting analysis will be a little more conservative.

R~0.1	Mean line (m=3)	$da/dN=1.5\times10^{-13}\ \Delta K^{3}$
	Design line (+2 Std. Devn.)	$da/dN=3.0\times10^{-13}\ \Delta K^{3}$
R$\geq$0.5	Mean line (m=3)	$da/dN=2.50\times10^{-13}\ \Delta K^{3}$
	Design line (+ 2Std. Devn.)	$da/dN=5.21\times10^{-13}\ \Delta K^{3}$

7.4.2 Steels tested in seawater - Free Corrosion

An R-ratio dependence was observed for ferritic steels in a seawater environment in a similar manner to that found in air, and separate recommendations have been made for each regime. Slight differences were also noted in the slopes of the Stage 1 lines for R~0.1 and R≥0.5, however for convenience a single value was adopted with minimal loss in accuracy.

FC R ~ 0.1

Stage 1	Mean line	$da/dN=3.00\times10^{-14}\ \Delta K^{3.42}$
	Design line (+2 Std. Devn.)	$da/dN=8.55\times10^{-14}\ \Delta K^{3.42}$
Stage 2	Mean line	$da/dN=1.27\times10^{-7}\ \Delta K^{1.30}$
	Design line (+2 Std. Devn.)	$da/dN=1.93\times10^{-7}\ \Delta K^{1.30}$

FC R ≥0.5

Stage 1	Mean line	$da/dN=5.37\times10^{-14}\ \Delta K^{3.42}$
	Design line (+2 Std. Devn.)	$da/dN=1.72\times10^{-13}\ \Delta K^{3.42}$
Stage 2	Mean line	$da/dN=5.67\times10^{-7}\ \Delta K^{1.11}$
	Design line (+2 Std. Devn.)	$da/dN=7.48\times10^{-7}\ \Delta K^{1.11}$

At low values of ΔK (close to the threshold in air) the rates for free corrosion exceed those for air or seawater with cathodic protection by a significant margin, and it appears that anodic dissolution at the crack tip makes a major contribution in crack extension. For this reason it is recommended that no fatigue crack growth threshold (Δk_{th}) is assumed for ferritic steels under free corrosion conditions.

7.4.3 Steels tested in seawater with Cathodic Protection

Data for Stage 1 was not well defined and regression analysis did not provide a rational basis for the formulation of design lines. However, in view of the similarity between air and seawater +CP behaviour in Stage 1 an approach was adopted of superimposing the statistically derived Stage 1 air lines onto the seawater data. This produced a very acceptable fit and it is therefore recommended that common Stage 1 constants are adopted for all non-corroding environments.

Data for Stage 2 was better defined, and a statistical analysis gave the following constants:

-850 mV : R ~ 0.1

Mean line	$da/dN=5.16\times10^{-12}\ \Delta K^{2.67}$
Design line (+2 Std. Devn.)	$da/dN=1.32\times10^{-11}\ \Delta K^{2.67}$

-850 mV : R ≥0.5

Mean line	$da/dN=6.00\times10^{-12}\ \Delta K^{2.67}$
Design line (+2 Std. Devn.)	$da/dN=2.02\times10^{-11}\ \Delta K^{2.67}$

-1050 mV R~0.1

Mean line	$da/dN=5.51x10^{-8}$	$\Delta K^{1.40}$
Design line (+2 Std. Devn.)	$da/dN=9.24x10^{-8}$	$\Delta K^{1.40}$

-1050 mV $R \geq 0.5$

Mean line	$da/dN=5.25x10^{-8}$	$\Delta K^{1.40}$
Design line (+2 Std. Devn.)	$da/dN=1.02x10^{-7}$	$\Delta K^{1.40}$

The slopes of the lines in Stage 2 were virtually independent on R-ratio and, in the same way as the air data, a very slight adjustment was made to make them the same.

7.5 Variable Amplitude Loading

Approaches for quantifying fatigue crack growth under variable amplitude loading in terms of models based on constant amplitude loading, may be broadly grouped into two categories depending on whether or not interaction effects are considered. These refer to effects of load cycles on subsequent cycles. For example, high stress cycles or overloads can cause retardation in crack growth rates, i.e. cycles which occur after an overload cause less growth (or no growth) than cycles which occurred before the overload.

7.5.1 Interaction models

Parameters that affect interaction include the amplitude of overload/underload and the loading history. These are considered in interaction models by determining crack growth on a cycle-by-cycle basis which may entail explicit modelling of effects of residual stresses in the plastic zone ahead of the crack tip, crack tip blunting and crack closure. A number of interaction models have been proposed including those of Willenborg (1971), Wheeler (1970), and the closure model (Newmann 1981). Key features of these models are outlined in UR33 (1985).

Cycle-by-cycle crack growth calculations can be used for structures subjected to deterministic loading. They have found the greatest use in industries where standardised load sequences exist, and where the materials exhibit appreciable interaction effects (e.g. aluminium alloys). However, such cycle-by-cycle calculations are not suited to offshore structures due to a number of factors including the random nature of wave and wind forces, the general lack of information on the sequential occurrence of the associated loading, and the need for time-history simulation. Even if the aforementioned difficulties are overcome, the cost of a cycle-by-cycle evaluation within the context of offshore structures can be prohibitive.

7.5.2 Non-interaction models

These enable a random loading spectrum to be reduced to an equivalent constant amplitude load range by considering the crack growth due to individual load ranges, using a constant amplitude crack growth law, and ignoring load interactions.

If there are p cycles of various magnitudes of stress intensity variations. ΔK_i, an effective constant amplitude ΔK may be defined as:

$$\Delta K_{eff} = \left[(\Delta K_1^m + \Delta K_2^m + \ldots . \Delta K_p^m) / p \right]^{1/m} \qquad 7.10$$

where m is the Paris exponent.

If the distribution of ΔK is expressed as a probability density function, $f(\Delta K)$, then Equation 7.10 may be generalised to give:

$$\Delta K_{eff} = \left[\int_0^\infty \Delta K^m \, f(\Delta K) \, d(\Delta K) \right]^{1/m} \qquad 7.11$$

Substituting ΔK_{eff} for ΔK in Equation 1.12 and performing the crack growth calculation gives the same total crack growth as for the cycle-by-cycle computation, if interaction effects are ignored.

Alternatively, substituting $\Delta\sigma$ for ΔK in the above equations, enables an equivalent constant amplitude stress range, $\Delta\sigma_{eff}$ to be quantified. If this is substituted for $\Delta\sigma$ in Equation 1.14 and crack growth calculation is performed according to Equation 1.12, similar results to those based on the ΔK_{eff} approach would be obtained.

This approach puts the emphasis solely on stress ranges, $\Delta\sigma$, or stress intensity factor ranges, ΔK, weighted by the material property factor, m. The effects of the mean stress and of isolated extreme stress ranges, are therefore lost.

A number of tests have been performed to validate the use of the ΔK_{eff} approach for various random loading sequences. Fatigue tests in air on low-alloy steels and BS 4360 50C steels have been reported to demonstrate good correlations with constant amplitude load cycling (Hibberd and Dover (1977), and Dover (1979)). More recently Thorpe and Rance (OTH 86 232, 1986), performed tests on BS 4360 50D steel in air and seawater under both cathodically protected and freely corroding conditions. They considered the ΔK_{eff} approach and an alternative variant based on the ΔK_{rms} parameter (obtained by substituting 2 for m in Equation 7.10) for comparing constant and variable amplitude crack growth rates. Their findings indicate that although at low crack growth rates, ΔK_{eff} resulted in variable amplitude rates which were higher than those measured under constant amplitude loading especially under cathodic protection, correlations based on ΔK_{eff} were superior to those achieved by using ΔK_{rms}.

The ΔK_{eff} and $\Delta\sigma_{eff}$ approaches can be refined by considering, at each crack increment, the effects of parameters such as residual stresses, stress ratio, and threshold SIF in connection with each loading cycle prior to averaging the weighted contribution of various cycles according to Equation 7.10. In this way, stress ranges which do not cause fatigue crack growth can be removed from the integration procedure. Examples of applications of these refinements are reported by Thurlbeck and Burdekin (1992) and Stacey (1993).

7.6 Paris Law and Proposed Modifications

The Paris simple power law (Equation 1.12) has proved to be a major breakthrough in fatigue crack growth characterisation. However, given the various factors which influence crack growth rates, a number of workers have proposed other crack growth formulae which are often claimed to be superior to the Paris Law. Most of the alternative laws account for the effects of stress ratio and threshold, and/or for the increase in crack growth rate at high values of the stress intensity factor when K_{IC} is approached.

Although a number of studies intended to validate some of the proposed formulae have been published, it is generally found that none of the equations has been proven to offer consistently good results in all crack growth regions under realistic loading and environmental conditions. An additional problem is that the proposed formulae have been derived for constant amplitude loading, and their performance under random loading conditions has rarely been considered. Therefore, in the light of the evidence available at present, these alternative formulae cannot be considered to offer a major advance over the simple Paris Law.

An approach which is frequently been adopted is to use simple modified versions of the Paris Law, rather than the more complicated variants. Such an approach may involve using an effective value of ΔK, which incorporates the effects of residual stresses, stress ratio and threshold, within the framework of the original Paris Law. The values of the constant C and exponent m may also be chosen to reflect different loading and environmental conditions.

An example of this simple approach is given in PD 6493:1991. It is suggested that when crack growth near the threshold is particularly significant, eg. under variable amplitude loading, the following less conservative version of the Paris Law may be justified:

$$\frac{da}{dN} = C(\Delta K_{eff})^m \qquad 7.12$$

where

$$\Delta K_{eff} = \Delta K \quad \text{for} \quad \Delta K > \frac{\Delta K_{th}}{R} \quad \text{and R is positive} \qquad 7.13$$

$$\Delta K_{eff} = \frac{\Delta K - \Delta K_{th}}{1-R} \quad \text{for} \quad \Delta K < \frac{\Delta K_{th}}{R} \quad \text{for any value of R} \qquad 7.14$$

where, ΔK_{th} is evaluated in terms of R according to Equations 7.8 and 7.9, and for welded joints, the effective value of R, incorporating residual stresses, is used (Section 7.2).

Although it is noted that, in the above case, the values of C and m will be usually different from those in the original Paris Equation, no specific recommendations regarding alternative values are given.

Other crack growth equations, some of which attempt to represent the whole (da/dN vs. ΔK) sigmoidal curve of Figure 1.5, are outlined in Appendix D. These include the models of Klesnil and Lucas (1972), Forman et al (1967), Austen et al (1981), and Hudak et al (1985).

7.7 Models for Crack Shape Development

As was noted in Section 2 fatigue cracks initiate from defects randomly distributed along the weld toe. These grow independently under fatigue loading until they are sufficiently close to interact, then coalesce to form a single dominant defect. Application of the Paris Law or one of its derivatives to predict the growth of the initial defects or that of the coalesced single defect may be performed according to a number of models. These can be classified into different categories depending on criteria such as the number of defects (eg. single or multiple), the size and shape of the defect(s), and interaction and coalescence models.

In the following review, crack models are considered in terms of the crack shape characterised by the aspect ratio a/c. This is an important parameter for both the multiple-defect pre-coalescence stage and the single-defect post-coalescence phase.

There are two basic a/c models which may be outlined as follows:

7.7.1 Variable aspect ratio

The aspect ratio is allowed to vary during the analysis, where the crack shape, characterised by a/c, is determined by the loading, geometrical and material conditions under consideration.

In other words, a/c is considered to be a part of the solution rather than a predetermined input parameter.

This model requires consideration of growth at the deepest and two surface points, for example, applying the Paris Law and restricting the attention to the deepest and one surface point only:

$$\frac{da}{dN} = C_a \, (\Delta K_a)^m \qquad 7.15$$

$$\frac{dc}{dN} = C_c \, (\Delta K_c)^m \qquad 7.16$$

where subscripts a and c refer to the deepest point and surface point, respectively. For an increment in crack depth, Δa, the corresponding increment in crack surface length, Δc, is:

$$\Delta c = \frac{C_c}{C_a} \left[\frac{\Delta K_c}{\Delta K_a} \right]^m \Delta a \qquad 7.17$$

This approach can be generalised to allow crack growth to be governed by the conditions under consideration. For example, if the crack grows in the depth direction beyond the region of influence of the weld notch stresses (eg. $a/T \geq 0.3$), ΔK_a may become lower than ΔK_{th}. As a result, growth will occur only at the surface. As the surface length increases, with the depth remaining unchanged, a/c decreases and ΔK_a increases probably until ΔK_a is larger than ΔK_{th} and growth in the depth direction resumes.

7.7.2 Predetermined aspect ratio

The aspect ratio may change or remain constant during the analysis, but in both situations a/c is forced to follow a predetermined function. This approach is normally based on observations of crack growth during experiments (see Section 2). The analyst may choose to adopt a simple model for a/c which may be intended to either resemble the observed experimental trends or represent a lower bound for the observed data. The functions used to represent a/c in terms of crack size and/or crack shape are known as the forcing functions. These may be of varying complexity depending on the type and purpose of the analysis. The simplest models consist of assuming that the crack aspect ratio remains constant, eg. a/c = 0 (straight fronted crack), or a/c = 0.1 (shallow crack). Evaluation of the fatigue life in this case requires integration of, eg. the Paris Law, either in the depth direction or on the surface only. More complex models include those proposed by Bell et al (1987) based on tests of welded plate joints, Eide and Berge (1987) based on tests of large scale plate girders, and Smith and Gurney (1986) based on data for stiffeners on plates in tension.

Each of these models involves two forcing functions, one for small defects, normally characterising the pre-coalescence phase, and another function describing the crack shape for deeper cracks after coalescence. The Bell et al model is as follows:

$$\frac{a}{c} = e^{-ka} \qquad 7.18$$

$$k = 2.09 * 10^{-6} (S_p)^{1.95} \qquad 7.19$$

$$S_p = K_t S_n = \left[1 + 0.512\, \theta^{0.572} \left(\frac{T}{r}\right)^{0.469}\right] S_n \qquad 7.20$$

where k is a function of stress level and weld toe geometry; k_p and k_n are the weld toe peak and nominal stresses, respectively; and the stress concentration K_t, given in terms of the weld angle, θ, and radius, r, is based on work by Niu and Glinka (1987).

Equations 7.18-7.20 are intended to represent the coalescence phase. This is assumed to end when a/c = 0.2. Thereafter, the coalesced crack is assumed to grow as a straight fronted crack (a/c = 0.0).

Dover et al (1988), based on data from a number of tubular joint tests, proposed the following model which assumes that crack coalescence occurs at a/T = 0.1.

$$\frac{a}{c} = \frac{a}{T} \qquad \text{for} \quad 0 < \frac{a}{T} < 0.1$$

$$\frac{a}{c} = 0.2\, \frac{a}{T} \qquad \text{for} \quad 0.1 < \frac{a}{T} < 1.0 \qquad 7.21$$

Haswell (1992) proposed a three-level approach providing models for crack shape development of varying sophistication, which range from simple forcing functions to combination of these with a general variable aspect ratio model. The proposed approach is reported in Table 7.1.

In general, forcing functions, based on specific crack growth data, will include all the parameters controlling the observed shape development for the joints considered. However, the validity of these functions is likely to be restricted to the conditions from which they were derived including global and local joint geometry, joint loading, and initial defect distribution.

Other approaches have been proposed, which, although would appear to offer more generality and less restrictions than the above models, still rely on some forcing elements. Two such approaches have been put forward by Snijder et al (1985) and Shetty and Baker (1990).

The Snijder model, also proposed by Morgan (1989), considers multiple initiated cracks of the same dimensions and intermediate spacing growing independently until they touch. Thus, if n initiation points are assumed, at coalescence the crack length increases discretely from 2c to n*(2c). It was reported that this model can be used to predict growth in T plate joints and in a tubular X joints with reasonable success. More recently, Thurlbeck (1991) applied the model in a wide ranging study and reported good agreement with experimental data. A disadvantage of the Snijder model is that it requires assumptions regarding the number and spacing of the initial defects as well as the initial defect geometry.

In the Shetty and Baker model, crack coalescence is modelled by considering a damage zone of length equal to 0.02d within which a number of cracks initiate and grow, where d is the brace diameter. Crack coalescence is assumed to be complete when the crack initiated at the hot spot reaches a depth of 3mm. On coalescence, the crack length is set to the length of the damage zone. Predictions based on the model are reported to be in good agreement with tubular joints experimental data.

7.8 Load Shedding

When the stiffness of a structural element in a redundant structure decreases, eg. as a result of hinge or crack forming, load paths in the structure change and the load sheds away from the element with the reduced stiffness. This phenomenon is often referred to as load shedding, and with regard to tubular joints, may be considered within a global or a local context.

Global load shedding concerns member forces which can be estimated from a linear elastic analysis of the whole three-dimensional frame. In this case, a structural element (eg. a tubular joint) would be expected to attract lower forces in the cracked than in the uncracked condition. The magnitude of decrease in member forces, resulting form load shedding, depends on the member under consideration and level of redundancy in the frame, ie. whether alternative load paths exist. The simplest method to quantify global load shedding is to reanalyse the frame with allowance made for the reduced member stiffness. It is beyond the scope of this section to elaborate on the issue of global load shedding, instead attention will be restricted to local load shedding (referred to hereafter simply as load shedding) which is usually dealt with on a component level, eg. in isolated tubular joints.

Most work on load shedding has been related to its effects on stress intensity factors and fatigue life of simple tubular joints. It is based on the observation that, in some cases, theoretical SIF predictions are higher than those obtained experimentally from laboratory tests. Such theoretical predictions are often based on plate models and stresses from the uncracked body in conjunction with either the Raju and Newman solutions for semi-elliptical surface cracks, or the O integral based weight function method. The experimental SIF data are obtained according to the empirical approach of Dover and co-workers at UCL, which is based on interpreting measured crack growth rates in tubular joints according to the Paris law.

Using such comparisons, Aaghaakouchak et al (1989) argued that overprediction of SIF is due to ignoring the load shedding associated with crack development and that, while in a plate model, the same stresses are assumed to be transferred through the cracked section regardless of the crack size and/or the stiffness of the cracked section, a partially cracked chord in a tubular joint is subjected to bending stresses which decrease as the crack becomes deeper. Based on this argument and a limited 2-dimensional FE study of edge-cracked flat plates and rings under different boundary conditions, Aaghaakouchak et al proposed a 'linear moment release model' to simulate the effects of load shedding. This model consists of reducing the bending component of the applied stresses at the hot spot according to the following relationship:

$$\sigma_b = \sigma_{bo} (1 - a/T) \qquad 7.22$$

where σ_b and σ_{bo} are the bending stresses in the cracked and uncracked body, respectively, a is the crack depth and T is the plate thickness.

Thus, the growth of a crack at the hot spot through the thickness leads to a significant decrease in the applied stresses and the associated crack driving force. This stress relaxation increases with the crack depth. When the crack penetrates the thickness, it is assumed to behave as a hinge which allows the transfer of membrane stresses only.

More recently, Forbes et al (1992) reported experimental data on the differences between load shedding in plate and in tubular joints. It was found that the decay of stresses in tubular joints was greater than in similarly loaded flat plates. In addition, the accuracy of SIF predictions in comparison with tubular joint empirical data, was reported to improve when the stresses used in the calculations were decreased by an amount similar to that measured experimentally. It was also noted that while load shedding was more important for deep cracks ($a/T > 0.5$) the effect of the non-linear stress distribution, associated with the weld notch stresses, was more important for early growth of small cracks. However, no load shedding model suitable for routine applications was proposed.

Berge et al (1994) measured stress relaxation in a tubular T joint subjected to IPB fatigue loading. They found that stresses in the chord at 24mm away from the weld toe (brace thickness is 16mm) agreed qualitatively with the aforementioned 'linear moment release model'. However the measured stresses were lower than those predicted using the model, ie. Equation 7.22.

It should be noted that while the available data on load shedding are very limited, caution is advised when applying the above or other models for stress relaxation. The following points should be considered:

- If stress intensity factors are evaluated using one of the direct methods, ie. with explicit crack modelling, load shedding will be implicitly accounted for in the structural model. In this case, the model does not require consideration of stresses in the uncracked condition and may involve three-dimensional crack idealisation or line spring finite elements. Empirical data also include the effects of load shedding.

- Known validations of load shedding models incorporate a large number of assumptions which are often inevitable in simplified fracture mechanics calculations. However, the influences of these assumptions on the predicted SIFs are often not reported or considered with sufficient detail, which is bound to affect the applicability of the results to more general practical cases.

- Ignoring load shedding is conservative because it leads to higher SIF and fatigue life predictions. The overprediction is most significant for deeper cracks, eg. $a/T > 0.5$. If most of the fatigue life is spent in the shallower regions ($a/T < 0.2$), the overall effect of ignoring load shedding on the predicted fatigue life will be relatively small. However, the effect on remaining fatigue life of defects found in-service may be significant.

- The degree of conservatism of models for SIF predictions using uncracked body stresses is in decreasing order:
  a) Load shedding is ignored.
  b) Load shedding is modelled using a parabolic moment release model which predicts higher stresses than the linear model.
  c) Load shedding is modelled using the linear moment release model.

- Strictly speaking, assuming that the brace nominal stresses are constant, any decrease of stresses at the centre of a semi-elliptical crack, occurs at the expense of an equivalent increase of stresses in the uncracked ligament near to the ends of the crack. Therefore, if may be argued that a theoretical model should not be restricted to consideration of the change of stresses at the deepest point only.

Assessment Level Parameter	1	2	3
SCF	Parametric Equations	Simple uncracked joint analysis	Complex uncracked joint analysis
DoB	0.5	As above	As above
a/T < 0.2 a/T = 0.2-0.8	Infinite plate x Mk Infinite plate	Infinite plate x Mk Tubular joint Fracture mechanics Model (Eqn. 12)	Complex cracked joint analysis
a a/T < 0.15 2c a/T > 0.15	0.1 (constant)	0.5 (constant) 0.1 (constant)	0.5 (constant) Variable/measured
Load history	Equivalent stress and no. of cycles	Full spectrum	Full spectrum

Table 7.1
Assessment level assumption, Haswell (1992)

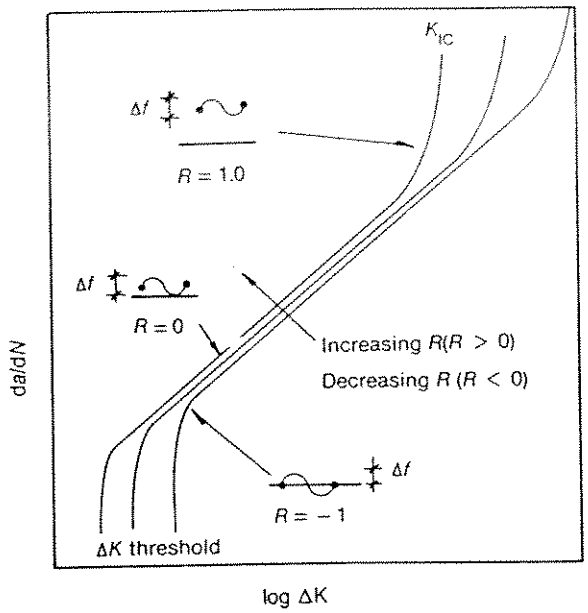

Figure 7.1 Schematic crack growth showing effect of R ratio for unwelded steels in air

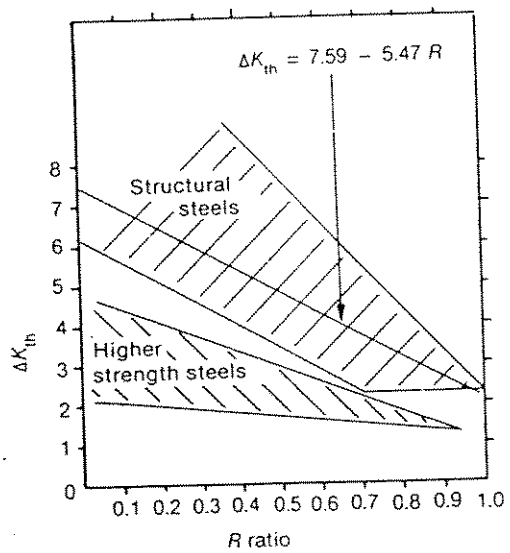

Figure 7.2 Effect of R ratio on threshold stress intensity

8. FACTORS AFFECTING FRACTURE ASSESSMENT

8.1 Some Aspects of the Failure Assessment Diagram

The Failure Assessment Diagram (FAD) approach is widely accepted as one of the most sophisticated and versatile techniques to conduct fitness-for-purpose fracture assessments (Section 1.6). However, this versatility and the potentials for improved accuracy associated with assessments using Level 2 or Level 3 were generally achieved at the expense of simplicity. Consequently, the Level 2 and 3 fracture procedures are relatively more complex to apply than the simpler treatment of the 1980 Edition of PD 6493 which was based on the CTOD design curve approach.

In practice, application of the fracture procedures of PD 6493:1991 may yield significantly different results depending on the input parameters and solution models that the analyst adopts. This is partly due to the fact that PD 6493:1991 is intended for general applications and does not necessarily provide optimal solutions for all types of welded joints. This would appear to allow the general recommendations given in the document to be interpreted in a number of different ways depending on the type of welded joint, its service conditions and the analyst experience.

Factors that could influence the outcome of a fracture assessment include:

- Applied stress model including through thickness stress distribution.
- Residual stress model and whether or not relaxation under the effect of high applied loading (primary loading) could be applied.
- Material properties in general and the material fracture toughness in particular. The absence of reliable and relevant data may necessitate the use of lower bound estimates and the application of pessimistic safety factors.
- Model adopted for the plastic collapse parameter S_r, eg. whether local or global collapse is considered.
- Crack geometry, its idealisation as a simple geometrical shape, and scope of the assessment, i.e. number and location of points along the crack front where fracture assessments are performed.
- Procedure adopted for determining critical solutions. In some cases it is possible to obtain non-unique critical solutions, i.e. multiple fracture assessment solutions.
- Scatter associated with input parameters, and whether partial safety factors which are intended to account for such scatter are applied. Appendix A of PD 6493:1991

provides guidance of safety factors relating to stress, fracture toughness and defect size.

- Choice of level of assessment and of the associated FAD. Level 2 is recommended for general structural steel applications including tubular joints. The Level 2 treatment which uses the strip yield model elastic plastic based FAD is reported to have been chosen as the Normal Treatment for assessing the significance of defects in welded structures because the stress-strain curves for weld metals usually shows high yield to ultimate strength ratios approximating to such behaviour (Burdekin et al 1992).

Some of the above issues are considered in more detail in the following sections.

8.2 Idealisation of Surface Defects and Scope of Assessment

Surface part thickness cracks found during in-service inspection may be non-symmetrical, i.e. the deepest point may be non-equidistant to the end-points. A simple method to assess this condition using solutions for symmetrical cracks, consists of assuming that the crack is formed of two independent halves with the deepest point common to both halves. In this way, each half is idealised as a quarter-elliptical crack and treated independently from the other half.

With regard to choice of positions on the crack front for consideration in a fracture assessment of a surface part thickness crack, it may be argued that since both the crack driving force and material toughness vary along the crack front, a comprehensive fracture analysis should involve assessing a large set of representative positions. However, due to a number of practical considerations, which include considerable uncertainties associated with determining both the driving force and material resistance parameters, assessments are generally carried out at only a limited number of positions, namely the deepest point and two end points.

While it is possible to determine the crack driving force parameter at any position on the front of a surface crack, eg. using finite element analysis, current codified fracture toughness testing procedures are restricted to determining one estimate only of the fracture toughness. This is associated with specimens containing deep fatigue precracked notches, designed to maximise geometric constraint and encourage the onset of crack extension, leading to a geometry-independent lower bound estimate of toughness.

With regard to plastic collapse, the distinction between solutions at various positions on the crack front depends on whether local elastic stresses or global joint capacities are used to determine the parameter S_r. Since joint capacities are associated with global collapse of the whole joint, only one estimate of collapse load is possible. However, with local elastic stresses different solutions for S_r may be obtained at the deepest and two end point positions.

8.3 Models for the Plastic Collapse Parameter

8.3.1 Introduction

This section provides a review of plastic collapse solutions for tubular joints containing weld toe defects at the brace/chord intersection.

A 'conventional' definition of the plastic collapse capacity of a flawed joint is that it represents the ultimate load that the joint can sustain in the absence of crack extension. However, in the context of the FAD approach, an additional requirement is that the plastic collapse load used for quantifying the parameter S_r (or L_r) must not exceed the load at which the value of J-integral becomes unbounded. Such an increase in J results from the increase in plasticity at the crack tip position and it characterises the shape of the FAD.

Therefore the solutions reviewed below are intended to characterise the proximity of a flawed joint to failure by plastic collapse, and to limit the plasticity at the crack tip to levels which are contained within those assumed in the assessment diagrams.

While local or global collapse solutions may be relevant for the assessment of surface cracks, only global collapse solutions are likely to apply in the case of through thickness cracks. Available collapse solutions are usually based on a plate or a tubular joint model. A plate model is appropriate for cracks on the brace side, while cracks on the chord side may be assessed using a plate or a tubular joint model.

8.3.2 Plate based collapse solutions

PD6493:1991 gives plastic collapse solutions for flat plates containing through thickness, surface and embedded cracks. The solutions are presented in the form of net section stresses. These are expressed in terms of the membrane and bending stresses, assumed to be calculated elastically in the crack free plate, and in terms of the crack and plate dimensions.

The background analysis given by Willoughby and Davey (1989) for part-wall defects, is based on two-dimensional limit load analysis of a plate containing an infinitely long part-wall (surface or embedded) crack. Since the presence of the crack causes the neutral axis to move away from the tensile axis, an additional bending moment will be present because of the eccentric tensile load. If there is negligible bending restraint, this additional moment will be applied to the net section, but if there is normal bending restraint, the additional moment will be carried externally.

Willoughby and Davey gave solutions for both types of restraints in the case of surface cracks, and solutions assuming negligible bending restraint in the case of embedded cracks.

These two-dimensional solutions which assume an infinitely long crack, are conservative for cracks of finite lengths, since a part of the load can be carried by the uncracked section on either side of the crack. To account for this condition, an effective crack depth/thickness ratio is used, which is broadly similar to what was proposed earlier in CEGB/R6 Revision 2. The crack is assumed to be rectangular in an effective cross section of B*(2c+2B), where B and 2c are the thickness of cross section and length of crack, respectively.

Thus, the effective crack depth/thickness ratio is given by:

$$C_{eff} = \frac{2ac}{B(2c + 2B)} \qquad 8.1$$

where a is the depth of a surface crack or hight of an embedded crack.

Using this approximation the following solutions were obtained:

$$\sigma_n = \frac{\sigma_b + [\sigma_b^2 + 9\sigma_m^2(1-\alpha)^2]^{0.5}}{3(1-\alpha)^2} \qquad 8.2$$

For surface cracks subjected to normal bending restraint, and

$$\sigma_n = \frac{\sigma_b + 3\sigma_m\alpha + [(\sigma_b + 3\sigma_m\alpha)^2 + 9\sigma_m^2(1-\alpha)^2]^{0.5}}{3(1-\alpha)^2} \qquad 8.3$$

For surface cracks subjected to negligible bending restraint.

where

$\alpha = (a/T)/[1 + (T/c)]$ for $W \geq 2(c+T)$

$\alpha = (2a/T)(c/W)$ for $W < 2(c+T)$

These and a similar solution for embedded cracks were then compared to experimental plastic collapse loads for cracked steel plates subjected to tension or bending loads. It was concluded that the solutions gave conservative estimates in all cases except for materials of very high work hardening capacity. This discrepancy was attributed to inappropriate estimates of the flow strength.

Since the above solutions are associated with failure of an effective area adjacent to the crack front, they are local collapse solutions which may potentially be very conservative for tubular joints with weld toe cracks on the chord side. The collapse behaviour in such geometries is more complex than in plates. It involves local yielding starting at one position around the intersection and spreading around the joint but remaining contained by elastic behaviour until full collapse occurs. The effect of cracks is basically to relieve local yielding conditions without causing a major redistribution of stresses.

Recent elastic-plastic finite element studies on a tubular T joint containing a weld toe surface crack in the chord, carried out by Kristiansen and Turner (1992), showed that the local collapse of the ligament was reached at a load level well below the global collapse load of the joint. It was noted that 'the first stage of yield through the remaining ligament has not led to a rapid upswing in J or any non-linearity in the load displacement', which indicates that, in this case, the use of the local collapse load to calculate S_r or L_r would lead to a very conservative fracture assessment.

With regard to through thickness cracks, PD 6493:1991 recommends the following solution based on a simple limit load analysis of a finite plate containing a through thickness crack and subjected to a combination of tensile and bending loading:

$$\sigma_n = \frac{\sigma_b + (\sigma_b^2 + 9\sigma_m^2)^{0.5}}{3[1-(2a/W)]} \qquad 8.4$$

8.3.3 Tubular joint based collapse solutions

These are usually based on relating the plastic collapse load of a cracked joint to that of an uncracked joint of nominally similar geometry and material properties. The advantage of this approach is that there is substantial empirical design guidance for assessing the ultimate strength of uncracked joints.

The plastic collapse load of a cracked joint is inferred from that of an uncracked joint by applying correction factors to the ultimate capacity in the uncracked condition. Such factors are functions of the crack and joint geometries, and are based on experimental and/or numerical data.

The data available at present are for simple T and DT joints containing through thickness cracks at the saddle position and subjected to tension loading, and gapped K joints containing through thickness cracks at the crown location in the gap and subjected to balanced axial loading (Cheaitani and Burdekin, 1994).

Analysis of the data indicates that, except at high β ($\geq$0.79), the reduction in strength due to the cracks was lower than the associated reduction in the punching shear area. Thus, it is suggested that estimates of the plastic collapse strength of cracked joints can be obtained by multiplying the strength of the uncracked joints, with the same geometry, by an 'area reduction factor' to take account of net section area as follows:

$$\textit{Area reduction factor} = \left[1 - \frac{\textit{crack area}}{\textit{intersection length} * T}\right] * \left[\frac{1}{Q_\beta}\right]^m \qquad 8.5$$

where

- T is the chord thickness
- $Q_\beta = 1$ for $\beta \leq 0.6$
  $Q_\beta = 0.3/(\beta(1-0.833\beta))$ for $\beta > 0.6$
- The uncracked joint strength (for K joints under balanced axial loading) is estimated as either the Department of Energy (DEn/HSE, 1990) characteristic compression design strength with m = 1, or the API (API, 1993) compression design strength with m = 0 (Q_β correction is not required).
- The uncracked joint strength (for T and DT joints under tension) may be estimated as either the Department of Energy (DEn/HSE, 1990) characteristic tension design strength with m = 1, or the API (API, 1993) tension design strength with m = 0 (Q_β correction is not required).

The above predictions of uncracked joint strength were obtained without applying the safety factors recommended by DEn/HSE and API for normal or severe operating loading conditions. In practice, the application of these factors would enhance the margin of safety.

It must be stressed that the above tubular joint model has been validated for a range of simple joints subjected to axial loading as outlined above. Therefore, it may be unconservative to apply the above approach to other joint types or joint loading.

It must also be stressed that plastic collapse models are independent of scale as far as plastic collapse behaviour is concerned and are intended only to assist in defining the plastic collapse parameter of the failure assessment diagram. Fracture behaviour requires separate consideration of the absolute effects of crack size and would be covered by consideration of the fracture axis on the failure assessment diagram.

8.4 Fracture Toughness Properties

Relevant fracture toughness data are one of the essential ingredients for any meaningful fracture assessment. The data should apply to the material in which the flaw under consideration lies. This is due to the fact that fracture assessment procedures assume that defects are located in materials of uniform properties.

In general, the fracture toughness for a specific material depends on a number of parameters which include constraint, microstructure, orientation, temperature and rate of loading. Therefore, a meaningful test must ensure that all these parameters are considered, eg. the test specimen should preferably be equal in thickness to the actual structure and should be produced using the same welding procedures, materials and consumables, used during construction.

Tests for measuring the fracture toughness are codified in a number of national and industry standards (see Section 9). The aim of these tests is to determine the critical value for a crack driving force parameter. This may be based on K, CTOD or J methods. While conversion between these parameters may be permitted (e.g. between K and J data), caution is advised due to the effects of ductility and constraint which may render a conversion inappropriate and unsafe.

An alternative to conversion between K and CTOD data, which is not permitted according to PD 6493:1991, is to adopt an appropriate assessment route, ie. based on K or CTOD methods.

Usually, the type and quality of the available toughness data determines which assessment route should be adopted, eg. PD 6493:1991 allows two routes, based on K and CTOD approaches, and three assessment levels. The lowest and most conservative of these, Level 1, may be appropriate when only Charpy or very limited data exist.

When no toughness data are available and only Charpy data exist, empirical correlations which are intended to enable K or CTOD estimates to be inferred from Charpy values may be used. However, caution should be exercised in selecting correlations relevant to the type of material under consideration. Uncertainties and scatter in the correlation data must be considered and accounted for conservatively.

8.5 Residual Stresses

Residual stresses can have a detrimental effect on the resistance of welded joints to fracture. They usually act as secondary stresses, ie. they do not contribute to plastic collapse, but may cause an increase in the severity of local conditions at the crack tip.

Within the context of the FAD approach, this effect is quantified in terms of an increase in the magnitude of the fracture parameter due to two contributions:

- The secondary stress intensity factor whose magnitude depends on the assumed residual stress distribution. A detailed evaluation of stress intensity factors due to typical residual stress distributions is reported by Stacey (1993).

- the plasticity correction factor which accounts for the non linear interaction between plasticity due to both primary and secondary stresses. The value of this factor depends on the ratio of secondary to primary stress. At primary stress levels approaching plastic collapse the magnitude of both the secondary stress and the plasticity correction factor approach zero.

Where the distribution of residual stresses in an as-welded joint is unknown, it is usual practice to assume that the residual stress is uniform across the thickness and equal to the yield strength. This assumption may be pessimistic but it is conservative and, at high applied stresses (high S_r), the assumed uniform residual stress may be relaxed to the lower of σ_y or:

$$\sigma_{residual} = \left(1.4 - \frac{\sigma_n}{\sigma_f}\right)\sigma_y \qquad 8.6$$

The philosophy behind this relaxation, which is allowed by PD 6493:1991, is that for high applied load levels (high primary stress) the sum of the net section stress, σ_n, and the secondary residual stress (assumed uniform across the thickness), is limited by the flow strength, σ_f, of the material (Burdekin el al 1988).

By contrast, PD 6493:1991 does not permit relaxation of alternative residual stress distributions under the effect of high applied load levels, presumably due to the general lack of data to support such relaxation.

An investigation illustrating the redistribution of residual stresses at the weld too of a T-butt joint under the effects of interaction with high applied load levels was undertaken by Mok and Pick (1990). Loads of 25 MPa and 50 MPa, corresponding to hot-spot stresses of 250 MPa and 500 MPa, respectively, were applied to the attachment of the T-butt joint. The residual stress distributions before and after application of the two loads are shown in Figure 8.1 (from Stacey 1993). This figure indicates significant redistributions especially in the immediate vicinity of the weld toe. In that region, the higher applied load (50 MPa) caused the residual stress to reverse sign and become compressive. Furthermore, both applied loads appear to have led to shifting of the regions of tensile residual stresses through the thickness away from the weld toe.

8.6 Tensile Properties

The behaviour of flawed structures under static tension loading is generally governed by brittle and ductile failure mechanisms which involve, respectively, limited and extensive yielding. As a result, the tensile properties of the material in which the defect lies play an important role, alongside its toughness properties, in determining the mode of failure and the ultimate load that the structure can sustain.

Assessments using Levels 1 or 2 of PD 6493:1991, require knowledge of the yield and tensile strengths together with the modulus of elasticity. The tensile properties are partly used to determine the flow strength, usually taken as the average of the yield and tensile strengths. This is an important parameter for determining the proximity of a flawed structure to failure by plastic collapse, and is intended to account implicitly for strain hardening.

At the more advanced Level 3, intended for tearing analysis and high strain hardening materials, PD 6493:1991 and CEGB/R6 allow assessment diagrams to be constructed as functions of the material stress-strain curve. In this case, detailed tensile information is required especially for strains below 1%.

While welded joints contain different regions which can have significantly different tensile properties, current fracture assessment procedures assume that defects are located in homogeneous materials of uniform properties. Consequently, differences in tensile properties between the weld, heat affected zone (HAZ) and parent metal can not be accounted for, and it is normal practice to use the tensile properties of the material in which the defect lies. However, if a defect is located in the heat affected zone or at the weld fusion boundary, the tensile properties are generally not known. In such cases and in order to ensure conservative assessments the lower properties of the adjacent weld and parent metal are used to estimate the crack driving force.

8.7 Uncertainties in Data

In order to account for the effects of uncertainties in input data on FAD-based fracture assessments using either the Level 2 or Level 3 treatments of PD 6493:1991, partial safety factors may be applied to key input parameters, namely stress, fracture toughness and defect size. Such factors are included in Appendix A of the document and are based on work undertaken jointly at Glasgow University and UMIST as a part of the MTD/SERC Defect Assessment Programme.

The approach taken in the above work was to use first order second moment β reliability index methods to determine the relationship between safety factors and probability of failure for different variabilities or uncertainties in the input parameters for the defect assessment equations. For design purposes the results were presented in the form of partial safety factors applied to stress, fracture toughness and defect size. These partial safety factors were calibrated using the Level 2 fracture assessment procedure of PD6493:1991 and different values were derived for moderate or severe consequences of failure (Plane et al 1987). The resulting partial safety factors have been included in PD6493 as an optional appendix in order that users may get familiar with the concepts (Burdekin et al 1992).

Alternatively users may continue to use worst case assumptions for the input data but this provides little idea of the real position on safety margins. The partial safety factors γ_s, γ_a, on stress and defect size respectively should be applied to best estimates of the input data, whilst γ_t on fracture toughness should be applied to the minimum value of three results or equivalent as given in PD 6493.

8.8 Non-Unique Critical Solutions

Non-unique critical solutions are possible when performing fracture assessments using the FAD approach. This can have serious implications since it may lead unwary analysts to conclude that critical solutions have been determined when other solutions associated with smaller critical defects or lower critical load levels have not been detected. Phaal (1994) considered a number of cases where multiple critical solutions could be predicted and concluded that possible causes for this phenomenon include:

- Decreasing stress field such as may be associated with primary or residual bending stresses, thermal shock or flaws at weld toes or other stress concentrations.
- Pure membrane loading, dependent on the Raju and Newman stress intensity factor solutions, resulting in a decreasing stress field.
- Residual stress relaxation because of prior proof testing or high primary loading, resulting in a decreasing stress field.
- Flaw re-characterisation.

In order to improve the capability of computerised automation of FAD-based assessment procedures to account for non-unique solutions, Phaal recommends the following two strategies:

- The iteration method chosen must always converge to the smallest critical flaw size or lowest critical stress.
- If a flaw of known dimension is assessed as being safe, a check must be to indicate whether smaller flaws may be unsafe. A similar check should be performed in terms of stress. It is also recommended that the assessment locus is plotted on the FAD to provide graphical evidence of the presence or absence of non-unique critical flaw solutions.

8.9 Fracture Implications for Material Selection and PWHT

Offshore welded joints are generally required to satisfy fracture toughness criteria in order to minimise the risk of brittle fracture (see Chapter 2). These criteria are more stringent for thicker joints due to the notion, based on test data, that as-welded joints become more susceptible to brittle fracture as the thickness increases. For joints exceeding specified thickness limits, post-weld heat treatment (PWHT) is usually recommended unless it can be shown, using fracture mechanics, that these joints are fit-for-service in the as-welded condition.

As is the case with any fitness-for-purpose based fracture assessment, the outcome of an analysis to determine whether PWHT is required, is highly dependent on the assumptions made regarding both input parameters and solution models. The task

is made harder by the uncertainties which may characterise some important parameters such as residual stress levels.

Two recent studies by Burdekin (1992) and Stacey (1994) provide useful insights into aspects of using fracture mechanics methods to determine PWHT requirements for offshore structures. In both investigations, the Level 2 procedures of PD 6493:1991 were used in order to determine the CTOD toughness levels required to tolerate postulated conditions relating to a number of parameters including: defect size, plate thickness, applied and residual stresses.

The approaches used in both studies were broadly similar. However, Stacey examined particularly the effects of models for through thickness residual stress distribution (Figure 8.2), while Burdekin explored the effects of applied and residual stresses via the SCF and welding heat input parameters, respectively. In addition, in order to illustrate the influence of joint redundancy, Burdekin applied partial safety factors as suggested in Appendix A of PD 6493:1991.

Conclusions from Burdekin's study include the following:

- The effects of residual stresses decrease proportionately as the SCF (ie. primary stresses) increases. As a result, PWHT becomes less influential and may be insufficient to allow defects to be tolerated at high values of SCF.

- The toughness required to tolerate deep defects, eg. a/T = 0.9, may be less than that for shallower defects, eg. a/T = 0.2. This can be attributed to the bending component of the applied stress and to the reduced effects of residual stresses as the crack becomes deeper.

Parameters used in Stacey's study and some results, expressed in terms of required CTOD levels vs. thickness, are illustrated in Figure 8.3. These indicate trends broadly similar to those of the preceding study and allow the following observations to be made:

- The selection of as-welded residual stress distribution is not as significant for shallow cracks as for deep cracks, since in all residual stress models the stress level in the region of shallow cracks is very close to yield. However, as the crack become deeper the stress level vary significantly depending on the residual stress model assumed in the analysis (Figure 8.2).

- The effect of the residual stress distribution is particularly significant for deep cracks and for high applied loads.

- The CTOD required for deep cracks at high applied loads is very high. However, this is the case for both as-welded and post-weld heat treated joints.

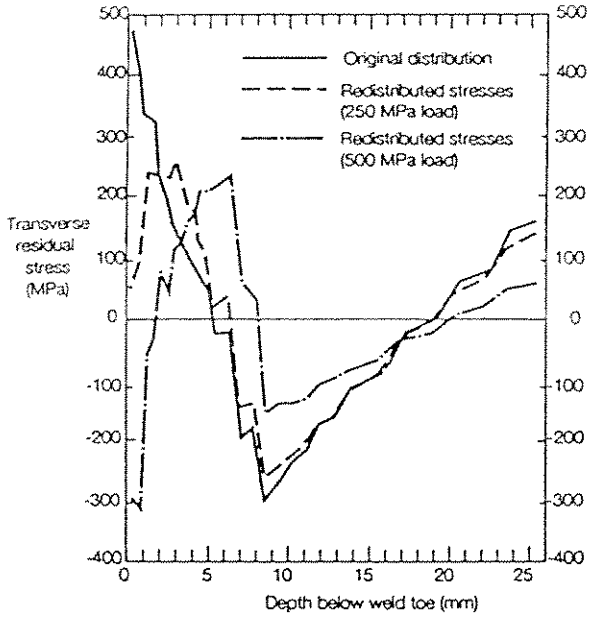

Figure 8.1 Predicted residual stress redistribution in T-butt/fillet joints (Stacey 1993)

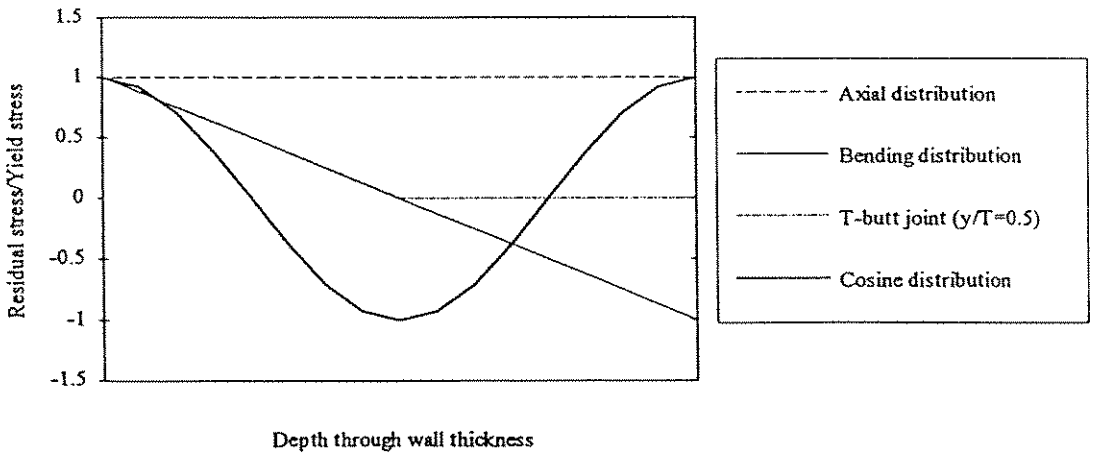

Figure 8.2 Idealised residual stress distributions (Stacey 1994)

Parameters used in Stacey's analysis

- Tensile properties of the parent material:
  Yield strength, σ_y = 315 - 345 N/mm^2
  Tensile strength, σ_u = 490 N/mm^2

- Applied primary stress (including SCF effects):
  High stress: σ_{total} = 2 σ_y, Degree of bending = 0.75.
  Low stress: σ_{total} = 0.8 σ_y, Degree of bending = 0.75

- Plastic collapse parameter Sr is determined according to the global collapse approach.

- Models for residual stress distribution (Figure 8.2):

1. A pure axial stress (constant through the thickness) equal to σ_y, reduced to allow for combined effects of applied and residual stresses according to: $\sigma_{residual}$ = lowest $\{\sigma_y , (1.4 - \sigma_n/\sigma_f)\sigma_y\}$.

2. A pure bending distribution.
3. A cosine distribution.
4. A T-butt joint distribution with y/T = 0.5.

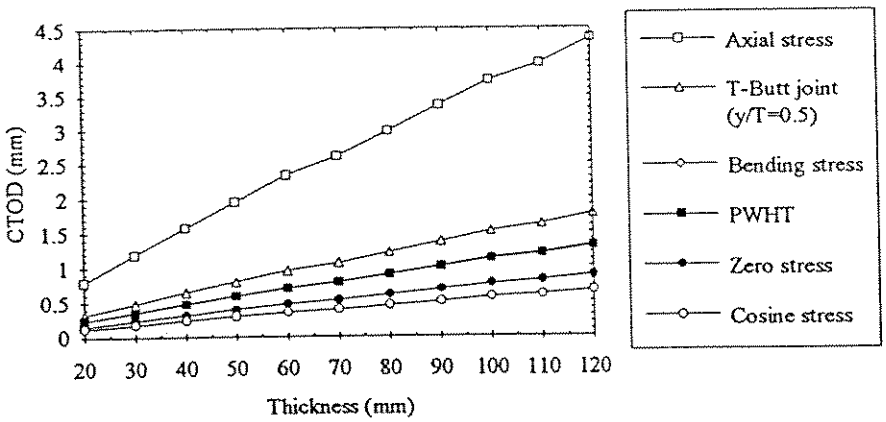

Figure 8.3 Predicted CTOD requirements for high stress nodal joints (a/T=0.8, a/c=0.2) (Stacey, 1994)

9. REVIEW OF RELATED CODES AND DOCUMENTS

9.1 Introduction

This section contains a review of the following codes and documents which provide guidance on performing fatigue and/or fracture analyses using fracture mechanics:

1. CEGB Document R/H/R6 Revision 3 'Assessment of the integrity of structures containing defects', 1986.

2. BS PD 6493:1991 'Guidance on methods for assessing the acceptability of flaws of fusion welded structures', 1991.

3. Det Norske Veritas RP D404 'Unstable fracture', 1988, and Det norske Veritas Note 30.2 'Fatigue strength analysis for mobile offshore units', 1984.

It should be noted that while this review aims at highlighting the main features of each document and includes extracts selected from some of the documents, it is not intended to provide sufficient information to apply the fatigue or fracture procedures under consideration. These are generally too complex to be covered adequately in the present review. Therefore, it is essential to consult the original documents prior to embarking on applying any of the fatigue or fracture procedures reviewed below.

For simplicity, each document is reviewed in the following order:

- Scope of guidance
- Fracture analysis
- Fatigue analysis
- Stress quantification
- Defect characterisation
- Stress intensity factors

Material quoted from the documents including section, figure, and table numbers are typed in italic.

9.2 CEGB Document R/H/R6 Revision 3 'Assessment of the Integrity of Structures Containing Defects', 1986.

9.2.1 General

This report was first published in 1976 with revisions in 1977, 1980 (Harrison et al), and 1986 (Milne et al). It describes what is known as the R6 method for the assessment of the integrity of structures containing defects under quasi-static loading.

Although intended for applications to pressure vessels typically used in electricity generating nuclear plants, the R6 method has found wide acceptance in other industries, especially since its partial incorporation in PD 6493:1991.

The third revision of the R/H/R6 report contains fourteen main sections and a number of appendices. The main sections detail the major steps to be followed when applying the FAD fracture procedure, while the appendices, considered to be advisory, provide guidance on how to perform the different aspects of the analysis. The failure mode considered is that caused by Mode I loading of planar flaws. However, guidance on treatment of mixed mode loading is provided in the appendices which cover the following topics:

1. *Determination of fracture toughness values*
2. *Plastic yield load analysis*
3. *Determination of stress intensity factors*
4. *Evaluation of* K_r^s
5. *Computing aids*
6. *Evaluation of fatigue and environmentally assisted crack growth*
7. *Evaluation under Mode I, II and III loads*
8. *Assessment of the integrity of structures made of C-Mn (Mild) Steels*
9. *A procedure for leak-before-break assessment*
10. *Probabilistic fracture mechanics procedure*

A unique feature of this report is that a detailed description of the extent of validation of its assessment procedures forms an integral part of the document. This is contained in *Section 14*, entitled the 'Status Notes', and in an additional 'Background and Validation' section at the end of the report

9.2.2 Fracture assessment

The R6 method uses the concept of a failure assessment diagram (FAD) to define the boundary between the safe and unsafe operating conditions of a flawed structure. This is based on the observation that there are two limiting loading regimes to a flawed structure: one is defined by linear elastic fracture conditions and one by plastic collapse. Interpolation between these two limiting regimes is provided by the general function $K_r = f(S_r)$, up to Revision 2 of R6, and $K_r = f(L_r)$ in Revision 3.

The function $f(S_r)$ was based on the strip yielding model of Bilby, Cottrell and Swinden (1963) which enabled the following relationship to be established:

$$K_r = S_r \left[\frac{8}{\pi^2} \ln \sec \left(\frac{\pi}{2} S_r \right) \right]^{-1/2} \qquad 9.1$$

The associated assessment curve is shown in Figure 1.6.

The stresses acting in the region of the flaw are divided into primary stresses σ^P which arise from loads that contribute to plastic collapse, and secondary stresses σ^S, which arise from loads that do not contribute to plastic collapse (eg. self equilibrating welding residual stresses). Hence:

$$S_r = \frac{\text{total applied load inducing } \sigma^P \text{ stresses}}{\text{plastic collapse load of flawed structure}} \qquad 9.2$$

or, alternatively

$$S_r = \frac{\sigma_n}{\sigma_f} \qquad 9.3$$

and

$$K_r = \frac{K^P + K^S}{K_{IC}} + \rho \qquad 9.4$$

where
σ_n is the net section stress
σ_f is the flow stress
K^P is the primary stress intensity factor
K^S is the secondary stress intensity factor
K_{IC} is the fracture toughness
ρ is the plasticity correction factor.

The plasticity correction factor ρ accounts for interaction between primary and secondary stresses. Since plasticity effects are not linearly additive, the direct addition of the elastic quantities K^P and K^S underestimates the actual severity of the crack driving force and so ρ increases the sum (K^P/K_{IC} + K^S/K_{IC}) in order to make the assessment conservative.

Work hardening effects are incorporated implicitly by means of the flow stress σ_f, which, is equivalent to the yield stress in an elastic perfectly plastic material. σ_f is commonly taken as the average of the yield and ultimate tensile stresses.

Revision 3 of R6 introduced a greater degree of complexity into the method. The concept of the FAD is retained but $f(S_r)$ is replaced by $f(L_r)$, where:

$$L_r = \frac{\text{applied load}}{\text{plastic yield load}} \qquad 9.5$$

Work hardening effects are incorporated explicitly by defining equations for $f(L_r)$ which are based on explicit formulations of J-integral.

The analysis can be performed at a variety of levels of sophistication, three options are given for the FAD and three categories of analysis may be performed for each option:

Option 3

This is based directly on the equivalence of the failure assessment curve to a J-integral analysis:

$$f_3(L_r) = \left[\frac{J_e}{J_{ep}} \right]^{1/2} \qquad 9.6$$

where J_e and J_{ep} are values of the J-integral obtained from an elastic analysis and an elastic-plastic analysis, respectively, for the same load ratio L_r.

Option 2

The FAD of Option 2 was developed by Ainsworth (1984), who used a reference stress approach to reformulate the J-integral equations of Kumar et al (1981) so that J-integral can be calculated using the actual stress-strain data of the material rather than the Ramberg-Osgood representation. 'Pessimistic' approximations were then introduced to remove the geometry dependence. The equation obtained is:

$$f_2(L_r) = \left[\frac{E\epsilon_{ref}}{L_r\sigma_y} + \frac{L_r^3\sigma_y}{2E\epsilon_{ref}} \right]^{-1/2} \qquad 9.7$$

where ϵ_{ref} is the uniaxial strain at stress $L_r\,\sigma_y$, σ_y is the yield or 0.2% proof stress, and E is Young's modulus.

Option 1

The Option 1 curve was developed for situations where the stress-strain data are not sufficiently complete for an Option 2 curve to be constructed. Based on the Option 2 curves corresponding to typical stress-strain data for a number of materials, the Option 1 curve is chosen to be biased towards the lower bound of the Option 2 curves. It has the form:

$$f_1(L_r) = (1 - 0.14L_r^2)\,(0.3 + 0.7\exp(-0.65L_r^6)) \qquad 9.8$$

Section 14.2 states that *'the Option 1 curve is most representative of austenitic materials, where the strain hardening rate is low at stresses close to yield. For ferritic materials which exhibit a sharp yield point and an extensive lower yield plateau the use of Option 2 may produce a curve which falls below the Option 1 curve at values of L_r near to but greater than 1. This a consequence of the discontinuities in the stress-strain data in the region of the yield point. These discontinuities are smoothed out in structural geometries except in the case of pure tension. In such circumstances Option 1 should not be used unless restricted to values of $L_r \leq 1.0$'.*

The plastic collapse criterion is inserted as a cut-off of the FADs, for all options, at a value $L_r = L_r^{max}$ given by:

$$L_r^{max} = \frac{\sigma_f}{\sigma_y} \qquad 9.9$$

Thus Equations 9.6-9.8 apply only up to $L_r = L_r^{max}$ and thereafter $K_r = 0$ (see Figure 9.1).

The three categories of analysis, permitted for each option, are designed to assess the flaw against crack initiation (Category 1) or ductile tearing (Categories 2 and 3). The choice of a category of analysis depends on the purpose of the analysis, and on the availability and level of confidence in the material's toughness data.

Guidance on methods to evaluate L_r is given in *Appendix 2* which, in addition, provides solutions for the cases of:

- a surface defect in a plate under tension loading, and
- through thickness defects in a cylinder or a sphere subjected to internal pressure loading.

These solutions are quoted from a CEGB Report by Miller (1987) which provides a comprehensive review of limit loads for structures containing defects. This report, however, does not include any solutions for tubular joints.

Detailed guidance on assessing the significance of results is provided in *Section 12* based on deterministic calculations. This states that confidence in assessments performed according to the procedures described in the document is gained in two stages: *'The use of lower bound material data and collapse expressions, together with upper bound loads, defect sizes and stress intensity factor values, provides the initial confidence. This should then be reinforced by investigating the sensitivity of the assessment point to variations of appropriate input parameters. Sensitivity analyses are facilitated by considering the effects that such variations have on reserve factors'*. For a particular parameter, the reserve factor is defined in terms of the values of the parameter which correspond to the assessed and limiting conditions. For example the reserve factor on applied load is:

$$\frac{\text{The load which would produce a limiting condition}}{\text{The applied load in the assessed condition}} \qquad 9.10$$

The alternative probabilistic approach for assessing the significance of results is described in *Appendix 10*.

9.2.3 Fatigue assessment

Appendix 6 provides guidance on fatigue and environmentally assisted crack growth, with regard to both analysis and derivation of data. Only sections concerning performing fatigue analysis are reviewed here.

It is noted that although a number of crack growth laws have been proposed to describe the entire sigmoidal relationship between fatigue crack growth rate (da/dN) and ΔK (Figure 9.2), these are often difficult to use and sometimes inaccurate in detail. Instead, it is suggested that it is preferable to use separate crack growth laws for each of the distinct regimes of the overall curve.

With regard to variable amplitude loading, it is remarked that in some circumstances enhancement or retardation of crack growth may occur in relation to overload/underload amplitude and loading history. However, quantification of these effects is considered beyond the scope of the document. The effects of 'short' fatigue cracks are also briefly discussed. It is noted that such cracks, which are both physically short (< 1mm) and small compared to relevant microstructural dimensions and the scale of local plasticity, may propagate faster than corresponding 'long' fatigue cracks subject to the same loading. In addition lower ΔK_{th} have been measured for 'short' cracks. Thus, in certain applications, defect assessments which use long crack growth data may result in non-conservative life predictions.

Guidance on specific crack growth laws for the three regimes, indicated on Figure 9.2, is given. This is outlined below.

For Regime A, near threshold crack growth, the following law is proposed:

$$da/dN = A' (\Delta K - \Delta K_{th})^p \qquad 9.11$$

where A' and p are constants.

It is suggested that a conservative form of this equation based on ambient temperature mild and low alloy steel data and including the high R regime, with ΔK in $MPa.m^{1/2}$, is:

$$da/dN = 8 \times 10^{-11} (\Delta K - 2)^3 \quad m/cycle \qquad 9.12$$

A lower bound expression for ΔK_{th}, based on data for a wide variety of mild and low alloy steels with $\sigma_y \leq 620$ MPa is also given:

$$\Delta K_{th} = 5 - K_{min} \quad \text{for } 0 \leq K_{min} \leq 3 \quad MPa.m^{1/2}$$
$$\Delta K_{th} = 2 \quad \text{for } K_{min} > 3 \quad MPa.m^{1/2} \qquad 9.13$$

For higher strength steels, a constant lower bound value of 2 $MPa.m^{1/2}$ is recommended.

For Regime B, at intermediate growth rates, the Paris law is recommended. The following version, where ΔK is in $MPa.m^{1/2}$, is suggested as an upper bound at room temperature for ferritic steels, including weld metal and HAZ, of all but the highest strength level.

$$da/dN = 1 \times 10^{-11} (\Delta K)^3 \quad m/cycle \qquad 9.14$$

For Regime C, near final failure, it is suggested that higher growth rates, which occur under the influence of static mode crack extension mechanisms, may be associated with K_{max} values larger than 0.7 K_{mat}. A relationship of the following form is proposed:

$$da/dN = \frac{D\ (\Delta K)^n}{[(1 - K_{min}/K_{max})\ K_{mat} - \Delta K]} \qquad 9.15$$

where D is a constant and K_{mat} represents a measure of the fracture toughness.

9.2.4 Stress quantification

For Options 1 or 2, an elastic stress analysis of the defective structure is required, while both elastic and elastic-plastic analyses are required if Option 3 is chosen. The stresses are classified as either primary or secondary depending on whether they contribute to plastic collapse or not (see above). However, *Section 5.2* suggests that such a classification may be a matter of some judgement, and that if there is doubt about the stress category, primary stresses should be assumed.

9.2.5 Defect characterisation

This is described in *Section 9* which notes that characterisation rules are required for flaw orientation, shape, interaction and any additional re-characterisation following ligament failure; and that any characterisation rule is suitable provided that it produces conservative results.

Simple guidelines, broadly compatible with those of PD 6493 and ASME Boiler and Pressure Vessel Code Section XI, are then given. With regard to defect interaction, three stages are suggested in order of increasing complexity and decreasing pessimism of assessment.

In the case of assessments which indicate ligament failure, *Section 9.3.2* states that *'when an embedded or a surface defect cannot be assessed as avoiding failure according to the procedure of Section 4, it may be re-characterised as a surface or through thickness defect. The resulting crack requires an allowance to be made for dynamic conditions and for possible crack growth at the ends during ligament breakthrough'.*

On re-characterising a part thickness defect, when ligament failure is by brittle mechanisms, the length on penetration is recommended to be set equal to the larger of:

- Twice the length of the original defect

- The sum of the depth, the ligament and the length associated with the original defect.

The depth of the re-characterised defect becomes equal to the sum of the depth and the ligament of the original defect.

9.2.6 Stress intensity factors

Appendix 3 contains information and source references for determining the Mode I stress intensity factor. However, the coverage is very brief and the guidance is restricted to general statements on: Code solutions, solutions for specific geometries including flaws at the edge of a notch, computer programs and finite element methods.

9.3 BS PD 6493:1991 'Guidance on Methods for Assessing the Acceptability of Flaws of Fusion Welded Structures', 1991.

9.3.1 General

The first edition of the BSI Document PD6493, published in 1980, provided one of the first codified approaches for assessing the significance of defects on a fitness for purpose basis. The document gives guidance particularly on the effects of planar defects on fracture and fatigue, based on fracture mechanics methods.

The fracture treatment is based on linear elastic fracture mechanics, if the sum of stresses in the region of the defect is below yield, or elastic-plastic fracture mechanics, using the crack tip opening displacement (CTOD) design curve approach, if the sun of stresses is above yield. Checks on plastic collapse are described separately within the framework of defect recategorisation procedures.

The fatigue guidance is based on linear elastic fracture mechanics and includes instructions on integration of the Paris crack propagation law. Alternatively a simplified procedure based on the quality category approach is presented graphically. This allows fatigue assessments to be carried out using the results of fracture mechanics calculations, already performed on selected geometries subjected to axial loading.

A major revision of PD6493, especially of its fracture clauses, took place during the 1980's and culminated in the publication of a new version in 1991. The revised document incorporates the latest advances in fracture mechanics and most importantly, in its fracture treatment, brings together the CTOD approach of the 1980 version and the failure assessment diagram (FAD) procedures of the CEGB R6 method. The fatigue treatment received minor changes, and although the data and procedures were reviewed and updated, the basic principles of the fatigue clauses of the 1980 version were effectively retained.

PD6493:1991 contains four main sections and a number of appendices. *Section 1* describes the scope of the document and the information required for performing defect assessments. *Sections 2 and 3* provide detailed procedures for fracture and fatigue assessments, respectively. Other modes of failure are considered briefly in *Section 3*, these include instability (buckling), creep and failures associated with environmental effects. Additional information on some aspects of the fatigue and fracture assessments are given in Eight appendices as follows:

A. Safety factors, number of tests and treatments of variability in input data for fracture assessment
B. Use of Charpy tests to indicate fracture toughness levels
C. Assessment of pop-in crack extensions
D. Stress due to misalignment
E. Stress intensity factor solutions for cracks in welded joints
F. Formulae for effective net section stress
G. Examples of Level 3 assessment diagrams
H. Approximate numerical integration methods

The document provides guidance for assessment of planar and non-planar defects using fracture mechanics and empirical data, respectively. Only aspects of assessing planar defects are described below.

9.3.2 Fracture assessment

The main features of the fracture treatment is that it brings together the CTOD concepts of PD6493:1980 and the FAD approach of the CEGB R6 procedures, providing a framework for fracture assessment which incorporates the three fracture parameters, K, CTOD and J-integral with regard to both crack driving force and toughness characterisation, in addition to explicit consideration of the interaction between fracture and plastic collapse.

Three alternative levels of treatment are available. These are termed Levels 1, 2 and 3, and provide, respectively, increasingly accurate and decreasingly conservative assessments.

The choice of level depends on the purpose of the analysis, available input data, and material under consideration. Level 1 is for preliminary assessments and is broadly compatible with PD 6493:1980. Level 2, based on the strip yield model, is intended for general structural steel applications and is similar to the CEGB R6 Revision 2 (Harrison et al. 1980), but with the alternative CTOD treatment as well as the K_{Ic} treatment. Level 3 corresponds to the CEGB R6 Revision 3 (Milne et al. 1986), and allows assessments involving high strain hardening and/or ductile tearing.

At each assessment level, alternative methods based on the stress intensity factor K or the crack tip opening displacement CTOD (or δ) are given. The choice of route depends usually on the form of available toughness data.

Each of the three levels has associated with it a specific failure assessment diagram. The definitions of the fracture and plastic collapse ratios are broadly similar to those of the R6, but in addition the fracture ratio can be defined as:

$$K_r = \sqrt{\delta_r} = \sqrt{\delta_i / \delta_c} + \rho \qquad 9.16$$

where δ_i and δ_c are the applied elastic CTOD and the critical CTOD, respectively.

The plastic collapse parameter is the ratio of applied load to flow strength collapse load (S_r : Levels 1 and 2), or yield collapse load (L_r : Level 3) of the flawed structure. Alternative definitions in terms of stresses are:

$$S_r = \sigma_n / \sigma_f \quad \text{and} \quad L_r = \sigma_n / \sigma_y \qquad 9.17$$

where
σ_n = net section stress
σ_y = yield strength or 0.2% proof stress
σ_f = flow stress, commonly taken as the average of the yield and ultimate tensile strengths

The main features of the three levels can be outlined as follows:

Level 1

The Level 1 treatment is consistent with the procedures of PD6493:1980. It is presented as a conservative preliminary assessment. The sum of the applied stress components (primary, secondary and peak stresses) is taken to act as a uniform stress across the section containing the defect.

The Level 1 FAD, shown in Figure 9.3, consists of two cut-offs at K_r (or $\sqrt{\delta_r}$) = 0.7 and S_r = 0.8. The limit of 0.7 on K_r maintains consistency with PD6493:1980 as it is equivalent to a factor of safety of 2 on defect size. The limit of 0.8 on S_r is based on a number of considerations. Among these is the need to prevent the use of the Level 1 procedure, in regions where the strip yield equation (of Level 2) predicts higher applied CTOD at high σ/σ_y, than the Level 1 CTOD design curve equation (Garwood et al, 1988).

Level 2

The Level 2 treatment is seen as the preferred (or normal) assessment level for the majority of applications. It incorporates the principles and FAD of the CEGB R6 Revision 2 procedure in addition to permitting the use of CTOD toughness data and CTOD driving force parameters.

The stress treatment adopted for Level 2 (and Level 3) assessments is based on the actual distribution of stresses in the vicinity of the defect. The stress may be split into membrane and bending components of the primary and secondary stresses.

The level 2 FAD, shown in Figure 9.3, is based on the strip yield model. It does not include explicit factors of safety (unlike the Level 1 FAD). Thus due allowance has to be made for uncertainties in the input data. As an alternative to worst case estimates of stress level, defect size and toughness, the document proposes the use of partial safety factors. These are given in *Appendix A*.

Level 3

The Level 3 treatment is the most advanced level of assessment. It is based on the CEGB R6 Revision 3 and is particularly appropriate for high strain hardening materials or for tearing analysis.

The assessment diagram at this level can be derived from the stress-strain curve of the material using the R6 Option 2 Equation 9.7. This equation is given here in terms of the engineering stress, σ, and engineering strain, ϵ, as follows:

$$K_r = \sqrt{\delta_r} = \left[\frac{E \ln(1+\epsilon)}{\sigma(1+\epsilon)} + \frac{\sigma^3 (1+\epsilon)^3}{2\sigma_y^2 E \ln(1+\epsilon)} \right]^{-1/2} \qquad 9.18$$

with a cut-off at $L_{r\,max} = (\sigma_y + \sigma_u)/2\sigma_y$, after which K_r or $\sqrt{\delta_r} = 0$. As with the R6 Revision 3, when the stress-strain data is uncertain or incomplete, the R6 Option 1 FAD defined by Equation 9.8 can be adopted (see Figure 9.1).

Although not stated in the document, the potential exists for both a material and geometry specific FAD based on elastic and elastic-plastic estimates of J-integral. This method corresponds to the R6 Option 3 approach.

9.3.3 Fatigue assessment

The fatigue treatment is based on linear elastic fracture mechanics and consists of estimating the fatigue life by integrating the Paris crack propagation law. Two methods for the assessment of planar flaws are described.

The simplified procedure, or quality categories approach, combines fracture mechanics with the S-N concept, and is based on a the results of fracture mechanics calculations already performed on simple geometries subjected to either tension or bending loading. While providing a simple and efficient method for assessment, the quality categories approach involves a number of simplifying assumptions and is limited to the simple geometries and loading considered in deriving the solutions. Thus, it is inappropriate for structures such as tubular joints where the assessment of weld toe defects lying in complex stress

fields requires refined modelling within a full fracture mechanics analysis. Such a treatment is described in the general procedure which is outlined below.

In the general procedure, it is noted that for many practical cases, it is sufficiently accurate to use the Paris Law bounded by the threshold stress intensity factor and the critical stress intensity factor for fracture. However, it is suggested that in some circumstances it may be advisable to use crack growth laws which describe the entire sigmoidal relationship, for example when a significant part of the fatigue life is spent in either the near-threshold or near-fracture regime. A modified version of the Paris Law is suggested for situations where crack growth near the threshold is particularly significant, eg. under variable amplitude loading (see Section 7.6).

With regard to fatigue crack growth data for use with the Paris Law, the following relationship between A and m corresponding to mean crack growth data is given:

$$A = \frac{1.315 * 10^{-4}}{895.4^{m}} \qquad 9.19$$

which gives $A = 1.832 * 10^{-13}$ for $m = 3$ with da/dN in mm/cycle and ΔK in $N.mm^{-3/2}$.

However, for compatibility with fatigue design rules for welded steels, and in the absence of specific fatigue growth propagation data, the following values are recommended for ferritic steels with yield or 0.2 % proof strength below 600 N/mm^2 operating in air or other non-aggressive environments at temperatures up to 100 °C: $m = 3$ and $A = 3 * 10^{-13}$

These are reported to correspond to the upper bound to many published data for ferritic steels. However, it is noted that higher growth rates have been observed in some weld metals and HAZ, particularly as the critical stress intensity factor for fracture is approached, in which case the recommended value of A is $6 * 10^{-13}$.

For structural steels operating in a marine environment at temperatures up to 20 °C, the following values are recommended: $m = 3$ and $A = 2.3 * 10^{-12}$

Detailed guidance is given on determining threshold stress intensity factors for carbon and carbon manganese steels. This is outlined in Section 7.3.

9.3.4 Stress quantification

Stresses are classified as either primary or secondary depending on whether they contribute to plastic collapse or not, and as peak stresses if due to concentrations at local discontinuities. Graphical guidance on linearisation of the through thickness distribution in order to split the primary and secondary stresses into membrane and bending components is given.

The principle behind such linearisation is that it should be conservative and in particular, it should not underestimate the surface stresses or the stresses acting in the region of the flaw.

Stresses for use in fracture assessments depend on the level at which the assessment is performed. Conservative models are used at Level 1, while realistic stress distributions can be used at levels 2 and 3 (see description of the three assessment levels above).

With regard to welding residual stresses, it is required that these are assumed equal to the room temperature yield strength of the material in which the flaw is located for flaws transverse to the welding direction, ie. stresses parallel to the weld, and to the lesser of the yield strengths of the weld or parent metal for flaws parallel to the welding direction, ie. stresses perpendicular to the weld. For post weld heat treated (PWHT) welds, it is stated that the residual stresses will not in general be reduced to zero. Thus, guidance on the residual stress levels likely to remain after PWHT is given, but it is stated that local heat treatment may leave significantly higher residual stresses and that specific assessments should be made for each case.

In addition, the document allows advantage to be taken of the reduction in residual stresses with preloads or applied loading. However, it would appear that such relaxation may be used only if the residual stress distribution is taken uniform through the thickness. A model to estimate the extent of the tensile component of the residual stress is recommended for transverse residual stresses at the toe of fillet or T-butt welds, eg. stress perpendicular to weld toe defects in tubular joints. The model allows the residual stresses to be represented as membrane and bending components which are functions of the heat input of the adjacent weld run.

In fatigue assessments, it is recommended to use the full stress range regardless of the stress ratio in both the as-welded and post-weld heat treated conditions. However, if it is required to take account of applied stress ratio, eg. when considering unwelded components or incorporating threshold effects, it is recommended to use the effective stress ratio obtained by superimposing applied and residual stresses.

9.3.5 Stress intensity factors

Detailed guidance is given on evaluation of stress intensity factors for embedded and surface cracks in plain plates based on the equations of Newman and Raju (1984). For weld toe cracks, it is recommended to use the Mk approach to account for the effects of weld geometry on stress intensity factors. The proposed Mk solutions are based on two-dimensional finite element analyses and are given for both tension and bending loading (see Section 6.3). Mk solutions for weld root cracks in cruciform joints are also given.

9.4 Det norske Veritas RP D404 'Unstable Fracture', 1988, and Det norske Veritas Note 30.2 'Fatigue Strength Analysis for Mobile Offshore Units', 1984.

These two documents are unique in that they are intended mainly to provide fracture and fatigue guidance relevant to offshore structures. The documents may be considered complementary to each other with the first, DnV RP D404, providing detailed guidance on fracture, and the second, DnV Note 30.2, addressing aspects of both S-N and fracture mechanics based fatigue analyses.

9.4.1 DnV RP D404 'Unstable fracture'

The document states that the potential implications of unstable fracture should be evaluated for the following three problem areas:

- Significance of defects on structural design for assurance of ductile structures (fracture mechanics design).
- Fitness for purpose evaluation of defects.
- Optimisation of inspection periods.

These three applications are covered in *Sections 2, 3 and 4*, respectively. Most of the material in *Section 2* applies to both fracture mechanics design and fitness for purpose evaluation. *Section 4* is very brief and merely introduces the concept of optimisation of inspection periods. In addition to the general guidance in the main text, specific recommendations regarding stress intensity factors, fatigue crack growth calculations, and fracture toughness testing are given in *Appendices 1, 2 and 3*, respectively.

9.4.2 Fracture mechanics design

The basic philosophy behind fracture mechanics design is that, for structures or structural elements which may contain significant cracks, fracture mechanics theory should be used as supplementary assessment of structural strength and safety in Ultimate/Progressive Limit States (ULS/PLS). The primary goal is to ensure ductile performance of the structure despite the presence of finite cracks. Within this context, guidance is given on evaluation of three alternative design parameters, namely, maximum tolerable stress, minimum required fracture toughness, and maximum allowable defect size. Procedures involving the use of partial safety factors applied to stress, defect and material parameters, are given according to ULS/PLS.

In *Section 2.1.2*, it is stated that the extent of request for fracture mechanics assessments of ULS is dependent on the importance of the structural elements and details in the structure, plate thickness, access for inspection and repair, probability of occurrence of crack-like defects, and accuracy of the predicted ultimate stress levels at the location of concern. Guidance on some of these issues is reproduced in Tables 9.1 to 9.3.

Examples of Category 1 structural elements, considered to be the most important, are given in *Section 2.1.5* and include rolled cans for tubular joints and through-going members in cruciform, tubular T, Y and K joints which are subjected to large stresses in the through thickness direction causing local plastic deformation in the ultimate limit state condition.

Section 2.2 gives the partial coefficients for use according to ULS/PLS for fracture mechanics design. The load coefficients are for live, permanent, deformation, and environmental loads. In ULS checks, the defect coefficient is 1.2, while the material fracture toughness coefficient is 1.15. In PLS checks, all load coefficients and the material coefficient are set to 1.0.

9.4.2.1 Fracture assessment

Criteria for fracture assessments are set out in *Section 2.3* for both linear elastic conditions and elastic plastic conditions. These criteria, which incorporate the aforementioned ULS partial coefficients, are effectively based on the CTOD design curve approach of PD 6493:1980. However, the document allows the use of other approaches such as those based on specific J integral solutions. The CEGB/R6 failure assessment diagram may also be used when *'proper solutions exist for J integral and plastic collapse of the structural geometry of concern'*. For load controlled structural elements and for structural elements with known 'exact' level of stresses, a modified version of Equation 6 (associated with the assessment curve of the Level 2 FAD, Equation 3.1), may be applied.

Section 2.6 deals with definition of the characteristic fracture toughness. In most cases, this is specified as the lower 5th percentile of an infinite number of relevant test data. For a finite number of test data, the equivalent characteristic value should be derived based on recognised statistical methods. Brief guidance on fracture toughness testing is provided in *Appendix 3* of the document, which is partly based on ASTM Designation E399-74 Part 10 and BSI BS 5762 1979, and deals with testing of the parent metal, weld metal as well as the HAZ and the associated local embrittled zones.

9.4.2.2 Fatigue assessment

This is covered in *Section 2.10.3* which suggests that integration of the Paris' law may be performed according to DnV Note 30.2. Some of the recommendations of this document are summarised in *Appendix 2*.

9.4.2.3 Stress quantification

In Section *2.3.8*, it is stated that the SCF for use in fracture assessment equations should be the effective SCF acting in the cross section of the possible locations of a defect accounting for possible overmatching of strength level in weld metal relative to parent plate and the associated yielding pattern.

Guidance on the level of welding residual stresses in the as-welded condition is given in Table 9.4 in terms of the ratio: residual stress / yield stress. The document does not state explicitly whether the yield stress is that of the parent or weld metal.

For structural elements where the exact stress levels are not known, it is suggested that the applied stress to be included in the fracture mechanics calculations should be set equal to the parent materials yield strength.

9.4.2.4 Defect characterisation

Recommendations regarding initial crack sizes for inclusion in fatigue crack growth analyses, integrated in the fracture mechanics design check, are partly reproduced in Table 9.5.

In *Appendix 1*, it is noted that SIF solutions are influenced significantly by the crack shape, and that relevant relations should be used in fatigue analyses in order to account for the evolution of crack shape during crack growth. It is suggested that theoretical or empirical crack shape models may be used. Some published empirical models for gusset and stiffener specimens are given, but it is warned that these are only valid for cases similar to the joints from which they were derived.

9.4.2.5 Stress intensity factors

Guidance on determining stress intensity factors is given in *Section 2.8* and *Appendix 1*. The compliance factor, Y, is expressed as follows:

$$Y = Y_E . Y_S . Y_T . Y_W . Y_G \qquad 9.20$$

where
Y_E is the basic crack shape factor
Y_S is the front face factor
Y_T is the back face or finite thickness factor
Y_W is the finite width factor
Y_G (= Y_{SS} * Y_K) is the stress gradient factor
Y_{SS} is the geometric stress gradient factor
Y_K is the localised stress gradient factor for surface irregularity.

Solutions for some of the above Y factors and SCF solutions are given for simple typical geometries including welded joints such as transverse butt welds and transverse load-carrying fillet welds. It is suggested that knowledge of the SCF provides important information on the SIF close to the surface, ie. with regard to the factor Y_G.

Figure 9.4 provides simple estimates for the SIF of chord surface defects at the hot spot for two specific geometries of T and K tubular joints.

9.4.2.6 Other issues

Although the main emphasis in the document is on the design against initiation of unstable fracture, it is allowed to consider a crack arrest design philosophy if this is deemed appropriate. It is also permissible to conduct design checks through component testing, in terms of wide plates or tubular joints containing cracks. This is addressed briefly in *Section 2.12*.

With regard to the effects of thickness, It is suggested that, for a given crack depth, the presence of a stress gradient through the thickness causes the stress gradient factor Y_G and the corresponding SIF to increase with increasing plate thickness. Therefore, the maximum allowable ultimate stress must decrease with increasing plate thickness if the same safety level is to be obtained.

9.4.3 Fitness for purpose evaluation

Guidance for performing fitness for purpose assessments are effectively similar to those outlined in the previous section except for some slight differences, eg. with regard to partial coefficients and defect characterisation. As an alternative, it is allowed to use other relevant documents. The most appropriate, according to *Section 3.1.3*, is the latest revision of BS PD 6493.

Partial coefficients for fitness for purpose evaluation, dealt with is *Section 3.2*, are as those for fracture mechanics design. However, if the ULS check is not fulfilled, reduced partial coefficients may be used in assessments for temporary conditions, eg. to determine whether immediate repair is necessary.

Section *3.3.1* provides guidance on characterisation of detected defects of irregular shape and on interaction of closely located defects. This guidance is effectively similar to that of PD 6493.

9.4.4 DnV Note 30.2 'Fatigue strength analysis for mobile offshore units', 1984.

9.4.4.1 **General**

Guidance is given on the following topics:

- Fatigue loading and stress distribution
- Fatigue analysis based on tests (S-N approach)
- Fatigue analysis based on fracture mechanics

Only recommendations relevant to the last subject are reviewed here.

9.4.4.2 Fatigue assessment

It is proposed that the Paris' law may be applied to predict fatigue crack propagation. Thus, the number of cycles necessary to grow the defect from an initial size a_o to a final size a_f, where a is the non-dimensional defect size, a/T, is expressed as:

$$N_B = \frac{1}{C\,T^{m/2-1}\,\Delta\sigma^m} \int \frac{d\alpha}{(Y\sqrt{\pi a})^m} \qquad 9.21$$

where solutions for the integral in Equation 9.21, denoted as I, are given for some configurations of butt-welds, cruciform joints and tubular joints in both air and seawater environments. The integrals are calculated assuming infinitely long cracks. The tubular joint solutions are reproduced in Figures 9.5a and 9.5b. These are reported to be based on upper bound values for crack growth measurements in simple unstiffened T, Y and K joints, and relevant for growth of surface cracks in the thickness direction in the hot spot region.

To calculate the compliance function Y, the document proposes that this may be obtained from numerical analyses, such as finite element calculations, but warns that due consideration should be given to the important influence of the boundary conditions. Alternatively, it may be assumed that the Y solutions given in *Appendix 1* of DnV RP D404 may be used.

Crack propagation constants, for use in integrating the Paris' law, are suggested if relevant data are unavailable (Table 9.6):

Values of C, corresponding to the mean plus two standard deviations, are recommended for use for design purposes in order to comply with the safety of the corresponding S-N approach.

Conversion factors for C values relevant to SI and other unit systems, given in *Section 4.2.1*, are reproduced in Table 9.7.

9.4.4.3 **Stress quantification**

In *Section 4.1.2*, the following is stated: '*normally, compressive stresses do not contribute to crack propagation. However, for welded connections containing residual stresses the whole stress range should be applied. Only stress components normal to the propagation plane are considered. The stresses to be used in* Equations 9.22 to 9.24 (given below) *is always the nominal stress of the plate. However, in the case of tubular joints the hot spot stress would be required'.*

It is also suggested that If the cumulative stress distribution is expressed as:

$$\Delta\sigma = \Delta\sigma_o \left[1 - \frac{\log N}{\log N_o} \right]^{1/h} \qquad 9.22$$

where $\Delta\sigma_o$ is the stress range exceeded once in N_o cycles, N_o is the total number of cycles, N is the number of cycles which

exceed $\Delta\sigma$, and h is the parameter of Weibull stress range distribution, then the equivalent effective stress range, $\Delta\sigma_{eff}$, may be calculated from:

$$\Delta\sigma_{eff} = \frac{\Delta\sigma_o}{(\ln N_o)^{1/h}} \left(\Gamma\left(\frac{m}{h} + 1\right)\right)^{1/m} \qquad 9.23$$

where m is the inverse slope of the S-N curve or material exponent in the Paris law. Values for $[\Gamma(m/h + 1)]^{1/m}$ are given in the document for m and h in the ranges 3.0-4.2 and 0.4-1.5, respectively.

However, If the long term stress distribution is given by a stress histogram consisting of a number of constant amplitude stress range blocks ($\Delta\sigma_i$) and a number of repetitions n_i, an effective stress range is calculated from:

$$\Delta\sigma_{eff} = \left(\frac{\sum_{i=1}^{n} \Delta\sigma_i^m \, n_i}{\sum_{i=1}^{n} n_i} \right)^{1/m} \qquad 9.24$$

9.4.4.4 Defect characterisation

With regard to initial crack sizes for inclusion in fatigue crack growth analyses, it is stated that *'the depth of the initial crack, $\underline{a}_o$ (= a_o/T), should be considered for each case, taking account of experienced imperfection or defect sizes for various weldments, geometries, access and reliability of the inspection method. For surface cracks starting from transitions welds/base material a crack depth of 0.5mm (eg. due to undercuts and microcracks at bottom of the undercut) may be assumed if not other documented information about crack depth is available'*. It should be noted that in the relatively more recent RP D404 document, an initial defect size of 0.3mm is suggested rather than 0.5mm.

As guidance on the limit of crack propagation corresponding to the final crack size, it is stated that *'since most of the stress cycles to failure are associated with the first part of the crack growth, an exact definition of failure is not essential, but may be assumed to be crack growth through the plate thickness. For high stresses or material with low ductility the relevant crack depth at unstable fracture, $\underline{a}_f$, should be evaluated and used in Equation* [9.21]'.

	Plate Thickness (mm)	Importance of structural element Secondary	Primary	Special
Access for inspection and repair	$t < 25$	No	No	No
	$25 \leqslant t \leqslant 50$	No	No	No
	$50 \leqslant t \leqslant 75$	No	No	Yes
	$75 < t$	No	Yes	Yes
No access for inspection and repair	$t \leqslant 25$	No	No	No
	$25 \leqslant t \leqslant 50$	No	No	Yes
	$50 \leqslant t$	No	Yes	Yes

Table 9.1 Recommended guidance on inclusion of fracture mechanics strength assessments at design stage welded offshore structures, stress relived condition

	Plate Thickness (mm)	Importance of structural element Secondary	Primary	Special
Access for inspect and repair	$t \leqslant 25$	No	No	No
	$25 \leqslant t \leqslant 50$	No	No	Yes
	$50 \leqslant t < 75$	No	Yes	Yes
	$75 < t$	Yes	Yes	Yes
No access for inspect and repair	$t < 25$	No	No	Yes
	$25 \leqslant t \leqslant 50$	No	Yes	Yes
	$50 \leqslant t$	Yes	Yes	Yes

Table 9.2 Recommended guidance on inclusion of fracture mechanics strength assessment at design stage, welded offshore structures, as welded condition

Category 1: Special structural elements.
These are elements which are essential to the overall integrity of the structures or subject to arduous stress conditions.

Category 2: Primary structural elements.
These are elements which contribute to the overall integrity of the structures and other elements of importance to the operational safety of the installation.

Category 3: Secondary structural elements.
These are elements which contribute to the strength of the structure, not defined as special or primary structural elements.

Category 4: Non-structural elements
These are elements not contributing to the strength of the structure.

Table 9.3 Importance of structural elements

Flaw type	Butt joint		Fillet joint		Tubular joint Chord/brace weld connections	
	Flaw parallel to weld line	Flaw normal to weld line	Flaw parallel to weld line	Flaw normal to weld line	Flaw parallel to weld line	Flaw normal to weld line
Through thickness flaw	0.2	0.8	0.2	0.8	0.2	0.8
Subsurface flaw	0.2	0.8	0.2	0.8	0.6	0.8
Surface flaw	0.4	0.8	0.8	0.8	0.8	0.8

Table 9.4 Weld residual stress level ratio residual stress/yield stress

Location	Surface Depth, a	Interior Heigth 2a
Parent rolled plate and tubular	0.1 mm x)	0.005 T ingot cast xxxx) 0.02 T continuous cast xxxx)
Welded connection MMA weld	0.3mm weldtoe xx)	Height 2a equal diameter of pores to be detected for diff. weld quality accoring to IIW chart
		When no NDE concerning pores, height 2a equal height of 1.weld pass.
Welded connection Fine grinding surface incl. min. 1 grinding depth at weld to.	0.1mm xxx)	as above xxx)

x) Length 2c considered 10a.
xx) Length 2c considered 5a.
xxx) Lack of fusion defects, length 2c =➧2T.
xxxx) May be set equal 0 if no segregation is present in final microstructure.

Table 9.5 Recommended characteristic size of initiation cracks to be included in a possible fatigue crack growth analysis integrated in the fracture mechanics design check

	m	C (N, mm)	
		Mean value	Mean + 2st.dev.
Welds in air	3.1	1.1×10^{-13}	3.3×10^{-13}
Welds subjected to seawater	3.5	3.4×10^{-14}	1.6×10^{-13}

Table 9.6 Crack growth parameters (DnV Note 30.2)

$Nmm^{-3/2}$ mm/cycle	$MPa\sqrt{m}$ mm/cycle	$kpmm^{-3/2}$ mm/cycle	$ksi\sqrt{in}$ in/cycle
1	31.6^m	9.81^m	$\frac{1}{25.4} 34.7^m$
0.0316^m	1	0.311^m	$\frac{1}{25.4} 1.1^m$
0.102^m	3.22^m	1	$\frac{1}{25.4} 3.54^m$
25.4×0.029^m	25.4×0.909^m	25.4×0.282^m	1

How to use this table:
Example: If the C-value is known in the units $ksi\sqrt{in}$ and in/cycle, a transformation into e.g $Nmm^{-3/2}$ and mm/cycle is as follows:
C ($Nmm^{-3/2}$, mm/cycle) = C ($ksi\sqrt{in}$, in/cycle) * 25.4 * 0.029^m

Table 9.7 Conversion factors for C-values (DnV Note 30.2)

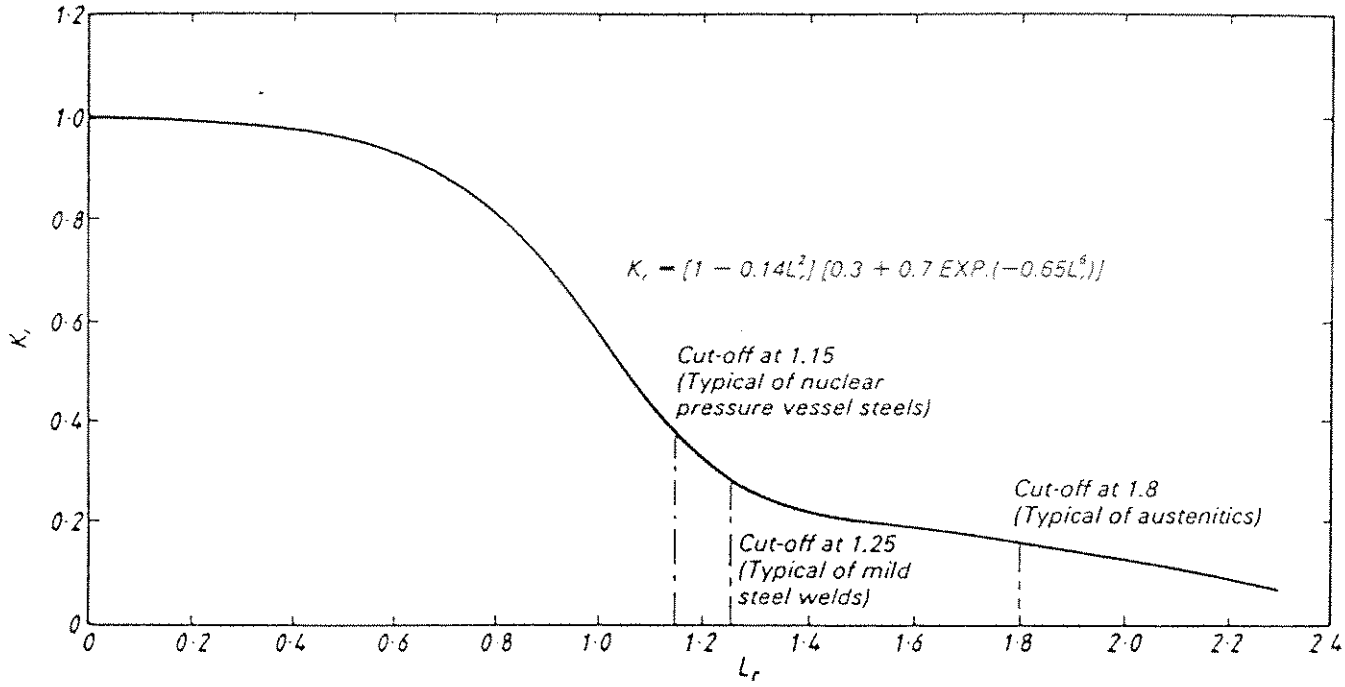

Figure 9.1 Failure assessment diagram for use with Option 1 when relevant stress-strain data is unavailable

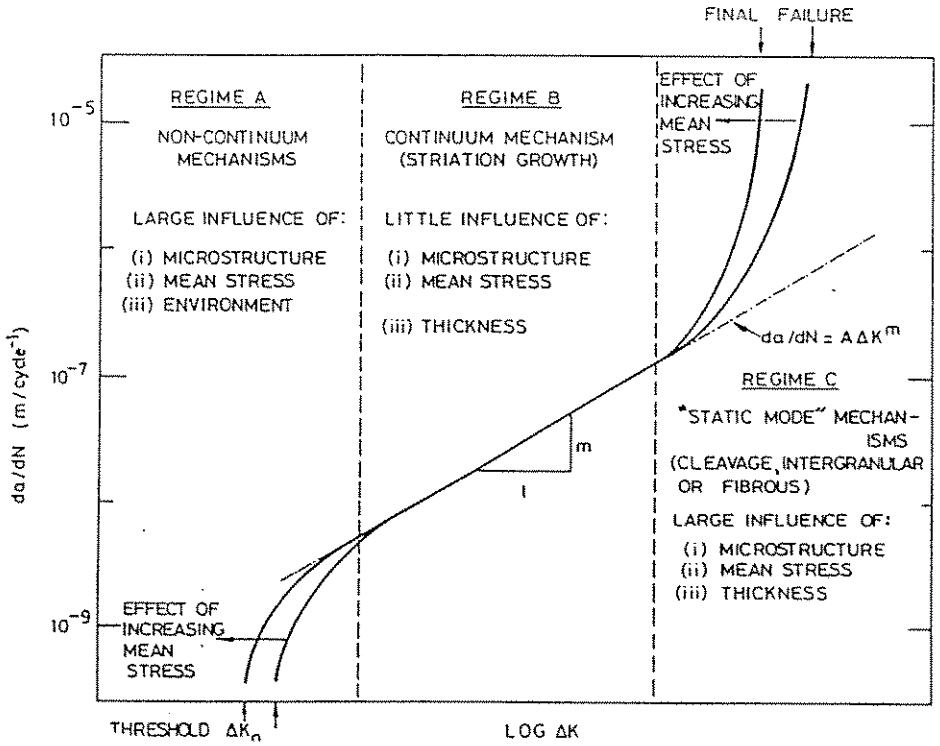

Figure 9.2 Sigmoidal variation of fatigue crack growth rate (da/dN) with alternating stress intensity (ΔK) and associated fracture mechanisms

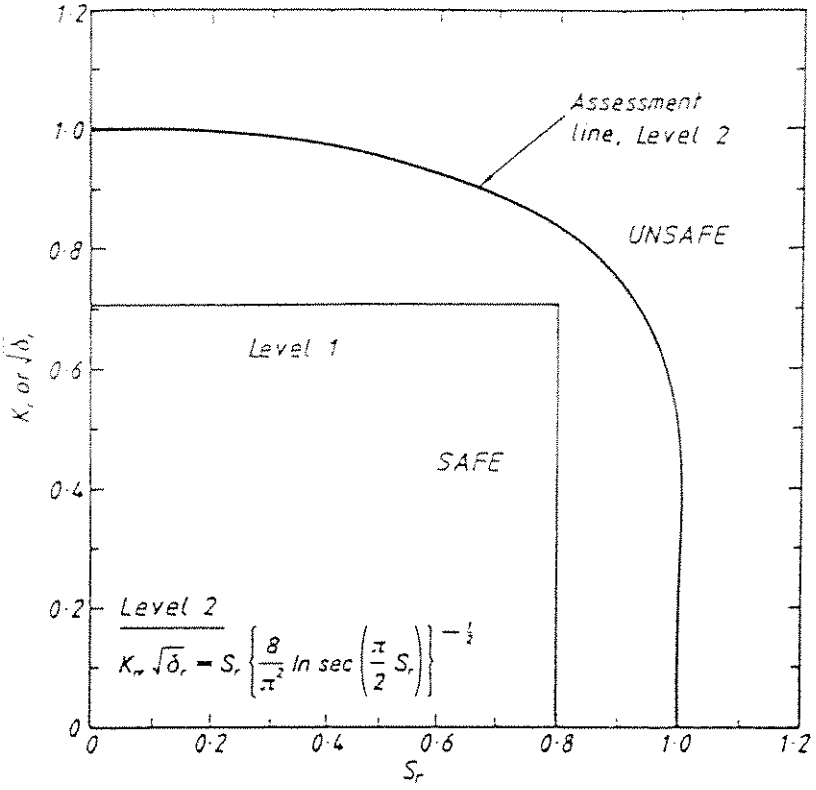

Figure 9.3 The failure assessment diagrams for Level 1 and Level 2

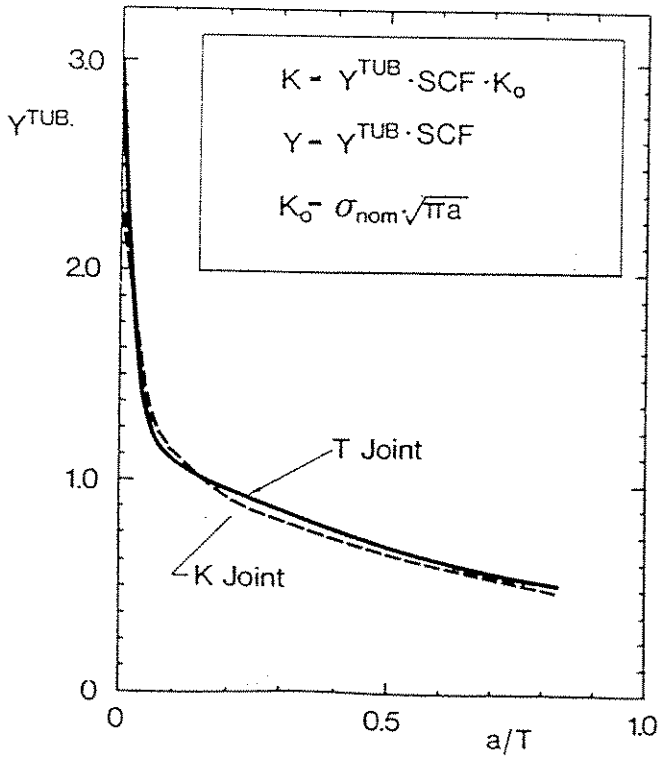

Joint-type	"T" 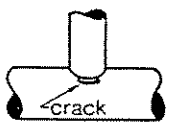	"K" 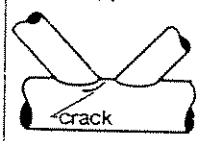
Crack location	Saddle chord side	Crown chord side
SCF	6.2	3.3
Geometry		
T (mm), chord	30	30
t (mm), brace	18	18
γ-D/2T	10	10
β-r/R	0.6	0.6
Loading	Axial	Axial balanced

Figure 9.4 Tubular joint, surface defect, chord side.
Y at cross section through bottom of surface defect

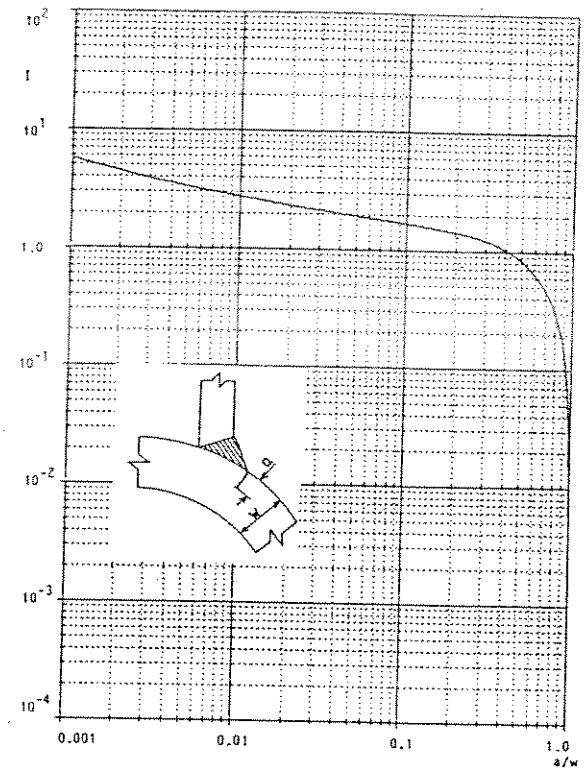

Figure 9.5a Tubular joints in air.
Surface cracks at the weld toe. m = 3.5

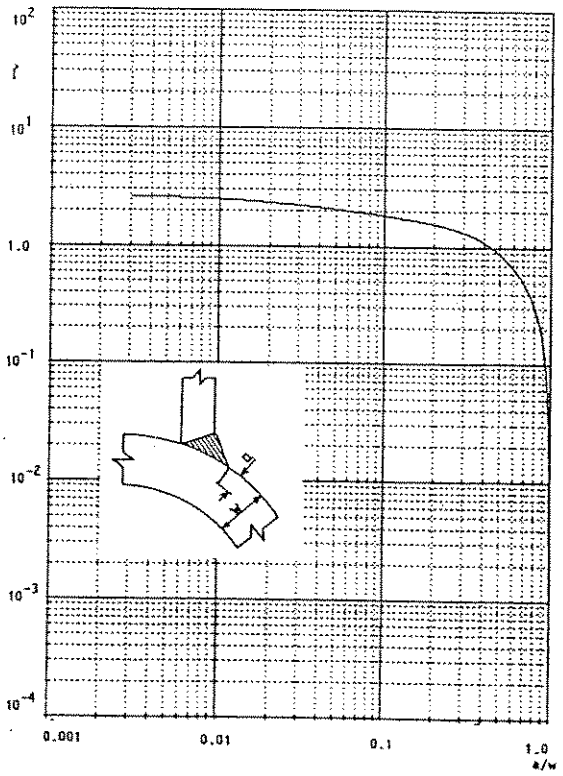

Figure 9.5b Tubular joints in seawater.
Surface cracks at the weld toe. m = 3.5

10. RECOMMENDATIONS

A comprehensive review of key analysis models and parameters which may be considered relevant to fracture mechanics based fatigue and fracture assessments has been performed. The review covers aspects of applying fracture mechanics in defect assessment of welded joints in general, and focuses on tubular joints in particular. This section provides general recommendations relating to performing fatigue and fracture assessments and includes references to relevant sections in this Chapter, which should be consulted for additional guidance.

Fracture mechanics design

The philosophy of fracture mechanics design should be applied in the design of new structures. The measures used to prevent failure by fatigue and fracture should be formalised as a fracture control plan for the structure (Section 1.2).

Determination of stress distribution

The stress distribution in uncracked joints, which may be required for determining stress intensity factors, may be quantified using three parameters, namely the SCF, DOB and notch stresses. Aspects of determining the SCF and DOB parameters are dealt with in detail in Chapter 4 and Section 4.1, respectively. Methods to account for notch stress by using the parameter Mk are covered in Section 6.3. Parametric equations for the DOB and Mk parameters are included in Appendices A and B, respectively.

There is limited information on welding residual stresses. Section 4.2 outlines the extent of available data and describes some models for quantifying distributions of these stresses.

Determination of stress intensity factors

The analyst is generally faced with one or a combination of the following two approaches:

1. Full modelling using finite element analysis which may involve explicit three-dimensional representation of the geometry of both the global joint and the local cracked region, with loading and restraint conditions which simulate the actual situation as accurately as possible.

2. Simplified modelling, which combines a number of approximations relating to geometry, stress distribution, or solution method.

The advantage of the first approach is that it may enable highly accurate solutions to be obtained. However, it is potentially very demanding in terms of computing time and it can only provide a finite number of solutions.

The main advantage of the second approach is that it can build on the wealth of reliable solutions obtained for simple geometries and idealised stress distributions, eg. flat plates subjected to either tension or bending. In order to adapt such solutions to complex configurations, eg. surface cracks in tubular joints, correction factors based on limited studies could be derived and calibrated using the first approach.

Parametric tubular joint SIF equations based on data generated using finite element analysis have been reviewed in Section 6.3. The most reliable of these equations appear to be those of Rhee et al (1991). However, their validity range is relatively limited. Further evaluation of other equations and of the available data is required in order to improve existing equations or produce alternative equations.

Simplified stress intensity factor solutions based on flat plate equations and the Mk approach have been reviewed in Sections 6.2 and 6.3. The Raju and Newman equations for plates subjected to tension or bending loads are recommended. A number of Mk equations may be used depending on the purpose of the analysis. The equations of Fu et al are recommended for their simplicity. However, they are restricted to a specific weld toe geometry. Other equations enable a wide range of weld toe geometries to be considered, thus more refined modelling is possible. The following Mk equations are arranged according to their range of application in an increasing order: Fu et al, PD 6493, Dijkstra et al, Thurlbeck et al. The Dijkstra et al equations appear to predict the lowest Mk values. Therefore, their use is not recommended pending further evaluation studies. The load shedding model reviewed in Section 7.8 may be unconservative according to a limited study, undertaken as a part of this work, and the OSU investigations reported in Section 6.3. It is therefore not recommended for use pending further evaluation studies. Due to various limitations associated with the approaches reviewed in this chapter, the most appropriate and viable option for quantifying stress intensity factors for general applications is to use the Raju and Newman equations together with the Mk approach.

It is recommended to consider the following basic guidelines for generating stress intensity factor solutions using FE analysis:

- Conventional requirements relating to use of finite element programs should be observed. These include the following:

  i) The program in general, and its routines and elements relating to prediction of fracture mechanics parameters, in particular, are validated.

  ii) The analysis parameters, eg. modelling of geometry and loading, boundary conditions, and interpretation of results are checked according to appropriate quality standards.

  iii) Due to limitations of line spring elements, data generated using these elements require, in general, more extensive validation than data from analyses with three-dimensional solid elements (Section 5.4.1).

- Unexperienced analysts should begin with simple problems which can be validated against known solutions (NAFEMS benchmark examples could be used). Another good starting point may be to consider the problems analysed by the program developers for validation purposes, and build on these gradually until sufficient experience has been gathered. Such a step-by-step approach may include analysis of the structure in the uncracked condition which allows the predicted stresses to be verified using reliable parametric SCF equations. Then, the relatively more complex case of analysing cracks in tubular joints may be tackled.

Indirect methods including weight function methods have been reviewed in Section 5.4.2. They are particularly useful for generating stress intensity factor solutions for non linear stress fields such as those associated with notch stresses. The accuracy of solutions based on indirect methods depend on a number of parameters including

- Stresses in the uncracked conditions. These are computed only once and used in evaluation of any number of cracks
- Accuracy of the reference solutions used, eg. weight functions, and their applicability to the problem under consideration, eg. with regard to geometry, boundary conditions, and loading
- Numerical integration procedure

It is recommended that validation studies of solutions generated using indirect methods include comparisons with relevant standard and/or finite element solutions at least for linear stress distributions.

Calibration of fatigue and fracture assessments

Reliable and meaningful fatigue and fracture assessments can only be obtained if:

- Appropriate analysis models are applied
- Relevant input parameters relating to material properties, defect geometry and loading conditions are used
- Uncertainties are considered within the context of deterministic or probabilistic approaches
- Relative importance of various parameters are taken into account. Thus, the most influential parameters can be given higher priority than other less significant parameters. If no data or previous experience are available, sensitivity analyses may be performed in order to determine the importance of selected parameters

With regard to calibration of both fatigue and fracture analyses, agreement with limited test data may not be sufficient. Such an agreement may be misleading if it is achieved despite unsuspected modelling errors. Errors due to an input parameter may cancel errors due to another input parameter. Ideally, calibration procedures should involve a systematic validation of various components of the analysis, ie. input parameters and assessment models.

If relevant test data are available, validation of assessment model against such data would increase the confidence in the assessment procedure. The scatter associated with individual or limited data must be considered. Effects of such scatter may be minimised if the calibration procedure involves a wide range or mean representation of data, eg. mean S-N curves.

Assessment for fatigue

For general use the Paris Law with suitably selected crack growth constants, should be employed for fatigue crack growth calculations. Although a number of crack growth models, some of which attempt to model the whole (da/dN, ΔK) sigmoidal curve have been proposed, it is generally found that none of the equations has been proven to offer consistently good results in all crack growth regions under realistic loading and environmental conditions. An approach which is frequently been adopted is to use simple modified versions of the Paris Law, rather than the more complicated variants. Such an approach is described in PD 6493:1991 and outlined in Section 7.6.

Consideration of effects of residual stresses, stress ratio and threshold, enable fatigue crack growth calculations to be refined (Sections 7.1-7.3). In addition, adopting realistic models for crack shape development by either pre-specifying the crack aspect ratio or by considering the crack shape to be a part of the solution, can have important effects on the predicted fatigue life (Sections 2 and 7.7).

It is recommended to use the fatigue crack growth constants due to be included in the new revision of PD 6493. These are applicable to a wide range of materials and cover growth rates in air environment and in seawater with and without cathodic protection (Section 7.4).

Aspects of quantifying fatigue crack growth under variable amplitude loading are addressed in Section 7.5. It is recommended to use the ΔK_{eff} approach and include refinements which allow effects of residual stresses, stress ratio and threshold to be considered before averaging the weighted contribution of various stress cycle.

Assessment for fracture

A limited evaluation of available tubular joint fracture tests, performed as a part of this work, indicates that FAD-based predictions of the fracture loads for the vast majority of tests are conservative. This limited study confirms that the failure assessment diagram approach offers an adequate framework for performing fracture assessments of tubular joints. However, further evaluation of the data is necessary before detailed guidance can be given.

Some aspects of applying the FAD approach have been covered in Section 8. In particular, the following factors which can have significant effects on the results of FAD-based assessments have been discussed:

- Idealisation of surface defects and scope of assessment
- Models for the plastic collapse parameter
- Fracture toughness properties
- Residual stresses
- Tensile properties
- Uncertainties in data
- Non-unique critical solutions

11. REFERENCES

Aaghaakouchak, A., Glinka, G and Dharmavasan, S. 'A load shedding model for fracture mechanics analysis of fatigue cracks in tubular joints'. 8th Int. Conf. on Offshore Mechanics and Arctic Engineering, 1989.

Ainsworth, R.A., Engineering Fracture Mechanics, Vol 19, 1984, pp.633-642.

Albrecht, P. and Yamada, K. 'Rapid calculation of stress intensity factors', ASCE Journal of the Structural Division, Vol 103 (ST2), February 1977.

ASME 1986 Boiler and Pressure Vessel Code Section III Nuclear Power Plant Components Division 1.

American Society of Mechanical Engineers. Boiler and Pressure Vessel Code, Section XI, Division I, Appendix A, 'Analysis of flaw indications', 1980.

Austen, I.M. 'Measurement of fatigue crack growth theshold values for use in design'. BSC Report No. SH/EN/9708/2/83/B, British Steel Corporation, January 1983.

Austen, I.M. Rudd, W.J. and Walker, E.F. 'Factores affecting corrosion fatigue and stress corrosion crack growth in offshore steels'. Conference on Steel in Marine Structures, Paris, 1981.

Barsom, J. M. and Rolfe, S. T. Fracture and fatigue control in structures, Prentice-Hall, New Jersey, 1987.

Barsoum, R. S. 'On the use of isoparametric finite elements in LEFM', International Journal for Numerical Methods in Engineering, 10, 1976.

Bell, R. and Vosikovsky, O. 'A fatigue life prediction model for multiple cracks in welded joints for offshore structures', Offshore Mechanics and Arctic Engineering Conference, 1992.

Bell, R. 'Stress intensity factors for weld toe cracks in welded T-plate joints', DSS Contract No OST84-00125, Faculty of Engineering, Carlton University, Ottawa, 1987.

Bell, R., Vosikovsky, O., Burns, D.J. and Mohaupt, U.H. 'A fracture mechanics model for life prediction of welded plate joints'. Steel and Marine Structures, 1987.

Berge, S., Haswell, J. and Engesvik, K. 'Fracture mechanics analysis of tubular joints tests: Degree of bending effects'. 13th Int. Conf. on Offshore Mechanics and Arctic Engineering, 1994.

Berge, S., Eide, O. and Tubby, P. 'Fatigue strength of tubular joints: some unresolved problems', Offshore Mechanics and Arctic Engineering Conference, 1994.

Booth, G.S and Dobbs, S.J. 'Corrosion fatigue crack growth in BS 4360 Grade 50D steel - an analysis. Welding Institute Research Bulleting, Vol 27, September 1986.

Boswell, L.F d'Mellow, C.A and Edwards, A.J. 'Residual stress in welded tubular joints'. International Conference on Mobile Offshore Structures, City University, London 1987.

Bowness, D. and Lee, M.K.K. 'Fatigue crack curvature under the weld toe in a tubular joint'. 6th Int. Symposium on Tubular Structures, Australia, December 1994.

Bowness, D. and Lee, M. M. K. 'Stress fields and stress intensity factors in tubular joints, Offshore Mechanics and Arctic Engineering Conference, 1993.

Bowness, D. and Lee, M. M. K. 'Fatigue crack curvature under the weld toe in a tubular joint', 6th International Symposium on Tubular Structures, Australia, December 1994.

British Standards Institution. 'Guidance on methods for assessing the acceptability of flaws in fusion welded structures'. BS PD6493:1991.

British Standards Institution. 'Guidance on some methods for the derivation of acceptance levels for defects in fusion welded joints'. BS PD6493:1980.

British Standards Institution. 'Crack opening displacement (COD) testing'. BS5762, 1979.

Brown, D. K. 'On the analysis of cracked tubular joints', International Conference on Fatigue and Crack Growth in Offshore Structures, London, 1986.

Bueckner, H. F. 'A novel principle for the computation of stress intensity factors', Zeitschrift fur Angewandte Mathematik und Mechanik, 50, pp 529-546, 1970.

Burdekin, F.M., Chan, W. T. W., Manteghi, S. and Thurlbeck, S. D. 'Design assessment support for tubulars by fracture mechanics methods', Conference on Fatigue of Offshore Structures, London, 1988.

Burdekin, F. M., Chu, W. H., Chan, W. T. W. and Manteghi, S. 'Fracture mechanics analysis of fatigue crack propagation in tubular joints', International Conference on Fatigue and Crack Growth in Offshore Structures, London, 1986.

Burdekin, F.M. Thurlbeck, S.D. and Cowling, M.J. 'Defect assessment in offshore structures'. Application of BSI Document PD 6493:1991, OMAE, 1992.

Burns, D. J., Lambert, S. B. and Mohaupt, U. H. 'Crack growth behaviour and fracture mechanics approach', Steel in Marine Structures Conference, Amsterdam, 1987.

Cambridge University Engineering Department. 'Residual stresses in nodes'. July 1983 - June 1985. From Cohesive Programme of R&D into the fatigue of offshore structures.

Cheaitani, M.J., Thurlbeck, S.D., and Burdekin, F.M. 'Fatigue, fracture and plastic collapse of offshore tubular joints', OMAE, 1995.

Clayton, A. M. 'Assessment of UKOSRP crack growth data to investigate the remaining life of offshore structures following inspection', UKAEA Report ND-R-852(R), HMSO, London, 1982.

Connolly, M. P., Hellier, A. K., Dover, W.D. and Sutomo, J. 'A parametric study of the ratio of bending to membrane stress in tubular Y and T joints', International Journal of Fatigue, Vol 12, No 1, 1990.

Det norske Veritas R P D404 'Unstable fracture', 1988.

Det norske Veritas Note 30.2 'Fatigue strength analysis for mobile offshore units', 1984.

Dharmavasan, S. and Dover, W. D. 'Non destructive evaluation of tubular welded joints', Offshore Tubular Joints Conference, OTJ'88, 1988.

Dijkstra, O. D., Snijder, H. H. and van Straalen, I. J. 'Fatigue crack growth calculations using stress intensity factors for weld toe geometries', Offshore Mechanics and Arctic Engineering Conference, 1989.

Dijkstra, O. D., van Straalen, I. J. and Noordhook, C. 'A fracture mechanics approach of fatigue of welded joints in offshore structures', Offshore Mechanics and Arctic Engineering Conference, 1993.

Dover, W. D. and Connolly, M. P. 'Fatigue fracture mechanics assessment of tubular welded Y and K joints', International Conference on Fatigue and Crack Growth in Offshore Structures, London, 1986.

Dover, W. D. and Dharmavasan, S. 'Fatigue fracture mechanics analysis of T and Y joints', Offshore Technology Conference, OTC 4404, 1982.

Dover, W.D., Niu, X, Aaghaakouchak, A., Katc, R. and Topp, D.A. 'Fatigue crack growth in X joints and multibrace nodes'. Conference on Fatigue of Offshore structures, 1988.

Dover, W.D. 'Variable amplitude fatigue of welded structures'. SEE Conf. on Fracture Mechanics - Current Status - Future Prospects (ed. R.A. Smith), pp 125-147, Cambridge, 1979.

Du, Z. Z. and Hancock, J. W. 'Stress intensity factors of semi-elliptical cracks in a tubular welded joint using line springs and 3D finite elements', Journal of Pressure Vessel Technology, Vol III, 1989.

Dufresne, J. 'Probabilistic application of fracture mechanics', Advances in Fracture Research (Fracture 81), Vol 2, ICF 5 - Conference, pp 517-531, 1981.

Efthymiou, H. 'Development of SCF formulae and generalised influence functions for use in fatigue analysis'. Offshore Tubular Joints Conference, OTJ '88, UK, 1988.

Eide, O.I. and Berge, S. 'Fatigue of large scale plate girders with plate thickness 20, 40 and 60mm' Steel and Marine Structures, 1987.

Forbes, J., Glinka, G and Burns, D.J. 'Fracture mechanics analysis of fatigue cracks and load shedding in tubular welded joints'. 11th Int. Conf. on Offshore Mechanics and Arctic Engineering, 1992.

Forbes, J., Glinka, G and Burns, D. J. 'Fracture mechanics analysis of fatigue cracks and load shedding in tubular welded joints', Offshore Mechanics and Arctic Engineering Conference, 1992.

Forbes, J., Desjardins, J., Glinka, G. and Burns, D. J. 'Calculation of stress intensity factors for surface semi-elliptical cracks in weldments', Offshore Mechanics and Arctic Engineering Conference, 1991.

Forman, R.G. Kearney, V.E. and Engle, R.M. 'Numerical analysis of crack propagation in cyclic-loaded structures'. Journal of Basic Engineering, September 1967.

Fu, B., Haswell, J. V. and Bettess, P. 'Weld magnification factors for semi-elliptical surface cracks in fillet welded T-butt joint models', International Journal of Fracture, Vol 63, 1993.

Fu, B. 'An elastic finite element analysis of shallow surface cracks in welded T-butt plates'. British Gas Report No. ERS R.4344, 1990.

Garwood, S.J. et al. 'Crack tip opening displacement (CTOD) methods for fracture assessments: Proposals for revisions to BSI PD6493'. Welding Institute Members Report 371/1988.

Garwood, S.J. 'Fatigue crack growth threshold determination', Welding Institute research Bulletin. September 1979, 20 (9).

Glasgow Marine Technology Centre (GMTC). Defect Assessment in Offshore Structures Phase 2 Report, 1992.

Gurney, T. R. 'Theoretical analysis of the influence of attachment size on the fatigue strength of transverse non-load-carrying fillet welds', Welding Institute Research Report 91/1979, 1979.

Harrison, R.P. et al 1980. 'Assessment of the integrity of structures containing defects'. CEGB Report R/H/R6, Revision 2.

Haswell, J. 'Simple models for predicting stress intensity factors for tubular joints', Fatigue Fracture Engineering Materials Structures, Vol 14, 5, 1991.

Haswell, J. V. 'A general fracture mechanics model for a cracked tubular joint derived from the results of a finite element parametric study', Offshore Mechanics and Arctic Engineering Conference, 1992.

Hellier A.K., Connolly M.P., Dover W.D., 1990. 'Stress concentration factors for tubular Y- and T- joints'. Int. Journal of Fatigue 12 1 pp 13 - 23.

Henshell, R. D. and Shaw, K. G. 'Crack tip finite elements are unnecessary', International Journal for Numerical Methods in Engineering, 9, 1975.

Hibberd R.D. and Dover W.D. 'The analysis of random load fatigue crack propagation'. Proc. of 4th Int. Conf. on Fracture (ed. D.M. Tapling), Vol 2, pp 1187-1194, Waterloo, 1977.

Ho, C.M. and Zwerneman, F.J. 'Assessment of simplified methods, Joint Industry Project on fracture mechanics investigation of tubular joints, Phase Two, Oklahoma State University, 1995.

Holbrook, S. J. and Dover, W. D. 'The stress intensity factor for a deep surface crack in a finite plate', Engineering Fracture Mechanics, 12, 1979.

Hudak, S.J.Jr. Burnside, O.H and Chan, K.S. 'Analysis of corrosion fatigue crack growth in welded tubular joints'. Journal of Energy Resources Technology, Vol 107, June 1985

Hsu, T. M. 'Prediction of fatigue crack growth in tubular T joints', Offshore Mechanics and Arctic Engineering Conference, 1990.

Huang, X., Du Z. Z. and Hancock, J. W. 'A finite element evaluation of the stress intensity factors of surface cracks in a tubular T joint', Offshore Technology Conference, OTC 5665, 1988.

Huget, W., Esser, K. and Grueter, L. 'Stress intensity factors for slender surface cracks', 7th International Conference on Structural Mechanics in Reactor Technology (SMIRT), Illinois, 1983.

Ingraffea, A. R. and Manu, C. 'Stress intensity factor computation in three dimensions with quarter-point elements', International Journal for Numerical Methods in Engineering, Vol 15, 1980.

Isida, M., Noguchi, H. and Yoshida, T. 'Tension and Bending of finite thickness plates with a semi-elliptical surface crack', International Journal of Fracture, Vol 26, 1984.

Kam, J. C. P., Topp, D. A. and Dover, W. D. 'Fatigue fracture mechanics modelling and structural integrity assessment of offshore welded tubular joints, Transactions of the ASME, Vol III, August 1989.

King, R.N. Private communication, October 1995.

King, R. and Stacey, A. 'A critical review of fatigue crack growth rates for structural steels in air and seawater environments used in the revision of PD6493:1991'. OMAE 1996 (in press).

Klesnil, M, and Lukas, P. 'Influence of strength and stress history on growth and stabilisation of fatigue cracks'. Engineering Fracture Mechanics, 1972, Vol 4, pp 77-92.

Koterazawa, R. and Minamisaka, S. 'Stress intensity factors of semi-elliptical surface cracks in bending', J. Soc. Mater. Sci. Japan, Vol 26, 1977.

Kumar, V. et al. 'An engineering approach to elastic plastic fracture analysis'. EPRI Report NP-1931, 1981.

Kristiansen, N. O. and Fu, B. 'The free-surface stress intensity factor of surface cracks in tubular joint models', Offshore Mechanics and Arctic Engineering Conference, 1993.

Lambert, S. B. 'Effects of seawater on fatigue crack shape development', Offshore Mechanics and Arctic Engineering Conference, 1992.

Milen , I et al 1986. 'Assessment of the integrity of structures containing defects'. CEGB Report R/H/R6, Revision 3.

Mok, D.H.B. and Pick, R.J. 'Finite element study of residual stresses in a plate T-joint fatigue specimen'. Part C: Journal of Mechanical Engineering Science, Proceedings of the Institution of Mechanical engineers, London, 1990, Volume 204 pp.127-134.

Morgan, H.G. et al. 'An investigation of the corrosion fatigue crack growth behaviour of structural steels in seawater'. Paper 5.1 of Conf. Steel in Marine Structures, Paris, 1981.

Morgan, H.G. 'The relevance of interaction rules in evaluating the growth of multiple fatigue cracks'. OTC 5985, Offshore Technology Conference, Houston, 1989.

Murakami, Y., 'Stress intensity factors handbook', Volumes 1 and 2, Committee on Fracture mechanics, The Society of Materials Science, Japan, Pergamon Press, 1986.

Newman, J. C. and Raju, I. S. 'An empirical stress intensity factor equation for the surface crcak', Engineering Fracture Mechanics, Vol 15, 1981.

Newman, J. C. and Raju, I. S. 'Stress intensity factor equation for cracks in three-dimensional finite bodies subjected to tension and bending loads', NASA Technical Memorandom 85793, NASA, Virginia, 1984.

Newman J.C. 'A crack-closure model for predicting fatigue crack growth under aircraft spectrum loading'. American Society for testing and Materials ASTM, STP 748, pp53-84, 1981.

Niu, X. and Glinka, G. 'The weld profile effect on stress intensity factors in weldments', International Journal of Fracture, 35, 1987.

Niu, X. and Glinka, G. 'Stress intensity factors for semi-elliptical surface cracks in welded joints', International Journal of Fracture, 40, 1989.

Oore, M. and Burns, D. J. 'Estimation of stress intensity factors for irregular cracks subjected to arbitrary normal stress fields, ASME Journal of Pressure Vessel Technology, Vol 102, pp 202-211, 1980.

Offshore Research Focus, June 1995.

Pang, H. L., J. 'A review of stress intensity factors for a semi-elliptical surface crack in a plate and fillet welded joint, The Welding Institute Research Report 426/1990, 1990.

Pang, H. L., J. 'A literature review of stress intensity factor solutions for a weld toe crack in a fillet welded joint', National Engineering Laboratory, Report No 721, 1991.

Pang, H. L., J. 'Fatigue crack growth and coalescence of surface cracks', Offshore Mechanics and Arctic Engineering Conference, 1993.

Petroski, H. J. and Achenbach, J. D. 'Computation of the weight function from a stress intensity factor', Engineering Fracture Mechanics, Vol 10, No 2, pp 257-266, 1978.

Paris, P. C. et al 'A rational analysis theory of fatigue', The Trend of Engineering, University of Washington, 13, pp 9-14, 1961.

Parks, D. M. 'A stiffness finite element technique for determination of crack tip stress intensity factors', International Journal of Fracture, Vol 10, No 4, December 1974.

Phaal, R. 'Non-unique solutions in PD 6493:1991 fracture assessment procedures'. Technology Briefing 493/1994, TWI, 1994.

Plane, C.A., Cowling, M.J. Nwegbu, V.K. and Burdekin F.M. 'The determination of safety factors for defect assessment using reliability methods', 3rd Int. Symp. on Integrity of Offshore Structures, Glasgow University, 1987.

Raju, I. S. and Newman, J. C. 'Stress intensity factors for a wide range of semi-elliptical surface cracks in finite thickness plates', Engineering Fracture Mechanics, Vol 11, 1979.

Rhee, H. C. 'The behaviour of stress intensity factors of weld toe surface flaw of tubular X joint', Offshore Technology Conference, OTC 5136, Houston, 1986.

Rhee, H. C. 'Fatigue crack growth analysis of offshore structural tubular joints', Offshore Mechanics and Arctic Engineering Conference, 1987.

Rhee, H. C. 'Fatigue life calculations for offshore structural tubular joint using fracture mechanics crack growth analysis', Offshore Technology Conference, OTC 5557, Houston, 1987.

Rhee, H. C. 'Fracture mechanics fatigue life analysis for a multiplanar K joint', Offshore Mechanics and Arctic Engineering Conference, 1988.

Rhee, H. C. 'Stress intensity factor evaluation from displacement along arbitrary crack tip radial lines for warped surface flaws', Engineering Fracture Mechanics, 32, 1989.

Rhee, H. C., Han, S. and Gipson, G. S. 'Reliability of solution method and empirical formulas of stress intensity factors for weld toe cracks of tubular joints', Offshore Mechanics and Arctic Engineering Conference, 1991.

Rhee, H. C. and Salama, M. M. 'On the evaluation of stress intensity factor for tubular joint fatigue study', Offshore Technology Conference, OTC 4998, Houston, 1985.

Rhee, H. C. and Salama, M. M. 'Mixed mode stress intensity factor solutions of a warped surface flaw by three-dimensional finite element analysis', Engineering Fracture Mechanics, 28, 1987.

Rice, J. R. and Levy, N. 'The part-through surface crack in an elastic plate', Journal of Applied Mechanics, 39, 1972.

Rice, J. R. 'Some remarks on elastic crack-tip stress fields', International Journal of Solids and Structures, 8, pp 751-758, 1972.

Ritchie, D., Voermans, C. W. M. and Vollan, K. 'Stress intensity factors in an offshore tubular joint test specimen, Fourth International Conference on Numerical Methods in Fracture Mechanics, San Antonio, Texas, 1987.

Rooke, D. P., Baratta, F. I. and Cartwright, D. J. 'Simple methods of determining stress intensity factors', Engineering Fracture Mechanics, Vol 14, 1981.

Rooke, D. P. and Cartwright, D. J. 'Compendium of stress intensity factors', HMSO, London, 1974.

Scott, P. M. and Thorpe, T. W. 'A critical review of crack tip stress intensity factors for semi-elliptical cracks', Fatigue of Engineering Materials and Structures, Vol 4, 4, 1981.

Shetty, N.K. and Baker, M.J. 'Fatigue reliability of tubular joints in offshore structures: crack propagation model'. OMAE 90', Houston, February 1990.

Smith, I. J. 'Stress intensity factors for toe defects in single-sided transverse attachments of varying thickness made with fully penetrating welds', Welding Institute Research Report 183/1982, 1982.

Smith, I. J. and Hurworth, S. J. 'The effect of geometry changes upon the predicted fatigue strength of welded joints', The Welding Institute Report 7819.01/84/394.3, Cambridge1984.

Smith, I.F.C. and Gurney, T.R. 'Changes in the fatigue life of plates with attachments due to geometrical effects'. Welding Research Supplement, September 1986, pp. 244-250.

Snijder, H.H. et al (1988). 'Fatigue crack growth modelling for multiple initiated cracks at the weld toes in tubular joints'. Behaviour of offshore structures, BOSS-88, Trondheim, Norway.

Stacey, A. 'Review of the post-weld heat treatment requirements for offshore structures'. Materials Engineering, Volume III, OMAE 1994, ASME 1994.

Stacey, A. 'The significance of residual stresses in the defect assessment of offshore structures', Offshore Mechanics and Arctic Engineering Conference, 1993.

van Straalen, I. J. J., Dijkstra, O. D. and Snijder, H. H. 'Stress intensity factors and fatigue crack growth of semi-elliptical surface cracks at weld toes', TWI International Conference - Weld Failures, London 1988.

Tada, H., Paris, P. C. and Irwin, G. R. 'The stress analysis of cracks handbook', Del Research Corporation, Pensylvania, 1973.

Thorpe, T.W. and Rance, A. 'Corrosion fatigue crack growth in BS 4360 Grade 50D structural steel in seawater under narrow band variable amplitude loading'. Department of Energy Offshore Technology Report OTH 86 232.

Thurlbeck, S. D. 'A fracture mechanics based methodology for the assessment of weld toe cracks in tubular offshore joints', PhD Thesis, UMIST, Manchester, 1991.

Thurlbeck, S.D. and Burdekin, F. M. 'Constant and variable amplitude LEFM fatigue assessment for tubular joints incorporating threshold effects', Offshore Mechanics and Arctic Engineering Conference, 1992.

Topp, D. A. and Dover, W. D. 'Validation of crack sizing and detection techniques for offshore structures', 21st Annual British Conference on Non-Destructive testing, Newcastle Upon Tyne, 1986.

Tubby, P., Eide, O., Skallerud, B. and Berge, S. 'Variable amplitude fatigue of steel tubular joints in sea water with cathodic protection', Offshore Mechanics and Arctic Engineering Conference, 1994.

Tweed, J. H. 'Remaining life of defective tubular joints: Depth of crack growth in UKOSRP II and implications', OTH 87 278, HMSO, London, 1987.

Tweed, J. H. and Freeman, J. H. 'Remaining life of defective tubular joints - An assessment based on data for surface crack growth in tubular joint fatigue tests', OTH 87 259, HMSO, London, 1987.

van Echo, J.A Roach, D.B and Hall, A.M. 'Short-time tensile and long-time creep-rupture properties of the HK-40 alloy and type 310 stainless steel at temperatures to 2000F'. Journal of Basic Engineering, September 1967.

Vosikovsky, O., Bell, R., Burns, D. J. and Mohaupt, U. H. 'Fracture mechanics assessment of fatigue life of welded plate T-joints including thickness effect', Behaviour of Offshore Structures Conference, BOSS'85, 1985.

Wheeler D.E. 'Crack growth under spectrum loading'. General Dynamics Report FZM 5602, 1970.

Willenborg, J. et al. 'A crack growthretardation model using ane ffective stress concept'. American Society for Testing and Materials AFFDL-TM-71-1-FBR, 1971.

APPENDIX A

PARAMETRIC EQUATIONS FOR DEGREE OF BENDING (DOB)

The following equations are reproduced from:

Connolly, M. P., Hellier, A. K., Dover, W.D. and Sutomo, J. 'A parametric study of the ratio of bending to membrane stress in tubular Y and T joints', International Journal of Fatigue, Vol 12, No 1, 1990.

Unless noted the validity range are as follows:

$$6.21 \leq \alpha$$

$$0.20 \leq \beta \leq 0.80$$

$$7.60 \leq \gamma \leq 32.0$$

$$0.20 \leq \tau \leq 1.00$$

$$35^\circ \leq \theta \leq 90^\circ$$

Brace axial loading

Parametric equation for the ratio of bending to total stress under axial loading at the chord hot-spot stress site:

$$\sigma_b/\sigma_{total} = 0.7026\ \alpha^{0.0236} \exp(-0.187\beta^4 + 0.0097\gamma + 0.0047/\theta^3 - 21.7\beta^3/\gamma^2 + 0.3038\beta\tau - 0.0867\beta^2/\theta^3 - 0.001\gamma^{1.5}\theta) \quad [A1]$$

Parametric equation for the ratio of bending to total stress under axial loading at the brace hot-spot stress site:

$$\sigma_b/\sigma_{total} = 0.6763\ \alpha^{0.0603}\gamma^{0.118}\tau^{0.24}\exp(-0.292\beta^{2.5} - 0.0407/\theta - 0.142\tau\theta + 0.0833\beta^3\theta) \quad [A2]$$

Parametric equation for the ratio of bending to total stress under axial loading at the chord saddle position:

$$\sigma_b/\sigma_{total} = 0.785\ \alpha^{0.0122}\gamma^{0.212\beta^{2.2}}\tau^{0.0117}\sin^{-0.1}\theta \times \exp(-0.799\beta^{2.5} + 0.165\beta\tau) \quad [A3]$$

Parametric equation for the ratio of bending to total stress under axial loading at the brace saddle position:

$$\sigma_b/\sigma_{total} = 0.6698\ \alpha^{0.0431}\gamma^{0.0834}\theta^{-0.0896} \times \exp(-0.1846\beta^2 - 0.0672/\tau + 0.0017\gamma\tau) \quad [A4]$$

Exceptions:

Axial brace saddle - where both $\theta < 45^\circ$ and $\tau < 0.40$, assume $\sigma_b/\sigma_{total} = 0$.

Brace in-plane bending

Parametric equation for the ratio of bending to total stress under in-plane bending at the chord hot-spot stress site:

$$\sigma_b/\sigma_{total} = 0.7984\ \alpha^{-0.0283}\tau^{-0.0017}\theta^{-0.024} \times \exp(0.0656/\beta + 0.00027\gamma^2 - 0.0819\theta/\alpha - 0.00036\theta/\beta^3 - 0.0001\gamma^2/\beta) \quad (A5)$$

Parametric equation for the ratio of bending to total stress under in-plane bending at the brace hot-spot stress site:

$$\sigma_b/\sigma_{total} = 0.6893\ \alpha^{0.0158}\beta^{0.226}\gamma^{(0.272-0.0443\tau+0.0196\theta)} \times \tau^{0.298}\theta^{0.0869}\exp(-0.0187\beta\gamma - 0.000343/\beta^2\tau - 0.1\beta\theta^2 - 0.114\tau\theta) \quad (A6)$$

Parametric equation for the ratio of bending to total stress under in-plane bending at the chord crown position:

$$\sigma_b/\sigma_{total} = 0.2886\alpha^{-0.0464}\gamma^{-0.242}\exp(-0.617\beta^{0.5} - 0.112\tau + 0.738\theta + 0.178\beta\tau - 1.34\gamma^{-0.2}\theta) \quad [A7]$$

Parametric equation for the ratio of bending to total stress under in-plane bending at the brace crown position:

$$\sigma_b/\sigma_{total} = 0.6683\alpha^{0.0143}\gamma^{(0.127+0.0968\tau^2-0.0038\theta)}\theta^{0.149} \times \exp(-0.00218/\beta^3 - 0.0143/\tau^2 + 0.000953/\beta^2\tau - 0.0145\beta\gamma - 0.162\tau\theta) \quad [A8]$$

Exceptions:

IPB brace hot spot - where both $\theta < 45°$ and $\tau < 0.45$, assume $\sigma_b/\sigma_{total} = 0$

IPB brace crown - where both $\theta < 45°$ and $\tau < 0.65$, assume $\sigma_b/\sigma_{total} = 0$.

Brace out-of-plane bending

Parametric equation for the ratio of bending to total stress under out-of-plane bending at the chord hot-spot stress site:

$$\sigma_b/\sigma_{total} = 0.768\ \beta^{-0.0882}\gamma^{0.0115}\tau^{0.00668} \times \exp(0.000122\alpha^2 + 0.04/\theta - 0.00249\tau/\beta^2 + 0.0123\tau/\theta^2) \quad \text{(A9)}$$

Parametric equation for the ratio of bending to total stress under out-of-plane bending at the brace hot-spot site:

$$\sigma_b/\sigma_{total} = 0.5174\ \alpha^{0.0211}\gamma^{0.203}\tau^{0.159}\theta^{-0.0919} \times \exp(-0.000048/\beta^5 - 0.00963\beta\gamma) \quad \text{(A10)}$$

Parametric equation for the ratio of bending to total stress under out-of-plane bending at the chord saddle position:

$$\sigma_b/\sigma_{total} = 0.7964\beta^{-0.0907}\gamma^{0.0092}\theta^{-0.0793} \times \exp(0.000159\alpha^2 + 0.0549\tau^2 - 0.0252\tau/\beta + 0.00223\theta^3/\beta + 0.000738\gamma\tau^3) \quad \text{(A11)}$$

Parametric equation for the ratio of bending to total stress under out-of-plane bending at the brace saddle position:

$$\sigma_b/\sigma_{total} = 0.61\alpha^{-0.0045}\gamma^{0.168}\theta^{-0.103} \times \exp(-0.000041/\beta^5 - 0.0665/\tau\ 0.0095\beta^2\gamma) \quad \text{(A12)}$$

Exceptions:

OPB brace hot spot - where both $\theta \leq 45°$ and $\beta \leq 0.25$, assume $\sigma_b/\sigma_{total} = 0$

OPB brace crown - where both $\theta < 45°$ and $\beta \leq 0.20$, assume $\sigma_b/\sigma_{total} = 0$.

Circumferential DOB Distribution (Cheaitani et al 1995, GMTC 1992)

For $0° < \phi < 90°$

$$\Omega_{\phi(AX)} = \Omega_{90°(AX)} - (\Omega_{90°(AX)} - \Omega_{0°(AX)})\ \mathrm{Cos}^3\phi$$
$$\Omega_{\phi(IP)} = \Omega_{0°(IP)} + (\phi/(180 - 2\phi)^2)\ \Omega_{0°(IP)}$$
$$\Omega_{\phi(OP)} = \Omega_{90°(OP)} + ((90 - \phi)/(\phi)^2)\ \Omega_{90°(OP)}$$

For $90° < \phi < 180°$

$$\Omega_{\phi(AX)} = \Omega_{90°(AX)} - (\Omega_{90°(AX)} - \Omega_{180°(AX)})\ \mathrm{Cos}^3(180 - \phi)$$
$$\Omega_{\phi(IP)} = \Omega_{180°(IP)} + ((180 - \phi)/(2\phi - 180)^2)\ \Omega_{180°(IP)}$$
$$\Omega_{\phi(OP)} = \Omega_{90°(OP)} + ((\phi - 90)/(180 - \phi)^2)\ \Omega_{90°(OP)}$$

For $180° < \phi < 270°$

$$\Omega_{\phi(AX)} = \Omega_{270°(AX)} - (\Omega_{270°(AX)} - \Omega_{180°(AX)})\ \mathrm{Cos}^3(\phi - 180)$$
$$\Omega_{\phi(IP)} = \Omega_{180°(IP)} + ((\phi - 180)/(540 - 2\phi)^2)\ \Omega_{180°(IP)}$$
$$\Omega_{\phi(OP)} = \Omega_{270°(OP)} + ((270 - \phi)/(\phi - 180)^2)\ \Omega_{270°(OP)}$$

For $270° < \phi < 360°$

$$\Omega_{\phi(AX)} = \Omega_{270°(AX)} - (\Omega_{270°(AX)} - \Omega_{0°(AX)}) \, Cos^3(360 - \phi)$$
$$\Omega_{\phi(IP)} = \Omega_{0°(IP)} + ((360 - \phi)/(2\phi - 540)^2) \, \Omega_{0°(IP)}$$
$$\Omega_{\phi(OP)} = \Omega_{270°(OP)} + ((\phi - 270)/(360 - \phi)^2) \, \Omega_{270°(OP)}$$

For $\phi = 0°$

$$\Omega_{\phi(AX)} = \Omega_{0°(AX)}$$
$$\Omega_{\phi(IP)} = \Omega_{0°(IP)}$$
$$\Omega_{\phi(OP)} = \Omega_{90°(OP)} + ((90 - 0.1)/(0.1)^2) \, \Omega_{90°(OP)}$$

For $\phi = 90°$

$$\Omega_{\phi(AX)} = \Omega_{90°(AX)}$$
$$\Omega_{\phi(IP)} = \Omega_{0°(IP)} + (89.9/(180 - 179.9)^2) \, \Omega_{0°(IP)}$$
$$\Omega_{\phi(OP)} = \Omega_{90°(OP)}$$

For $\phi = 180°$

$$\Omega_{\phi(AX)} = \Omega_{180°(AX)}$$
$$\Omega_{\phi(IP)} = \Omega_{180°(IP)}$$
$$\Omega_{\phi(OP)} = \Omega_{90°(OP)} + ((179.9 - 90)/(180-179.9)^2) \, \Omega_{90°(OP)}$$

For $\phi = 270°$

$$\Omega_{\phi(AX)} = \Omega_{270°(AX)}$$
$$\Omega_{\phi(IP)} = \Omega_{0°(IP)} + (89.9)/(180-179.9)^2) \, \Omega_{0°(IP)}$$
$$\Omega_{\phi(OP)} = \Omega_{270°(OP)}$$

0° and 180° denote crown positions
90° and 270° denote saddle positions
ϕ denotes angular location, measured from 0° crown location
AX, IP, and OP denote axial, in-plane, and out-of-plane loading

Note: The expressions for $\Omega_{0°(OP)}$, $\Omega_{90°(IP)}$, $\Omega_{180°(OP)}$ and $\Omega_{270°(IP)}$, were chosen in order to avoid developing infinite DOB values as σ_{tot} approaches zero.

APPENDIX B

PARAMETRIC EQUATIONS FOR STRESS INTENSITY MAGNIFICATION FACTORS (Mk)

APPENDIX B COEFFICIENTS FOR THE MK EQUATIONS PROPOSED BY DIJKSTRA ET AL AND REPORTED IN:

Dijkstra, O. D., Snijder, H. H. and van Straalen, I. J. 'Fatigue crack growth calculations using stress intensity factors for weld toe geometries', Offshore Mechanics and Arctic Engineering Conference, 1989.

Dijkstra, O. D., van Straalen, I. J. and Noordhook, C. 'A fracture mechanics approach of fatigue of welded joints in offshore structures', Offshore Mechanics and Arctic Engineering Conference, 1993.

1. g_L (a/T.L/T):

g_L (a/T.L/T) = 10^p for a/T ≤ 0.4

g_L (a/T.L/T) = 1.0 for a/T > 0.4

where $p = B0+B1*\log(a/T) + B2*[\log(a/T)]^2$

and $B0 = A00 + A01*(L/T) + A02*(L/T)^2 + A03*(L/T)^3$

$B1 = A10 + A11*(L/T) + A12*(L/T)^2 + A13*(L/T)^3$

$B2 = A20 + A21*(L/T) + A22*(L/T)^2 + A23*(L/T)^3$

The curve fit coefficients A00 - A23 are as follows:

Coefficient	Bending	Membrane
A00	0.064786	0.056799
A01	-0.092831	-0.069547
A02	0.037914	0.041922
A03	-0.003925	-0.009259
A10	0.225863	0.207689
A11	-0.261891	-0.219371
A12	0.097998	0.138435
A13	-0.006443	-0.031627
A20	0.104874	0.100385
A21	0.025918	0.021066
A22	-0.034588	-0.015169
A23	0.011765	0.003573

2. f_θ (a/T, θ):

f_θ (a/T, θ) = $(10.a/T)^{-1/2(\log A\theta)}$ for $0.001 \leq a/T \leq 0.1$

where $A_\theta = 13.096.10^{-3} + 28.119.10^{-3}\ \theta - 139.45.10^{-6}\ \theta^2$

f_θ (a/T, θ) = 1.0 for a/T > 0.1

3. $f_r\ (a/T,\ r/T)$:

$$f_r\ (a/T,\ r/T) = 1 - A_r.e^{-Br.a/T} \qquad \text{for } a/T \leq 0.1$$

where $A_r = A_{r1} + A_{r2}/\ (r/T - A_{r3})$

$$B_r = B_{r1} + B_{r2}.\ (r/T)^2$$

$$f_r\ (a/T,\ r/T) = 1.0 \qquad \text{for } a/T > 0.1$$

The coefficients A_{r1} - B_{r2} are as follows:

Coefficient	Bending	Membrane
A_{r1}	0.70754	0.71032
A_{r2}	-0.020160	-0.024015
A_{r3}	-0.024502	-0.028061
B_{r1}	75.323	105.29
B_{r2}	-1541.7	-1993.8

Mk Correction Factor Equations for Membrane Stress - Peak Path (Cheaitani et al 1995, GMTC 1992)

$$Mk_{m(combined)} = Mk_{m(L/T)} \times \frac{Mk_{m(\theta)}}{Mk_{m(\theta=45°)}} \times \frac{Mk_{m(r/T)}}{Mk_{m(r/T=0.01)}} \times f(r/T, \theta)$$

$$Mk_{m(n)} = C_m0_{(n)} + C_m1_{(n)} \text{Log}_e\frac{a}{T} + C_m2_{(n)}\left[\text{Log}_e\frac{a}{T}\right]^2 + C_m3_{(n)}\left[\text{Log}_e\frac{a}{T}\right]^3$$

where n = L/T, θ, or r/T. If Mk < 1.0 or a/T > 0.2, Mk = 1.0

For the base case, i.e. L/T = 1.0, θ = 45° and r/T = 0.01, $Mk_{m(combined)} = Mk_{m(L/T)}$.

<u>Attachment Length Parameter - L/T</u>

Validity ranges: $0.375 \leq L/T \leq 3.0$

For $0.375 \leq L/T \leq 1.0$

$$C_m0_{(L/T)} = 0.671 + 1.779(L/T) - 0.965(L/T)^2$$
$$C_m1_{(L/T)} = -0.204 + 1.735(L/T) - 0.9145(L/T)^2$$
$$C_m2_{(L/T)} = -0.033 + 0.5114(L/T) - 0.248(L/T)^2$$
$$C_m3_{(L/T)} = -0.0048 + 0.0368(L/T) - 0.0176(L/T)^2$$

For $1.0 < L/T \leq 3.0$

$$C_m0_{(L/T)} = 1.7832 - 0.5433(L/T) + 0.2966(L/T)^2 - 0.0507(L/T)^3$$

$$C_m1_{(L/T)} = 0.8870 - 0.4978(L/T) + 0.2750(L/T)^2 - 0.0474(L/T)^3$$
$$C_m2_{(L/T)} = 0.2750 - 0.0877(L/T) + 0.0529(L/T)^2 - 0.0096(L/T)^3$$
$$C_m3_{(L/T)} = 0.0184 - 0.0077(L/T) + 0.0046(L/T)^2 - 0.0008(L/T)^3$$

Weld Angle Parameter - θ

Validity range: $22.5^\circ \leq \theta \leq 90^\circ$ (Note θ_r is equivalent in radians)

For $22.5^\circ \leq \theta \leq 60^\circ$

$$C_m0_{(\theta)} = -0.2723 + 4.5636(\theta_r) - 2.9600(\theta_r)^2$$
$$C_m1_{(\theta)} = -1.0830 + 4.2240(\theta_r) - 2.6204(\theta_r)^2$$
$$C_m2_{(\theta)} = -0.1978 + 0.9575(\theta_r) - 0.5245(\theta_r)^2$$
$$C_m3_{(\theta)} = -0.0111 + 0.0569(\theta_r) - 0.0311(\theta_r)^2$$

For $60^\circ < \theta \leq 90^\circ$

$$C_m0_{(\theta)} = 5.3391 - 7.1219(\theta_r) + 3.0815(\theta_r)^2$$
$$C_m1_{(\theta)} = 3.8342 - 5.8670(\theta_r) + 2.5297(\theta_r)^2$$
$$C_m2_{(\theta)} = 0.8704 - 1.1015(\theta_r) + 0.4677(\theta_r)^2$$
$$C_m3_{(\theta)} = 0.0547 - 0.0691(\theta_r) + 0.0293(\theta_r)^2$$

Weld Toe Radius Parameter - r/T

Validity Range: $0.01 \leq r/T \leq 0.5$

For $0.01 \leq r/T < 0.1$

$$C_m0_{(r/T)} = 1.6167 - 13.553(r/T) + 46.281(r/T)^2$$
$$C_m1_{(r/T)} = 0.7262 - 11.244(r/T) + 31.193(r/T)^2$$
$$C_m2_{(r/T)} = 0.2515 - 2.1006(r/T) + 1.8965(r/T)^2$$
$$C_m3_{(r/T)} = 0.0143 + 0.0247(r/T) - 0.9807(r/T)^2$$

For $0.1 < r/T \leq 0.5$

$$C_m0_{(r/T)} = 0.9127 - 2.2231(r/T) + 3.3824(r/T)^2$$
$$C_m1_{(r/T)} = 0.1521 - 2.6884(r/T) + 3.7842(r/T)^2$$
$$C_m2_{(r/T)} = 0.1480 - 1.0050(r/T) + 1.2918(r/T)^2$$
$$C_m3_{(r/T)} = 0.0142 - 0.0824(r/T) + 0.1027(r/T)^2$$

Membrane r/T and θ Interaction Parameter

For $0.01 \leq r/T \leq 0.1$

$$f(r/T,\theta) = -11.111(1-Mk_{m(BASE)}/Mk_{m(\theta)})(r/T) + 1.111 - 0.111(Mk_{m(BASE)}/Mk_{m(\theta)})$$

For $0.1 < r/T \leq 0.5$

$$f(r/T,\theta) = Mk_{m(BASE)}/Mk_{m(\theta)}$$

Mk Correction Factor Equations for Bending Stress - Peak Path (Cheaitani et al, 1995)

$$Mk_{b(combined)} = Mk_{b(L/T)} \times \frac{Mk_{b(\theta)}}{Mk_{b(\theta=45°)}} \times \frac{Mk_{b(r/T)}}{Mk_{b(r/T=0.01)}} \times f(r/T, \theta)$$

$$Mk_{b(n)} = C_b0_{(n)} + C_b1_{(n)} Log_e \frac{a}{T} + C_b2_{(n)} \left[Log_e \frac{a}{T}\right]^2 + C_b3_{(n)} \left[Log_e \frac{a}{T}\right]^3$$

where n = L/T, θ, or r/T. If Mk < 1.0 or a/T > 0.2, Mk = 1.0

For the base case, i.e. L/T = 1.0, θ = 45° and r/T = 0.01, $Mk_{b(combined)} = Mk_{b(L/T)}$.

Attachment Length Parameter - L/T

Validity ranges: $0.375 \leq L/T \leq 3.0$

For $0.375 \leq L/T \leq 1.0$

$$C_b0_{(L/T)} = 0.9638 + 0.5183(L/T) - 0.254(L/T)^2$$
$$C_b1_{(L/T)} = 0.0464 + 0.6654(L/T) - 0.276(L/T)^2$$
$$C_b2_{(L/T)} = 0.0465 + 0.2100(L/T) - 0.046(L/T)^2$$
$$C_b3_{(L/T)} = 0.0016 + 0.0119(L/T)$$

For $1.0 < L/T \leq 3.0$

$$C_b0_{(L/T)} = 1.4656 - 0.4793(L/T) + 0.2948(L/T)^2 - 0.0529(L/T)^3$$
$$C_b1_{(L/T)} = 0.6386 - 0.3976(L/T) + 0.2370(L/T)^2 - 0.0423(L/T)^3$$
$$C_b2_{(L/T)} = 0.2232 - 0.0455(L/T) + 0.0422(L/T)^2 - 0.0092(L/T)^3$$
$$C_b3_{(L/T)} = 0.0145 - 0.0037(L/T) + 0.00356(L/T)2 - 0.0008(L/T)^3$$

Weld Angle Parameter - θ

Validity range: $22.5° \leq \theta \leq 90°$ (Note θ_r is equivalent in radians)

For $22.5° \leq \theta \leq 60°$

$$C_b0_{(\theta)} = 0.8030 + 0.7397(\theta_r) - 0.2526(\theta_r)^2$$
$$C_b1_{(\theta)} = -0.2153 + 1.1941(\theta_r) - 0.4643(\theta_r)^2$$
$$C_b2_{(\theta)} = -0.0464 + 0.4840(\theta_r) - 0.2000(\theta_r)^2$$
$$C_b3_{(\theta)} = -0.0047 + 0.0398(\theta_r) - 0.0211(\theta_r)^2$$

For $60° < \theta \leq 90°$

$$C_b0_{(\theta)} = 0.1445 + 1.6688(\theta_r) - 0.5394(\theta_r)^2$$
$$C_b1_{(\theta)} = -1.0531 + 2.2865(\theta_r) - 0.7444(\theta_r)^2$$
$$C_b2_{(\theta)} = -0.3365 + 0.8420(\theta_r) - 0.2765(\theta_r)^2$$
$$C_b3_{(\theta)} = -0.0441 + 0.0853(\theta_r) - 0.0286(\theta_r)^2$$

Weld Toe Radius Parameter - r/T

Validity Range: $0.01 \leq r/T \leq 0.5$

For $0.01 \leq r/T < 0.1$

$$C_b0_{(r/T)} = 1.2784 - 5.2218(r/T) + 19.935(r/T)^2$$
$$C_b1_{(r/T)} = 0.5044 - 7.1937(r/T) + 31.128(r/T)^2$$
$$C_b2_{(r/T)} = 0.2305 - 2.0478(r/T) + 7.9234(r/T)^2$$
$$C_b3_{(r/T)} = 0.0137 - 0.0172(r/T) - 0.1580(r/T)^2$$

For $0.1 < r/T \leq 0.5$

$$C_b0_{(r/T)} = -0.2049 + 0.2654(r/T)^{-0.5} + 1.016(r/T)^{0.5}$$
$$C_b1_{(r/T)} = -1.5810 + 0.3995(r/T)^{-0.5} + 1.3089(r/T)^{0.5}$$
$$C_b2_{(r/T)} = -0.3637 + 0.1201(r/T)^{-0.5} + 0.2813(r/T)^{0.5}$$
$$C_b3_{(r/T)} = -0.02211 + 0.00871(r/T)^{-0.5} + 0.01576(r/T)^{0.5}$$

Bending r/T and θ Interaction Parameter

For $0.01 \leq r/T \leq 0.08$

$$f(r/T,\theta) = -14.29(1-Mk_{b(BASE)}/Mk_{b(\theta)})(r/T) + 1.1429 - 0.1429(Mk_{b(BASE)}/Mk_{b(\theta)})$$

For $0.08 < r/T \leq 0.5$

$$f(r/T,\theta)=Mk_{b(BASE)}/Mk_{b(\theta)}$$

Ma Correction Factor Equations

For Membrane Stress

For: $a/T < 0.001$

$$MM_1 = 0.8$$

For: $0.001 \leq a/T \leq 0.1$

$$M_1 = 1.662 - 1.637(a/c)^{0.1} + 0.596(a/c)^{0.2}$$
$$M_2 = -1.783 + 4.337(a/c)^{0.1} - 1.589(a/c)^{0.2}$$
$$M_3 = 5.1 - 11.92(a/c)^{0.1} + 4.29(a/c)^{0.2}$$
$$MM_1 = M_1 + M_2(a/T)^{0.25} + M_3(a/T)$$

For: $0.1 < a/T \leq 0.5$

$$MM_1 = 0.91(a/c)^{-0.015}$$

For: $0.5 < a/T \leq 1.0$

$MM_1 = 1 - 2(1-M_{0.5})(1-a/T)$; where $M_{0.5} = MM_1$ at $a/T = 0.5$

$$Ma_m = 1 + ((Mk_m-1)/MK_{m(BASE)}).(Mk_{m(BASE)}(1-MM_1)/(1-Mk_{m(BASE)})$$

For the base case, $Ma_m = MM_1$.

For Bending Stress

For: $a/T < 0.001$

$MB_1 = 0.8$

For: $0.001 \leq a/T \leq 0.2$

$M_1 = 1.685 - 1.535(a/c)^{0.1} - 0.0754(a/c)$

$M_2 = 0.100 - 0.923(a/c)^{0.2} - 1.3700(a/c)^{0.8}$

$M_3 = -0.91 + 2.040(a/c)^{0.1} + 0.2000(a/c)$

$MB_1 = M_1 + M_2(a/T) + M_3(a/T)^{0.1}$

For: $0.2 < a/T \leq 0.5$

$MB_1 = 0.91(a/c)^{-0.0125} - 2(0.91(a/c)^{-0.0125} - e^{(0.0054-0.584(a/c))})(a/T)$

For: $0.5 < a/T \leq 1.0$

$MB_1 = 1 - 2(1-M_{0.5})(1-a/T)$; where $M_{0.5} = MB_1$ at $a/T = 0.5$

$Ma_b = 1 + ((Mk_b-1)/MK_{b(BASE)}).(Mk_{b(BASE)}(1-MB_1)/(1-Mk_{b(BASE)})$

For the base case, $Ma_b = MB_1$.

APPENDIX C

PARAMETRIC EQUATIONS FOR STRESS INTENSITY FACTORS

APPENDIX C STRESS INTENSITY FACTOR EQUATIONS FOR T JOINTS. REPRODUCED FROM:

Rhee, H. C., Han, S. and Gipson, G. S. 'Reliability of solution method and empirical formulas of stress intensity factors for weld toe cracks of tubular joints', Offshore Mechanics and Arctic Engineering Conference, 1991.

	d	T	t	a	c
1	400.00	25.00	7.50	20.00	160.00
2	400.00	25.00	7.50	1.25	93.33
3	400.00	25.00	7.50	1.25	6.67
4	400.00	25.00	25.00	5.00	93.33
5	400.00	25.00	25.00	1.25	160.00
6	400.00	25.00	25.00	20.00	6.67
7	400.00	33.33	10.00	26.67	13.33
8	400.00	33.33	33.33	3.33	13.33
9	400.00	50.00	15.00	40.00	6.67
10	400.00	50.00	15.00	2.50	160.00
11	400.00	50.00	15.00	10.00	93.33
12	400.00	50.00	32.50	20.00	46.67
13	400.00	50.00	50.00	40.00	160.00
14	400.00	50.00	50.00	2.50	6.67
15	600.02	25.00	7.50	10.00	70.00
16	600.02	25.00	7.50	2.50	10.00
17	600.02	25.00	25.00	1.25	20.00
18	600.02	33.33	21.67	6.67	20.00
19	600.02	33.33	21.67	6.67	70.00
20	600.02	33.33	21.67	3.33	190.00
21	600.02	33.33	21.67	6.67	70.00
22	600.02	33.33	21.67	20.00	190.00
23	600.02	33.33	21.67	3.33	70.00
24	600.02	50.00	15.00	2.50	70.00
25	600.02	50.00	50.00	20.00	20.00
26	800.03	25.00	7.50	1.25	320.01
27	800.03	25.00	7.50	20.00	13.33
28	800.03	25.00	16.25	20.00	26.67
29	800.03	25.00	25.00	2.50	93.34
30	800.03	25.00	25.00	1.25	13.33
31	800.03	25.00	25.00	20.00	320.01
32	800.03	10.00	10.00	1.67	26.67
33	800.03	33.33	33.33	13.33	13.33
34	800.03	50.00	15.00	2.50	13.33
35	800.03	50.00	15.00	20.00	320.01
36	800.03	50.00	15.00	40.00	186.67
37	800.03	50.00	32.50	5.00	26.67
38	800.03	50.00	50.00	2.50	186.67
39	800.03	50.00	50.00	2.50	320.01
40	800.03	50.00	50.00	40.00	13.33
Note: Chord Diameter D = 1000.000					

Table 1

Dimensions (mm) of analysed cracks

Stress intensity factor empirical formula of T-joint under brace tension

$$K_e = \sigma_n F_g F_i F_s \sqrt{(\pi a)}$$

Model AKA1 (Axial): Deepest Crack Front Point (K_a)

$$F_g = 0.2749\beta^{-0.6225-1.2685\ln\beta}\,\gamma^{1.3191-0.1661\ln\tau}\,\tau^{1.6621+0.3704\ln\beta}$$

$$F_i = \beta^{0.3561A-0.0956C}\,\gamma^{0.0983A+0.2298C+0.0817C^2}\,\tau^{-0.0762A}$$

$$F_s = (a')^p(c')^r$$

$$p = -0.8669-0.2198A-0.0162A^2-0.4750C^2-0.1667C^3-0.0193C^4$$

$$r = 0.0777+1.0531A+0.5820A^2+0.0810A^3-0.07001C-0.0604C^2+0.0060C^3$$

$$A = \ln(a/T) \text{ and } C = \ln(3c/d)$$

Model AKC2 (Axial): Surface Crack Front Point (K_c)

$$F_g = 204.08\beta^{-0.5858-0.7492\ln\beta}\,\gamma^{-2.6713-0.2884\ln\beta+0.5646\ln\gamma}\,\tau^{1.1491-0.2936\ln\gamma-0.5043\ln\tau}$$

$$F_i = \beta^{0.0680A}\,\gamma^{0.0478A-0.5344C-0.1218C^2}\,\tau^{-0.1299A-0.0370C}$$

$$F_s = (a')^p(c')^r$$

$$p = 1.0787+0.6397A+0.1569A^2+0.0186A^3-(0.0770+0.0478A+0.0099A^2)C^2$$

$$r = 0.8617+0.4888A+0.1816A^2+0.0123A^3-0.3252C-0.2210C^2-0.0275C^3$$

$$A = \ln(a/T) \text{ and } C = \ln(3c/d)$$

Stress intensity factor empirical formula of T-joint under out-of-plane bending

$$K_e = \sigma_n F_g F_i F_s \sqrt{(\pi a)}$$

Model OKA2 (OPB): Deepest Crack Front Point (K_a)

$$F_g = 0.1718\beta^{0.9626-0.5003\ln\beta}\ \gamma^{1.5274}\ \tau^{0.6488\ +\ 0.3353\ln\beta-0.2962\ln\tau}$$

$$F_i = \beta^{0.3066A-0.0598C}\ (a')^{0.1315\ln\gamma-0.0775\ln\tau}$$

$$F_s = (a')^p(c')^r$$

$$p = -1.3130-0.4253A-0.0584A^2 + 0.9843C-0.3278C^2-0.0308C^3$$

$$r = 0.7184 + 0.5401A^2 + 0.0889A^3 -0.4186C-0.0496C^2 -0.04210A^2C$$

$$A = \ln(a/T) \text{ and } C = \ln(3c/d)$$

Model OKC1 (OPB): Surface Crack Front Point (K_c)

$$F_g = 4.7016\beta^{0.7362-0.9523\ln\beta}\ \gamma^{0.2227-0.7169\ln\beta}\ \tau^{0.6663-0.1040\ln\gamma-0.3802\ln\tau}$$

$$F_i = \beta^{0.1388A-0.2143C}\ \gamma^{0.0573A-0.5026C-0.1175C^2}\ \tau^{-0.1548A}$$

$$F_s = (a')^p(c')^r$$

$$p = 1.5044 + 0.8350A + 0.1258A^2 +0.6624C-0.0202C^2$$

$$r = 0.2954 + 0.3328A^2 + 0.0453A^3 -0.6990C-0.3648C^2 -0.0473C^3$$

$$A = \ln(a/T) \text{ and } C = \ln(3c/T)$$

Stress intensity factor empirical formula of T-joint under in-plane bending

$$K_e = \sigma_n F_g F_i F_s \sqrt{(\pi a)}$$

Model IKA5 (IPB): Deepest Crack Front Point (K_a)

$$F_g = 0.0887\beta^{1.3433-0.4798\ln\beta}\,\gamma^{5.2247-0.5555\ln\beta-0.8310\ln\gamma}\,\tau^{0.6928-0.4302\ln\beta}$$

$$F_i = 0.0887\beta^{-0.0758A-0.2391C}\,\gamma^{0.1406A+0.4341C+0.1543C^2}\,\tau^{-0.1771A}$$

$$F_s = 0.0887(a')^p(c')^r$$

$$p = 1.8586 + 2.2859A + 0.9035A^2 + 0.1215A^3 - 1.0918C - 0.4785C^2$$

$$r = -1.3298 - 0.3040A^2 + 0.4834C + 0.7030C^2 + 0.1130C^3 - 0.1207A^2C$$

$A = \ln(a/T)$ and $C = \ln(3c/d)$

Model ICK3 (IPB): Surface Crack Front Point (K_c)

$$F_g = 0.1395\beta^{-0.6498-1.1883\ln\beta}\,\gamma^{1.0779-0.3414\ln\beta}\,\tau^{0.8168-0.2149\ln\beta}$$

$$F_i = \beta^{0.0422A-0.2452C}\,\gamma^{1.4558A+0.4173A^2-0.9276C-0.3297C^2}\,\tau^{-0.0905A-0.0338C}$$

$$F_s = (a')^p(c')^r$$

$$p = -2.4921 - 0.0063A + 0.2056A^2 + 0.9804C + 0.3916C^2 + 0.0620C^3 - 0.0110C^4$$

$$r = 2.8298 + 0.5682A^2 + 0.0704A^3 + 0.6562C - 0.0453C^2 + 0.0022C^3 + A^2C(0.1621 + 0.0384C)$$

$A = \ln(a/T)$ and $C = \ln(3c/d)$

APPENDIX D

ALTERNATIVE CRACK GROWTH EQUATIONS

APPENDIX D ALTERNATIVE CRACK GROWTH EQUATIONS

This appendix is intended to complement Section 2.6.6. It outlines a number of crack growth equations which have been proposed by various workers as alternatives to the Paris Law. The emphasis is placed on reporting the form of the equations in addition to some related background information, but it is not attempted to reproduce all the parameters necessary for the application of these equations.

Forman et al (1967)

The equation has an exponential component similar to the Paris Law, but in addition, it incorporates a singularity at $[(1 - R)K_c - \Delta K]$, which implies infinite growth rate when K_{max} exceeds the fracture toughness K_c:

$$\frac{da}{dN} = \frac{C(\Delta K)^m}{(1-R)K_c - \Delta K}$$

where, C, m and ΔK correspond to the usual parameters in the Paris Law; and R is the stress ratio.

The equation has been shown to correlate well with data from a number of sources on fatigue of two Aluminum alloys, namely 7075-T6 and 2024-T3, tested at different R values.

Klesnil and Lukas (1972)

This is a simple variant for the Paris Law obtained by incorporating ΔK_{th} into the equation as follows:

$$\frac{da}{dN} = C\left[(\Delta K)^m - (\Delta K_{th})^m\right]$$

where C, and m are reported to be dependent on the strength of the material; and, ΔK and ΔK_{th} are, respectively, the applied and threshold stress intensity factor ranges.

The equation is shown to produce good predictions of the fatigue behaviour of four types of steels having different mechanical tensile and fatigue properties.

Austen et al (1981)

The equation incorporates the effects of the stress ratio R on both the threshold, at low ΔK, and fracture, when K_{max} approaches the fracture toughness K_c. It has the form:

$$\frac{da}{dN} = C\ \Delta K^{n} \left[\frac{\Delta K - \Delta K_{th}}{K_c - \Delta K/(1 - R)} \right]^{p}$$

where

$$\Delta K_{th} = K_{th}^{o}\ (1 - R)^{\gamma}$$

This relationship is reported to accurately represent fatigue crack growth behaviour in air for BS 4360 Grade 50D, API X65 and other steels. Values for the parameters C, n, α and ΔK_{th} are suggested based on limited data.

Hudak et al (1985)

This formulae, referred to as the 'three-component model', incorporates terms to account for growth across the range of ΔK, and is proposed together with the parameters required to cover several environmental and loading conditions. It is expressed in terms of the inverse of the crack growth rate as follows:

$$\frac{1}{da/dN} = \frac{A_1}{\Delta K^{n1}} + \frac{A_2}{\Delta K^{n2}} - \frac{A_2}{[(1 - R)\ K_c]^{n2}}$$

where the parameters A1, n1, A2 and n2 are empirical constants defined in Figure AD1 and given in Table AD1 for structural and low alloy steels. K_c, the fracture toughness, is set equal to 250 MPa $m_{1/2}$.

Application of the model to tubular joints in air and seawater environments is reported to give reasonable agreement with constant amplitude experimental data in the majority of the cases considered.

Condition[a]	A_1	A_2	n_1	n_2
Air, Low-R	1.9×10^{29}	2.5×10^{11}	32.0	3.15
Air, High-R	1.0×10^{14}	9.1×10^{10}	13.3	3.15
Seawater, free Corrosion potential, Low-R	1.9×10^{20}	3.3×10^{11}	17.5	3.65
Seawater, free Corrosion potential, High-R	1.0×10^{14}	1.7×10^{11}	13.3	3.65
Seawater, cathodic polarization,[b] Low-R	8.0×10^{24}	2.9×10^{13}	32.0	5.93
Seawater, cathodic polarization, High-R	—	Constants not estimated because of lack of experimental data		

[a] Low-R: $R < 0.2$; high-R: $R \geq 0.5$

[b] The plateau rates occurring under these conditions were modeled by adding an additional constant to equation (3) equal to 1×10^{6} cycles/m for the 0.1 Hz data and 1.5×10^{7} for the 1.0 Hz data.

Table AD1 Constants in three-component crack growth equation

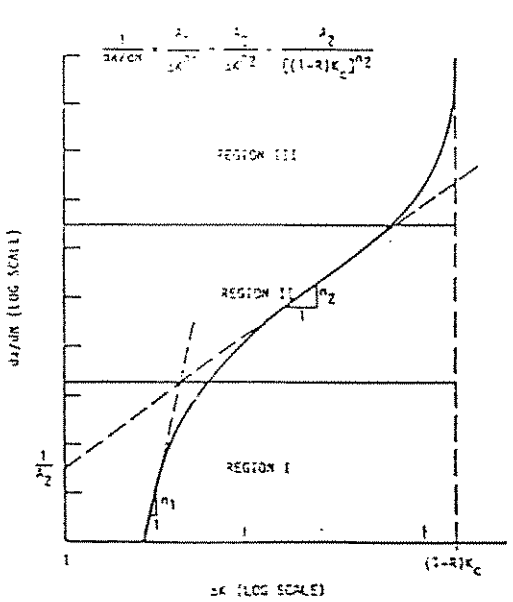

Figure AD1 Schematic representation of three-component crack growth rate equation